Universidad de Oviedo
University of Oviedo

Programa de Doctorado en Biogeociencias

Dissolution-crystallisation processes of Ca-Pb-carbonate, Ca-Pb-sulphate and Ca-phosphate-sulphate systems under Earth's surface and diagenetic conditions

Procesos de disolución – cristalización de los sistemas Ca-Pb-carbonatos, Ca-Pb-sulfatos y Ca-fosfatos-sulfatos en condiciones de la superficie terrestre y diagenéticas.

TESIS DOCTORAL

ANA ROZA LLERA

2023

Universidad de Oviedo

University of Oviedo

Programa de Doctorado en Biogeociencias

Dissolution-crystallisation processes of Ca-Pb-carbonate, Ca-Pb-sulphate and Ca-phosphate-sulphate systems under Earth's surface and diagenetic conditions.

Procesos de disolución – cristalización de los sistemas Ca-Pb-carbonatos, Ca-Pb-sulfatos y Ca-fosfatos-sulfatos en condiciones de la superficie terrestre y diagenéticas.

TESIS DOCTORAL (mención internacional)

ANA ROZA LLERA

Dirigida por Amalia Jiménez Bautista y Mª Lourdes Fernández Díaz

2023

Universidad de Oviedo

RESUMEN DEL CONTENIDO DE TESIS DOCTORAL

1.- Título de la Tesis	
Español/Otro Idioma: Procesos de disolución-cristalización en sistemas Ca-Pb-carbonato, Ca-Pb-sulfato y Ca-fosfato-sulfato en condiciones de la superficie terrestre y diagenéticas.	Inglés: Dissolution-crystallisation processes in Ca-Pb-carbonate, Ca-Pb-sulphate and Ca-phosphate-sulphate systems under Earth's surface and diagenitic conditions.

2.- Autor	
Nombre: ANA ROZA LLERA	DNI/Pasaporte/NIE:
Programa de Doctorado: BIOGEOCIENCIAS	
Órgano responsable: Centro Internacional de Postgrado.	

RESUMEN (en español)

En la corteza terrestre se producen diferentes procesos como la diagénesis, el metamorfismo o el metasomatismo, dónde la circulación de fluidos facilita el desarrollo y progreso de diferentes reacciones minerales. En las últimas décadas, el estudio de los procesos que tiene lugar durante la interacción de fluidos acuosos con las superficies minerales se ha convertido en un importante tema de investigación debido a sus implicaciones diagenéticas y medioambientales. Trabajos previos a esta investigación, demuestran que las interacciones entre minerales y fluidos pueden controlar la movilidad y concentración de contaminantes ambientales peligrosos, como los metales pesados, a través de diferentes mecanismos de sorción.

En esta tesis doctoral se estudian las reacciones de disolución-precipitación que tienen lugar en ambientes de la superficie terrestre y en condiciones diagenéticas, en los sistemas Ca-Pb-carbonato-sulfato, Ca-Pb-Carbonato biogénico y Ca-fosfato-sulfato, con el fin de avanzar en la comprensión de procesos minerales de interés geológico y medioambiental. Para ello, se han diseñado experimentos de interacción a temperatura ambiente entre carbonatos y sulfatos de calcio con disoluciones acuosas ricas en plomo, y experimentos de interacción entre sulfatos de calcio y disoluciones de fósforo en condiciones hidrotermales.

Para el estudio del sistema Ca-Pb-carbonatos-sulfatos (capítulo 3) se han seleccionado fragmentos de calcita y yeso. A pesar de que estos minerales aparecen a menudo asociados en cuencas sedimentarias, todos los estudios experimentales previos de la interacción entre disoluciones de Pb con calcita o yeso se habían realizado considerando estas fases por separado, sin tener en cuenta que la disolución de cualquiera de estos minerales, puede alterar significativamente las características fisicoquímicas de la solución acuosa pudiendo influir en las características de la interacción de la fase fluida con el mineral. Por ello, se han llevado a cabo experimentos de interacción entre disoluciones de plomo con yeso, calcita y con mezclas de yeso y calcita. En todos los casos, se observa la precipitación de sulfatos de plomo (anglesita) o de carbonatos de plomo (cerusita e hidrocerusita) que son los responsables de la eliminación del plomo disuelto. El resultado más llamativo es que las mezclas de yeso y calcita son mucho más efectivas ya que se obtienen concentraciones finales de plomo más bajas que cuando la interacción se produce con yeso o calcita por separado.

La mayoría de estudios experimentales sobre la eliminación de metales pesados, a través de la interacción con superficies minerales de carbonatos de calcio, utilizan como material inicial

calcita y aragonito de origen geológico. Sin embargo, hay muchos menos trabajos que hayan investigado la sorción de metales pesados con carbonatos de calcio de origen biogénico. En esta tesis doctoral se estudia el sistema Ca-Pb-Carbonatos biogénicos (capítulo 4) donde se han realizado experimentos de interacción entre disoluciones de plomo y biominerales de composición calcítica (Chlamys opercularis) y aragonítica (Sepia officinalis). Los resultados obtenidos permiten confirmar que estos biominerales son más eficaces en la eliminación del Pb de disoluciones acuosas que la calcita y aragonito de origen inorgánico, siendo el más efectivo de ambos el biomineral de composición calcítica.

Por último, con el objetivo de avanzar en el estudio de los mecanismos de eliminación de P a través de reacciones acopladas de disolución – cristalización (ICDP) y en el origen de las acumulaciones de apatito asociadas a rocas sedimentarias evaporíticas, se ha llevado a cabo el estudio del tercer sistema Ca-fosfatos-sulfatos (capítulo 5). En este sistema se han efectuado experimentos de interacción entre cristales de anhidrita y disoluciones acuosas de P en condiciones hidrotermales. Los resultados muestran que se produce el reemplazamiento pseudomórfico de la anhidrita por agregados de fosfatos cálcicos (hidroxiapatito y β-TCP). El progreso de la reacción se ve facilitado por la formación de porosidad, que está a su vez fuertemente influenciada por la relación hidroxiapatito/β-TCP y las características texturales y morfológicas de ambas fases. Se ha determinado la energía de activación empírica (Ea) del reemplazamiento mediante dos métodos (iso-conversion y Avrami) obteniéndose un valor de Ea próximo a 40 kJ/mol. Los resultados indican que el reemplazamiento de minerales de origen evaporítico es un mecanismo factible para la formación de acumulaciones de fosfato cálcico en cuencas sedimentarias durante la diagénesis.

RESUMEN (en Inglés)

Different processes such as diagenesis, metamorphism or metasomatism occur in the Earth's crust, where the circulation of fluids involves the development and progress of different mineral reactions. During the last decades, the interaction of aqueous fluids with mineral surfaces has been the subject of numerous studies due to its diagenetic and environmental implications. Previous works show that the interactions between minerals and fluids can control the mobility and concentration of dangerous environmental pollutants, such as heavy metals, through different sorption mechanisms.

This PhD thesis studies the dissolution-precipitation reactions that take place under Earth's surface and diagenetic conditions in the Ca-Pb-carbonate-sulphate, Ca-Pb-biogenic carbonate and Ca-phosphate-sulphate systems, in order to advance in the understanding of mineral processes of geological and environmental interest. For this purpose, interaction experiments at room temperature between calcium carbonates, sulphates and Pb-bearing aqueous solutions, and hydrothermal interaction experiments between calcium sulphates and P-bearing aqueous solutions have been performed.

For the study of the Ca-Pb-carbonate-sulphate system (chapter 3), calcite and gypsum crystals have been selected. Although gypsum and calcite minerals are often associated in sedimentary basins, all previous experimental works of the interaction between Pb-bearing aqueous solutions with these minerals have been conducted considering these phases separately, without taking into account than the dissolution of any of these mineral phases can both significantly alter the physicochemical characteristics of the aqueous solution and influence the characteristics of the fluid phase interaction with the mineral. Therefore, interaction experiments between Pb-bearing aqueous solutions with gypsum, calcite and mixtures of gypsum and calcite

crystals have been carried out. In all cases, it is observed the precipitation of lead sulphates (anglesite) or lead carbonates (cerussite and hydrocerussite), which are the main mechanism of Pb removal from aqueous solutions. The most striking result is that mixtures of gypsum and calcite are much more effective, resulting in lower final lead concentrations than when the interaction occurs with gypsum or calcite separately.

The majority of experimental studies of the removal of heavy metals from aqueous solution through their interaction with calcium carbonates mineral surfaces have used mineral samples of carbonates from metamorphic origin as starting material. However, there is much less works that investigates the sorption of heavy metals with calcium carbonates of biogenic origin. In this PhD thesis, Ca-Pb-Biogenic carbonates system is studied (chapter 4) using two different biominerals in the interaction experiments with Pb-bearing aqueous solutions, one of them of calcitic composition (Chlamys opercularis) and the other of aragonitc composition (Sepia officinalis). The results obtained confirm that biominerals are more effective in Pb removal from aqueous solutions than their geological counterparts, being the most effective the calcitic biomineral, Chlamys opercularis.

The study of Ca-phosphate-sulphate system (chapter 5) has been conducted in order to advance in the study of the mechanisms of P removal through the development of interface coupled dissolution-precipitation (ICDP) reactions and the origin of apatite accumulations associated to evaporitic sedimentary rocks. In this system, hydrothermal interaction experiments have been carried out between P-bearing aqueous solutions and anhydrite crystals. The results show the pseudomorphic replacement of anhydrite by calcium phosphate aggregates (hydroxyapatite and β-TCP). The progress of the reaction is facilitated by porosity formation, which is in turns strongly influenced by the hydroxyapatite/β-TCP ratio and the morphological characteristics of both phases. The empirical activation energy (Ea) of the replacement has been determined by two methods (iso-conversion and Avrami) yielding Ea values around 40 kJ/mol. The results show that the replacement of evaporitic minerals is a feasible mechanism for the formation of some calcium phosphate accumulations in sedimentary basins during diagenesis.

SR. PRESIDENTE DE LA COMISIÓN ACADÉMICA DEL PROGRAMA DE DOCTORADO EN BIOGEOCIENCIAS

A Mar

Inocencia y alegría

¡Cuatro años de pura felicidad!

Agradecimientos

Con estas palabras me gustaría agradecer a todas aquellas personas que de modo alguno han contribuido a la realización de esta Tesis Doctoral:

En primer lugar, quiero agradecer a mis directoras Amalia Jiménez Bautista y Lurdes Fernández Díaz la oportunidad de realizar esta tesis doctoral con ellas. Gracias Lurdes por enseñarme a escribir y reflexionar, sin lugar a duda tienes el don de mejorar aquello que tocas, tienes una capacidad de esfuerzo y trabajo encomiable. Gracias Amalia por enseñarme tanto, por estar siempre disponible, por tu apoyo y dedicación diaria, sin lugar a duda esta tesis no habría salido adelante sin tu ayuda y tus consejos, después de cinco años puedo decir que me une a ti algo más que una simple relación académica o profesional.

Quiero agradecer a todos los miembros del Departamento de Geología de la Universidad de Oviedo (Personal Docente Investigador y Personal de Administración y Servicios) su buena acogida. Una mención especial para el área de Cristalografía y Mineralogía, habéis conseguido que me sintiese como en casa, muchas gracias por tener siempre palabras de ánimo y apoyo.

Muchas gracias a Sergey Churakov y a Fulvio Di Lorenzo por su acogida durante la estancia en la Universidad de Berna. Fulvio, ha sido un placer compartir tiempo contigo en el laboratorio, gracias por enseñarme tanto en tan poco tiempo. Georgia, Matteo, Michelle, Annita, y Feredica, sin vosotros mi estancia en Berna no habría sido lo mismo, siempre la recordaré con mucho cariño, gracias.

Agradecer también a los Servicios Científico Técnicos de la Universidad de Oviedo y al Centro de Ayuda a la Investigación (CAI) de Difracción de Rayos

X, de la UCM, por su buena disposición y ayuda para llevar a cabo los diferentes análisis.

Muchas gracias a los compañeros que durante estos años hemos compartido tan buenos momentos: Rosa, Irene, Adriana, Manuel, Adriana Georgina, Bea e Indira. Hago una mención especial a aquellos que me han tenido que sufrir en los momentos más difíciles: Iván, Emma Marta y Alba, gracias por vuestro apoyo, comprensión y sinceridad.

Quiero agradecer a mis amigas geólogas, aquellas con las que empecé a estudiar la licenciatura, aquellas que se hacen llamar "las paleosomeras", por vuestra confianza y palabras de aliento.

Gracias a mi familia, por su apoyo incondicional en los buenos y malos momentos, especialmente a mis padres, quienes con su esfuerzo y sacrificio han hecho posible mi carrera académica. Virgi, no hay persona más comprensiva y paciente que tú, suerte de hermana que tengo, siempre dispuesta a escucharme. Berto, nos vemos en los bares.

Finalmente quiero agradecer a Marcos su paciencia, comprensión y sinceridad, a veces incomoda, pero absolutamente necesaria. Has sido, sin lugar a duda, quién más ha sufrido a mi lado, espero que también sientas la misma liberación y satisfacción que yo al cerrar este capítulo de mi vida.

Este trabajo ha sido financiado por el Ministerio de Ciencia e Innovación con la ayuda FPI MINECO-18-BES-2017-081759 y los proyectos MINECO-CGL2016-77138-C2-1-P, MINECO-CGL2016-77138-C2-2-P y PID2021-125467NB-I00

INDEX

CHAPTER 1

INTRODUCTION

1. Introduction

1.1. State of the art

Over the last decades, the study of the processes that take place during the interaction between mineral surfaces and aqueous fluids has become a main topic of research which has far-reacing implictaions for minerals genesis theory as well as the use of mineral surfaces in industrial and environmental applications (Hochella 2002). The circulation of fluids plays a major role in a wide variety of geological settings in the Earth's crust, facilitating the progress of mineral reactions during diagenesis, metamorphism and metasomatism and the achievement of thermodynamic equilibrium in the mineral-fluid systems (Putnis 2002; Putnis and Fernández-Díaz 2010). During the interaction between aqueous solutions and mineral surfaces several processes can occur simultaneously: (i) dissolution of the prymary mineral phases, (ii) transport of dissolved chemical species both to and from the mineral-fluid interface, (iii) adsorption of ions on reactive positions on the mineral surface and (iv) precipitation of secondary mineral phases on the surface of the primary ones, among others. Mineral surface-aquoeous solution interactions can result in the removal of chemical species from the fluid through four different sorption mechanisms that can operate siumulatenously Sposito (1986): adsorption, absorption, precipitation and co-precipitation (Figure 1.1). Absorption involves the diffusion of ions or molecules from the mineral-fluid interface into deeper layers of the mineral, to occupy structural interstices. In contrast, adsorption involves the incorporation of ions or molecules at the mineral-fluid interface without the development of a three-dimensional periodic structural framework. Finally, precipitation and co-precipitation also involve the incorporation of ion or molecules at the mineral-fluid interface, but result in the heterogeneous

nucleation and growth crystals of new mineral phases that would partially or totally cover the original mineral-fluid interface. The newly formed mineral phase incorporates into its crystal structure the previously dissolved chemical species. The main difference between precipitation and co-precipitation mechanism relates to the relationship between the primary and the secondary phase(s). In the first case, the new precipitate is not related to the original mineral, while the mineral phase(s) formed during co-precipitation incorporates chemical species that came from both the bulk aqueous solution and the dissolving surface of the primary mineral phase. Thus, co-precipitation involves the development of dissolution-precipitation reactions and results in the formation of randomly oriented as well as epitatic overgrowhts of varying compositions, including the solid solution series through heterogeneous nucleation, or even topotactic reactions (Sposito 1986). Thus, in the case of heterogeneous nucleation when the new phase shares crystallographic similarities with surface of the substrate epitaxy may occur (Sposito 1986).

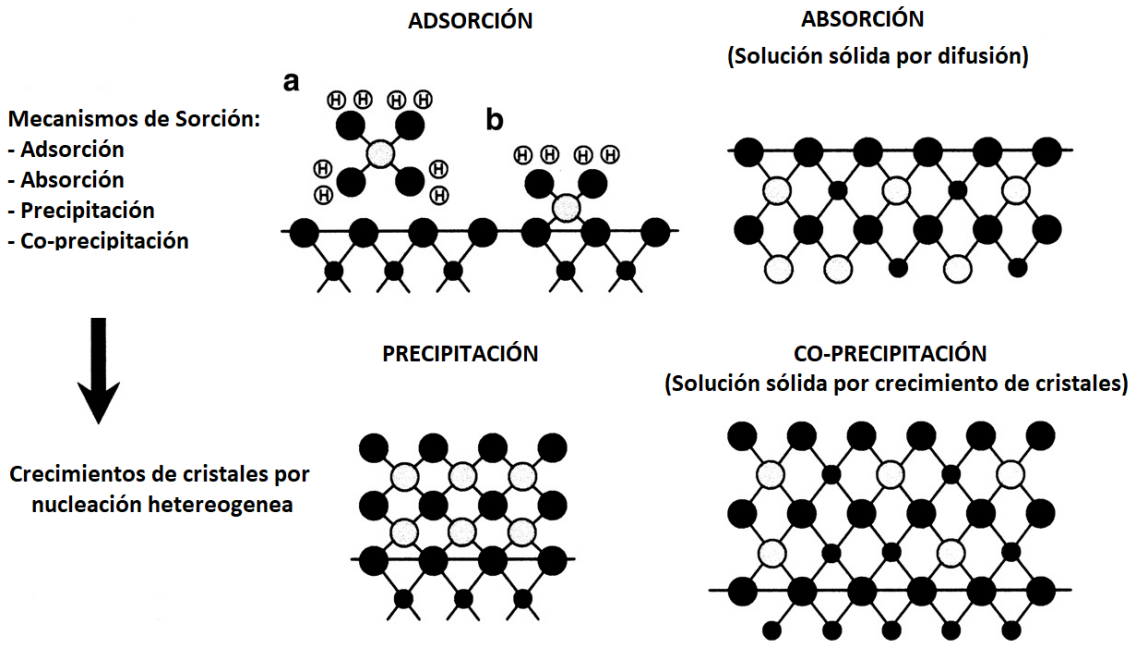

Figure 1.1. Sorption mechanism at the mineral-water interface (after Brown et al. 1995).

These sorption processes are of great interest within the field of mineralogy and environmental geochemistry as they play a key role in the quality of drinking or irrigation water, as well as in the fertility and production of soils. The interactions between minerals and fluids can determine the mobility and concentration of some of the most dangerous environmental pollutants, such as cadmium, lead or mercury, controlling the dispersion and accumulation of heavy metals, as well as their geoavailability and bioavailability in surface environments (Hochella 2002; Godelitsas and Astilleros 2010)

In addition to sorption processes, other dissolution-crystallisation reactions known as ICDP (coupled dissolution-crystallisation reactions) are also common in sedimentary, diagenetic, metamorphic and metasomatic environments. Thermodynamic and kinetic properties of minerals, together with physicochemical conditions of the fluids, can promote a coupling between the dissolution rate of the primary phase and the precipitation rate of the secondary one. When this occurs, both the shape and the volume of the primary phase is preserved, resulting in the formation of pseudomorphic crystal aggregates of the secondary phase(s) (Putnis 2002, 2009a). When the dissolution rate of the primary phase is the limiting kinetic factor of the ICDP reaction, the degree of coupling between the dissolution and precipitation rates is so accurate that every primary phase nanotopographic as well as textural and/or microtextural features are preserved during the mineral replacement reaction and can be found in the secondary phase pseudormoph (Xia et al. 2009; Ruiz-Agudo et al. 2014; Altree-Williams et al. 2015). Moreover, the size of the crystals that build up the latter srongly depends on the degree of coupling during the dissolution-precipitation reactions, so that the tightest the coupling the secondary phase pseudomorph consist of smallest crystals (Fernández-Díaz et al. 2009).

The progress of ICDP reactions requires a continuous communication between the fluid phase and the primary phase-secondary phase interface. This communication between the interphase and the fluid phase is ensured by the formation of porosity and/or fractures during the mineral replacement reaction. Porosity formation is an intrinsic characteristic of all ICDP reactions that involve a negative molar volume change between the primary (dissolved) and secondary phase(s) (precipitated). In addition to molar volume change, a negative solubility change that can also add up in determining that further porosity volume is generated during ICDP reactions (Zhao et al. 2009; Pollok et al. 2011; Jonas et al. 2013; Ruiz-Agudo et al. 2014; Putnis 2015). The amount of porosity formed during ICDP mineral replacements strongly influence the rate of mass transport to and from the primary phase-secondary phase interface reaction (Jonas et al. 2013; Pedrosa et al. 2017). However, the overall kinetics of the replacement reaction is not only determined by the newly formed porosity volume but also by the textural features of this porosity including the size, shape, and connectivity of pores as well as porosity permeability (Putnis et al. 2005; Jonas et al. 2013; Putnis 2015; Yuan et al. 2018; Forjanes et al. 2020b).

The existence of epitaxial relationships between primary and secondary phases can play a role in both mineral replacements and sorption processes. When the substrate of the parent mineral (sorbent) shares crystallographic elements with the secondary phase (sorbate), it is very likely that the newly formed nuclei will grow epitaxially on the surface of the primary phase. This allows the formation of an oriented crystals layer that can partially or totally cover the substrate of the parent mineral and prevent the interaction of the fluid phase with the substrate (Van Der Merwe 1978; Putnis et al. 2005; Xia et al. 2009; Chernov 2012). This can result in a total or partial hindering of the progress of the dissolution-precipitation reaction depending on the nature of the epitaxy between the mineral phases involved. If both phases are isostructural, the

coincidence between the structures can be almost perfect and two-dimensional nuclei can form and grow according to the Frank van der Merwe or Stransi Krastanov growth mechanism (Van Der Merwe 1978; Chernov 2012; Cuesta Mayorga et al. 2018; Forjanes et al. 2020a). In such cases, the epitaxial layer covering the parent phase usually is only a few nanometers thick and presents perfect continuity (Astilleros et al. 2003, 2010; Prieto et al. 2003; Pérez-Garrido et al. 2007). In this case, the epitaxial layer effectively armours the substrate from further interaction with the aqueous phase, resulting in a complete stoppage of the dissolution-crystalizacion reaction.

There are numerous experimental examples of sorption and mineral replacement processes that rapidly stop due the growth of epitaxial layers. This has been observed durint the sorption of Mn and Cd by calcite ($CaCO_3$) surfaces after to the formation of epitaxial nanolayers of rhodochrosite ($MnCO_3$) and otavite ($CdCO_3$) respectively (Prieto et al. 2003; Köhler et al. 2007; Pérez-Garrido et al. 2007), during the sorption of Cr and Sr by barite ($BaSO_4$) surface due to the formation of epitactid layers of hashemite ($BaCrO_4$) (Shtukenberg et al. 2005), and celestite ($SrSO_4$) (Sánchez-Pastor et al. 2005), respectively, during the sorption of As by gypsum ($CaSO_4 \cdot 2H_2O$) surface after the formation of epitaxial layer of pharmacolite ($CaHAsO_4 \cdot 2H_2O$) on gypsum (Rodríguez-Blanco et al. 2007), during the sorption of Pb by aragonite ($CaCO_3$) after the epitactic growth of cerussite (Di Lorenzo et al. 2020) and during the replacement of anhydrite ($CaSO_4$) by celestinte crystals (Forjanes et al. 2020a).

The study of dissolution-precipitation reactions in the mineral-fluid system has encouraged the appearance of new lines of research focused on environmental remediation with the aim of developing new strategies to reduce the concentration of inorganic in soils and waters. In many countries around the world, mining activities have resulted in extensive contamination of soils and

waters, causing significant environmental damage and threatening drinking water supplies and the viability of farming activities (Li et al. 2014). Moreover, over the last century, a variety of industries, including chemical, pharmaceutical, battery manufacturing or nuclear industry have been responsible, have also significantly contributed to the contamination of soil and groundwater by organic and inorganic pollutants (Hassaan et al. 2016). Among the latter, heavy metals pose a major risk for the health of humans and, in general, living organisms as these elements can be adsorbed and accumulated. Indeed, the accumulation of heavy metals in the human body has been related to the development of serious diseases such as cancer or strong damage to the nervous system (Zhuang et al. 2009; Li et al. 2014). In recent years, different decontamination methods, such as coagulation and flocculation, electrolysis, electrocoagulation, and electrodeionization, have been applied to treat water polluted by heavy metals (Johnson et al. 2008; Al Aji et al. 2012; Peng et al. 2014; Lu et al. 2015). Although good results have been obtained, a common drawback of these techniques is their elevated cost, which makes their application in developed countries impossible. Therefore, research and development of more efficient and less expensive decontamination strategies is essential (Crini and Lichtfouse 2019; Guo et al. 2021).

Among heavy metals, lead is one of the most dangerous, causing long-lasting damage in underwater environments with a major impact on soil fertility and productivity, as well as biodiversity (Li et al. 2014). The U.S. Environmental Protection Agency lists lead as a very toxic element and ranges its toxicity immediately after that of arsenic because of the risks lead poses to human health. Besides the damage it can cause to circulatory, nervous, endocrine and immune systems of the human body (Zhuang et al. 2009; Li et al. 2014), it is considered an important mutagenic, teratogenic and carcinogenic agent, especially dangerous for vulnerable groups, such as pregnant women, children and the

elderly (Jung and Thornton 1997; Ryan et al. 2000; Tong et al. 2000; Zheng et al. 2007, 2010; Luo et al. 2012; Hassaan et al. 2016; Piekut et al. 2019).

The presence of heavy metals in water is a serious environmental problem, but it is not the only environmental threat our society faces nowadays. Extensive use of ammonium phosphate as a fertiliser in intensive agriculture has resulted in phosphorus contamination of aquifers and running waters (Smith 2003; Wei and Bailey 2021). Phosphorus (P) is an essential macronutrient for plant growth; however, excessive use of this element can lead to eutrophication of water bodies. The excess nutrients in an aquatic environment can cause the uncontrolled proliferation of different organisms and the excessive development of toxigenic algae. As a result, the environmental balance can be disrupted, leading to the interruption of oxygen production due to a lack of light, which makes the environment anoxic. Much of the surface water bodies in Europe are deteriorated by an excess of nutrients (Poikane et al. 2019; Mallin and Cahoon 2020).

Due to the environmental importance of the concentration of these elements in water bodies, as it is a conditioning factor for the drinking suitability of waters, several works have addressed the study of the interactions between minerals and polluted water as a way of understanding the role that minerals surface play in the fate of pollutin elements. Dissolution-precipitation reactions are common in surface and subsurface geological environments, where calcium carbonates and sulphates, such as calcite, aragonite, gypsum and anhydrite, are common rock-forming minerals in sedimentary basins as the main constituents of carbonate and evaporites rocks (Ma et al. 1993; Traina and Laperche 1999; Warren 2006). Altree-Williams et al. (2015) reviewed macroscopic and microscopic studies, which had addressed the development of dissolution-precipitation reactions that occurred as a result of aqueous fluids and mineral

surface, highlighting the widespread nature of this type of reactions in natural environments. Different authors have demonstrated the effectiveness of dissolution-precipitation reactions for the elimination of heavy metals. These reactions have proven to be effective mechanisms in the control of inorganic pollutants from wastewaters, through the immobilization of toxic elements in the crystalline structure of the precipitated secondary mineral phasess. The efficiency of this process depends on several factors such as the solubility of the solid phases, the reactive surface of the primary phase, the formation of solid solutions and the epitaxial relationships between the primary and secondary phases as explained above. Several studies have shown that sorption proceses (adsorption, absorption and co-precipitation) that take place on the surface of mineral calcium carbonates and sulfates, and often are the starting point of pseudomorphic mineral replacement processes can help to control the concentration of different pollutant in natural environments. Thus, different experimental studies have confirmed the effectiveness of calcium carbonates, such as calcite and aragonite surfaces as scavengers of dissolved toxic elements as lead (Godelitsas et al. 2003; Yuan et al. 2016; Di Lorenzo et al. 2019, 2020; Kim et al. 2023), manganese (Pérez-Garrido et al. 2009), cadmium (Stipp et al. 1992; Chada et al. 2005; Pérez-Garrido et al. 2007; Callagon et al. 2017) phosphate (Wang et al. 2012a, 2012b) and chromate (Guren et al. 2020), from aqueous solutions through coupled dissolution-precipitation reactions that result in the immobilization of the pollutant within the crystal structure of a mineral sorbate. The same ability has been experimentally confirmed for the surfaces of the mineral calcium sulfates, gypsum and anhydrite. Dissolution-crystallisation reactions that take place on the surface of these latter mineral result in the effective uptake dissolved barium and strontium (Forjanes et al. 2020a, 2020b), lead (Astilleros et al. 2010; Morales et al. 2013, 2014), arsenic (Rodríguez et al.

2008) and phosphate (Pinto et al. 2009, 2010), and their immobilization in the structure of the secondary mineral phases.

The majority of experimental studies of the removal of heavy metals from aqueous solution through their interaction with calcium carbonates mineral surfaces have used mineral samples of carbonates from metamorphic origin as starting material (Stipp et al. 1997; Chada et al. 2005; Elzinga et al. 2006; Pérez-Garrido et al. 2007, 2009; Yuan et al. 2016). Comparatevely, very few studies have been carried out using calcium carbonates of biogenic origin to investigate heavy metal sorption (Köhler et al. 2007; Alidoust et al. 2015; Zhou et al. 2017). However, these latter works have shown that biominerals, such as marine shells, eggshells or sepia cuttlebone, are much more efficient materials scavenging heavy metals from polluted waters than their geological counterparts (Zhou et al. 2017; Lee et al. 2018; Nkutha et al. 2021). Interestingly, the biocarbonates are waste products of mariculture and canning industries. Incorporating these materials into polluted water decontamination strategies contains the added value of giving an use to these waste and thereby contributing to some extent solve its disposal, which often is problematic. Currently, only small amounts of these residues are recycled in fertiliser production and as additives in animal feed (Arvanitoyannis and Kassaveti 2008; Soto 2009). Most biogenic calcium carbonates are characterized by a hierarchical structure comprising two intimately interlinked components: pliant polymers (up to 10 wt. %) and hard inorganic minerals (≥ 90 wt%) (Lowenstam and Weiner 1989). The mineral component consists mainly of nanoparticulate calcite and/or aragonite, which appear arranged in mineral units (Berman et al. 1993; Weiner and Dove 2003; Checa et al. 2007, 2016, 2018; Harper et al. 2009; Kim et al. 2016; Lee et al. 2018). The compliant polymers consist of biopolymers of complex assemblages of polysaccharides, proteins, glycoproteins, and glycosaminoglycans, which appear arranged as membranes surrounding

calcite/aragonite mineral units, and networks of fibrils (occluded within the mineral units). Each species presents a specific composition and distribution of biolpolymers, as well as a characteristic texture and microstructure of the biominerals, which may even vary between different parts of a single biomineral (Addadi and Weiner 1992; Checa et al. 2016).

This thesis has addressed the study of reactions between mineral and fluids that take place in conditions close to those prevailing on the Earth's surface in order to shed light on some mineral processes of great geological and environmental interest.

From an environmental point of view, special attention has been paid to the interaction of calcium carbonates and/or sulphates with Pb-bearing aqueous solutions. Although gypsum and calcite minerals are often associated in sedimentary basins, all previous experimental works of the interaction between Pb-bearing aqueous solutions with these minerals have been conducted considering these phases separately, without taking into consideration that the dissolution of any of these Ca-bearing minerals can both significantly alter the physicochemical characteristics of the aqueous solution and influence the characteristics of the fluid phase interaction with the mineral. On the other hand, the effectiveness of biominerals (BIO-calcite and BIO-aragonite) for the removal of dissolved Pb from polluted water has been studied and the results have been compared with those obtained in previous works where calcite and aragonite were used. In the context of diagenesis, previous experimental studies confirm that the interaction of phosphate-bearing fluids with sedimentary rock-forming minerals such as aragonite and calcite results in their replacement by aggregates of apatite crystals (Kasioptas et al. 2010, 2011; Jonas et al. 2013; Reinares-Fisac et al. 2017). However, the mechanisms of P-sequestration by mineral surfaces through ICDP reactions and the origin of apatite accumulations associated to

evaporitic sedimentary rocks still need to be studied in depth. Here, we investigate the pseudomorphic replacement of anhydrite single crystals by aggregates of calcium phosphates and the overall kinetic of the replacement reaction.

1.2. Structures of the primary minerals used in this thesis

In this thesis, the experimental study of three systems is carried out:

1. Removal of dissolved Pb from contaminated waters through its interaction with calcite and gypsum mixtures.

2. Removal of dissolved Pb from contaminated waters through its interaction with biominerals (BIO-Calcite and BIO-aragonite).

3. Anhydrite replacement by calcium phosphates under hydrothermal conditions.

In this section, the crystal structures of the primary minerals involved in the above-mentioned systems are briefly described.

Calcite structure

Calcite ($CaCO_3$) is the most abundant mineral of the rhombohedral carbonate group, which includes other minerals that contain cations of smaller radius than Ca (Mg, Fe, Ni, Cd, Co, Mn or Zn). Calcite crystallizes in the hexagonal system (space group R-3c, no. 167). Its crystalline structure is formed by CO_3 groups in which the carbon atom is enclosed by three oxygen atoms forming a flat equilateral triangular group (Figure 1.2) that enjoys a limited degree of rotation, especially at low temperatures. Calcium cation appear in nine coordinated with the nearest oxygens belonging to six adjacent triangular groups. The crystal structure consists of cation layers alternating with carbonate layers perpendicular to the c-axis, with the triangular carbonate groups pointing in opposite directions in successive layers (Reeder 1983). This feature is responsible for the strong anisotropy of calcite, which is reflected in the

difference of physical property values when measured parallel or perpendicular to the c-axis. For example, birefringence can be observed in the direction perpendicular to the c-axis, whereas along the direction parallel to the c-axis (which coincides with the optical axis) this phenomenon is hardly noticeable.

Calcite is the most abundant mineral, within the rhombohedral group, in sedimentary rocks of chemical or biogenic origin. The hard parts of bivalves are also the result of biogenic precipitation of calcite crystals that grow in marine environments where specific parts present different proportions of organic components depending on the biological species.

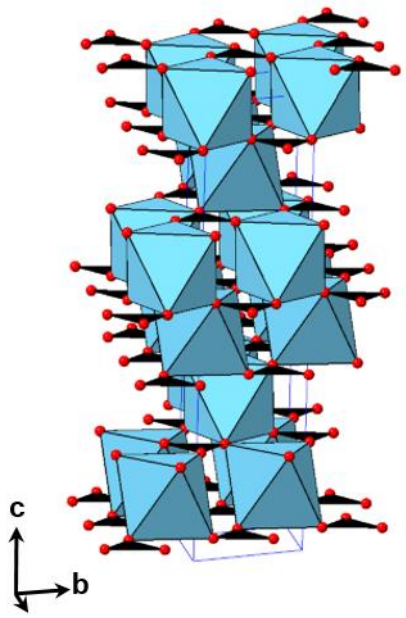

Figure 1.2. Structure of calcite ($CaCO_3$).

Gypsum structure

Calcium sulphates such as gypsum ($CaSO_4 \cdot 2H_2O$) are very abundant in sedimentary basins forming evaporite deposits. Gypsum belongs to the monoclinic system, with spacial group A2/a and lattice parameters a = 6,277 Å, b = 15,181 Å, c = 5,672 Å (Heijnen and Hartman 1991; Comodi et al. 2008). The

structure consists of layers of tetrahedra (SO_4) parallel to (010) strongly bound to irregular calcium polyhedra in coordination eight, two of the oxygen atoms of the calcium polyhedra belong to water molecules and the other six oxygen atoms to sulphate groups (Figure 1.3). These layers are bonded together by water molecules via hydrogen bonds, which connect one oxygen of the calcium polyhedra (CaO_8) with another oxygen of the tetrahedra (SO_4). These bonds are weak, which explains the exfoliation of the gypsum parallel to the (010) planes. The sulphate tetrahedra are not regular and form chains along [101] (Cole and Lancucki 1974; Pedersen and Semmingsen 1982; Heijnen and Hartman 1991).

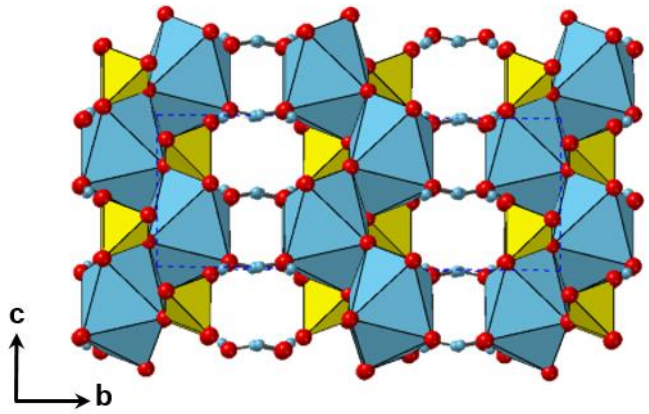

Figure 1.3. Structure of gypsum ($CaSO_4 \cdot H_2O$).

Anhydrite structure

Anhydrite ($CaSO_4$) is a common mineral in sedimentary basins, where it appears as a major component of evaporites, as well as forming nodules and cements in sandstones, limestones and dolostones (Murray 1964). Anhydrite crystallizes in the rhombic system (Amma space group) and its lattice parameters are a=6.993Å, b=6.995 Å, c=6.245 (Hawthorne and Ferguson 1975). Its crystal structure consists of SO_4 groups with tetrahedral geometry and Ca

cations coordinated with the eight nearest oxygens of the sulphate groups (Figure 1.4). The distances between calcium and oxygen vary between 2,345 and 2,564 Å, which generates a distorted triangular dodecahedron (Hawthorne and Ferguson 1975). In the structure of anhydrite SO_4 tetrahedra and Ca dodecahedra alternate to form chains parallel to [001]. These chains in turn are joined together sharing edges (dodecahedra) and vertices (SO_4) along the [100] direction and sharing only vertices along the [010] direction. Due to these characteristics, the anhydrite exhibits perfect exfoliation parallel to the three main planes (001), (010) and (100), which correspond to F-type faces according to the Hartman-Perdok model (Hartman and Perdok 1955a, 1955b).

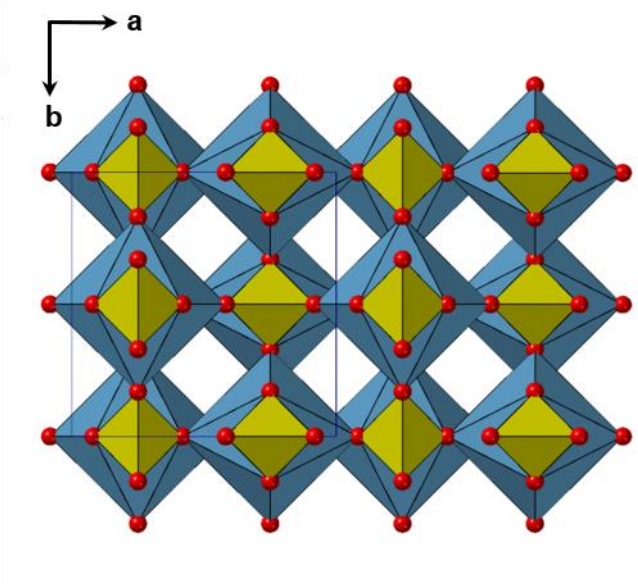

Figure 1.4. Structure of anhydrite ($CaSO_4$)

1.3. Objectives

Experimental studies focused on the reactions between mineral surfaces and fluids have allowed a better understanding of those geological processes that take place on long time scales under very different temperature conditions. However, physicochemical factors that govern the evolution and kinetics of reactions under epigenetic conditions still remains poorly understood. The main objective of this thesis is to understand the factors involved in dissolution-crystallisation processes of mineral phases that are relevant in different natural scenarios such as diagenesis or the environment. In these contexts, mineral transformations that involves Ca-Pb-carbonates-sulphates, Pb-biogenic calcium carbonates and Ca-phosphate-sulphate have been investigated. To approach the study of these systems, the physicochemical conditions of aqueous solutions interacting with calcium carbonates (calcite, biocalcite or bioaragonite) and/or with calcium sulphates (gypsum or anhydrite) under epigenetic conditions have been reproduced to understand the relationship between the physicochemical changes of the fluid and the textural changes of the mineral phases involved. To address this main objective, a series of specific objectives have been established:

- Analyze the evolution of the chemical composition of the fluid during the interaction of Pb-bearing aqueous solutions with two systems: a) calcite - gypsum and b) biocalcite or bioaragonite

- Determine the Pb-removal mechanism during its interaction with single crystals of calcite and gypsum and its mixtures or with biogenic calcium carbonates.

- Evaluate and compare the effectiveness of dissolved lead removal by different biogenic calcium carbonates and abiogenic calcium carbonates.

- Study the replacement of anhydrite single crystals by calcium phosphates upon interaction with P-bearing aqueous solutions analyzing the influence of physicochemical and textural parameters.

- Determine the mechanism and kinetics of the replacement reaction in the system Ca—sulphates -phosphates.

1.4. Structure of the thesis

This thesis is structured in the following chapters:

Chapter 2 details the experimental methods conducted to study the three systems as well as the analysis and characterization techniques used.

Chapter 3 (Ca-Pb-carbonates and sulphates system) shows the experimental results of the interaction of Pb-bearing aqueous solutions with gypsum, calcite and mixtures of gypsum and calcite. The results of this chapter correspond to a work already published: "Removal of Pb from Water: The Effectiveness of Gypsum and Calcite Mixtures" by Ana Roza-Llera, Amalia Jiménez and Lurdes Fernández-Díaz.

Chapter 4 Ca-Pb-Biogenic carbonates System presents the results attained in the study of Pb^{2+} uptake by the surface of two biominerals, the shell of the bivalve Chlamys opercularis (Aequipecten opercularis) and the cuttlebone of the cephalopod Sepia officinalis. The results of this chapter correspond to a work already accepted: "Pb removal efficiency by calcium carbonates: biogenic versus abiogenic materials" by Ana Roza-Llera, Fulvio Di Lorenzo, Sergey V. Churakov, Amalia Jiménez and Lurdes Fernández-Díaz.

Chapter 5 Ca-phosphates-sulphates System studies the interaction of a P-bearing aqueous solution with anhydrite single crystals and determines the kinetics and reaction mechanisms of anhydrite replacement by calcium phosphates. The results of this chapter correspond to a work already published: "Mechanism and kinetics of the pseudomorphic replacement of anhydrite by calcium phosphate phases at hydrothermal conditions" by Ana Roza-Llera, Amalia Jiménez and Lurdes Fernández-Díaz.

Chapter 6 General discussion of the results presented in this thesis.

Chapter 7 summarizes the most important conclusions obtained during the course of this thesis.

CHAPTER 2

METHODS

2. Methods

In this experimental thesis, three systems have been studied, two of them in conditions of the earth's surface with significant environmental interest and the third one in hydrothermal conditions close to those prevailing during diagenesis. The three systems have been studied by performing interaction experiments of Pb or P-bearing aqueous solutions with minerals abundant in the earth's crust such as calcium carbonates (calcite and aragonite) and calcium sulphates (gypsum and anhydrite). Specific experiments have been designed for each system in order to reproduce the most accurate scenario according to the environmental or diagenetic interest of lead or phosphate, respectively. Thus, the experimental procedures carried out for each system studied are detailed in the corresponding chapters. Therefore, in this chapter, a global description of the experiments and techniques used in this doctoral thesis is described. The methods chapter has been divided into 4 categories: (2.1) room temperature experiments, (2.2) hydrothermal experiments, (2.3) liquid phase characterization and (2.4) solid phase characterization.

2.1. Experiments at room temperature.

The experiments carried out at room temperature are specifically designed to study two processes: (a) the interaction of Pb-bearing aqueous solutions with abiogenic calcium carbonates and calcium sulphate (chapter 3) and, (b) the interaction of Pb-bearing aqueous solutions with biogenic calcium carbonates (chapter 4). Here, the prior preparation of the starting solids used and the batch type experiments designed for each case are described below.

2.1.1. Preparation of Starting Solids

Chapter 3 evaluates the efficiency of calcium carbonates and sulphates in the removal of dissolved lead. In this case, gypsum and inorganic calcite samples were used. The calcite samples belong to the Iceland spar variety and come from Proaza (Asturias, Spain) whereas the gypsum crystals belong to the selenite variety and come from Alameda de la Sagra (Toledo, Spain) (Figure 2.1). Both mineral samples were crushed mechanically, using an agate mortar, until the selected grain size (3-4 mm) was obtained. The mineral grains were then introduced in an ethanol bath to clean any impurity fragments that could be adhered to the surface. Once clean and dry, they were inspected under a stereomicroscope and those specimens free of impurities were selected.

Chapter 4 studies the effectiveness of biogenic calcium carbonate to remove dissolved lead. For this purpose, sepia cuttlebones (*Sepia officinalis*) and shells of bivalve (*Chlamys opercularis*) were selected. The cuttlebone of the cephalopod *Sepia officinalis* were collected in the bay of Lastres (Asturias, Spain) and is composed of aragonite, while the bivalve shell of *Chlamys opercularis* come from the Galician coast (Spain) and is composed of calcite. Both samples were ground in an agate mortar and sieved to separate the selected grain size fraction $125 < ø < 200$ μm. The samples were then cleaned by immersing in technical grade ethanol in an ultrasonic bath to remove any impurity fragments. Finally, they were washed with Milli-Q deionized water and then dried in an oven at 105°C for 12 h.

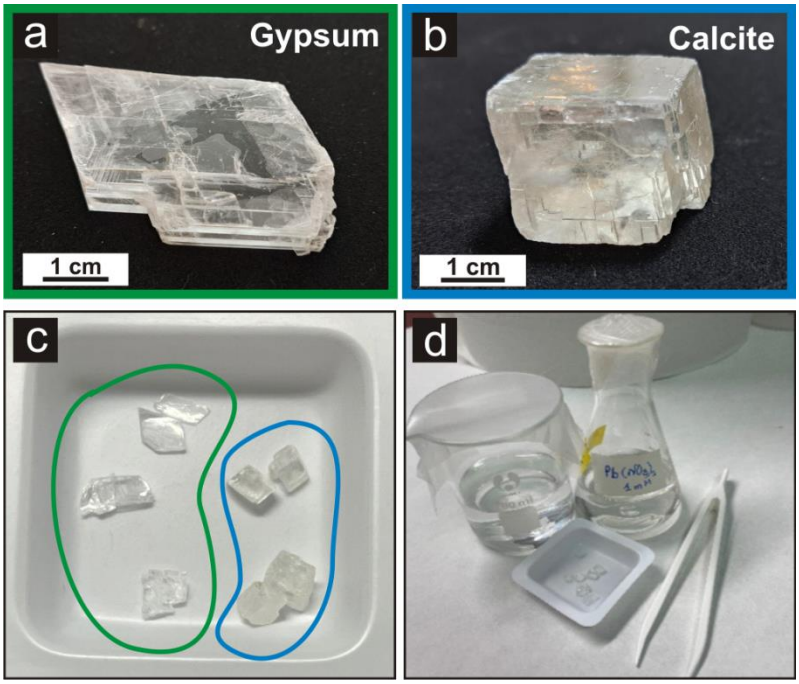

Figure 2.1. Calcite and gypsum single crystals used in the interaction experiments at room temperature. (c) Fragments of calcite (blue circle) and gypsum (green circle) (2-3 mm).(d) Pyrex Erlenmeyer flasks and beakers were experimets were performed.

2.1.2. Overview of experiments

The interaction experiments, carried out at room temperature and atmospheric pressure, involve the interaction of solid mineral samples (inorganic and organic) with Pb-bearing aqueous solutions. These solutions were prepared with the reagent-grade $Pb(NO_3)_2$, Panreac (Chapter 3) or Sigma Aldrich (Chapter 4) and high purity deionized water (MiliQ) (18 MΩ cm). Borosilicate glass beakers (VWR) were used to perform the experiments and were sealed with parafilm to avoid water evaporation during experiments. The experiments were also stirred at a constant speed for reaction times varying from a few minutes to ten days (Figure 2.2).

After the end of each experiment, the liquid phase was extracted by filtering with 0.45 μm nitrocellulose filters (Millipore, Ø = 0.45 μm). The recovered solid phases were dried at room temperature for further analysis.

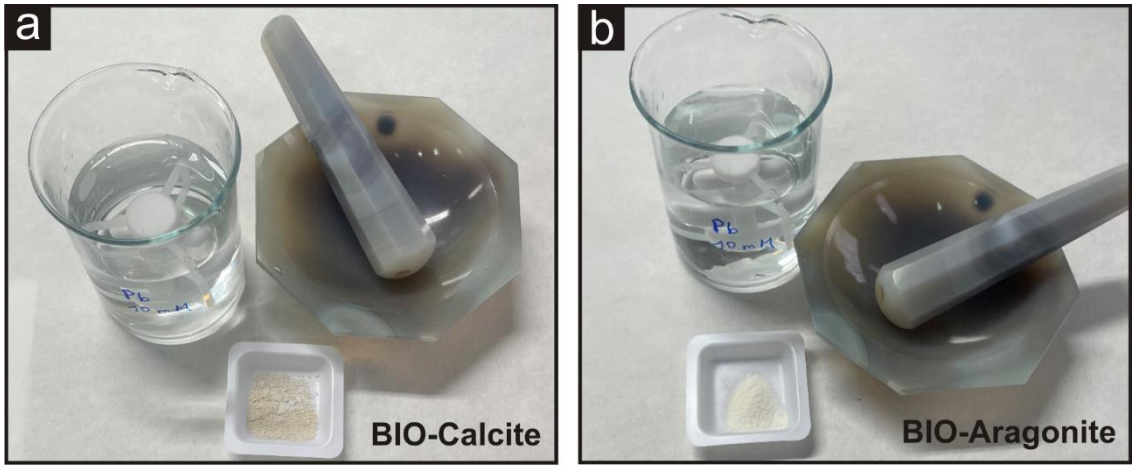

Figure 2.2. Biogenic calcium carbonate powder used in the interaction experiments at room temperature. (a) BIO-Calcite powder of Chlamys opercularis (Aequipecten opercularis) shells and (b) BIO-Aragonite powder of Sepia officinalis endoskeleton.

2.2. Hydrothermal experiments

The procedure conducted to study the interaction of calcium sulphates with phosphate-bearing solutions under hydrothermal conditions is described below (Chapter 5).

2.2.1. Preparation of Starting Solids

Chapter 5 studies the replacement of calcium sulphates (anhydrite) by calcium phosphates under hydrothermal conditions. In this system, anhydrite single crystals from Naica mine (Chihuahua, Mexico) were used. The anhydrite crystals were cleaved along (100), (010) and (001), to obtain anhydrite samples of similar size (3 x 3 x 3 x 3 mm). The selected crystals were cleaned in an ethanol bath, to remove surface impurities, and then were dried overnight in a silica gel desiccator at room temperature.

2.2.2. General description of experiments

Hydrothermal interaction experiments were conducted using propylene reactors, which were placed in stainless steel autoclaves (Figure 2.3). Four

anhydrite crystals were introduced into each reactor together with a 2 M phosphorus aqueous solution prepared with the reagent $(NH_4)_2HPO_4$ (Acros Organics) and high purity deionized water (MiliQ). The reactors were placed in preheated ovens at temperatures in the range between 120°C and 200°C for different reaction times between 2 and 72 h. After reaction, the solid samples were removed and washed with distilled water and dried overnight at 30°C in a thermostatic chamber.

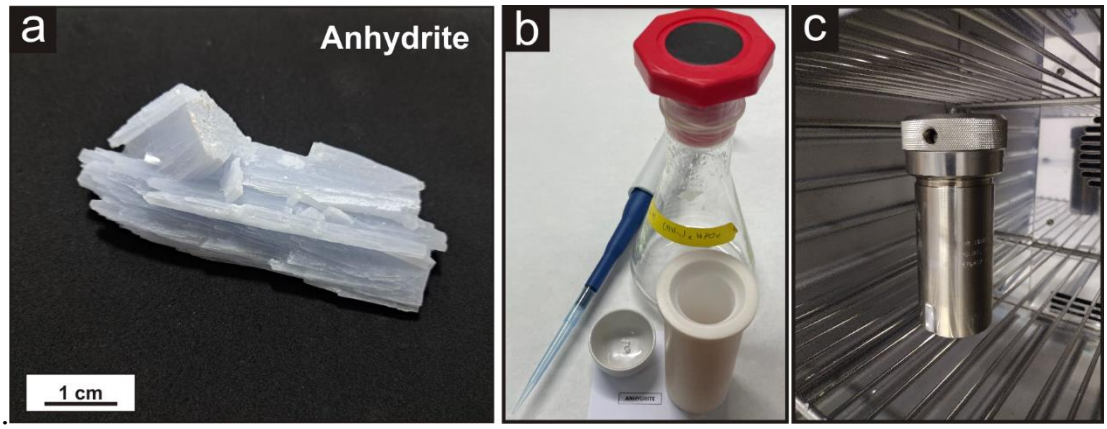

Figure 2.3. (a) Anhydrite crystal used in Hydrothermal experiments. (b) Pyrex Erlenmeyer flasks and Teflon reactors in which hydrothermal experiments were performed (c) Steel hydrothermal reactors in which the high temperature experiments were conducted.

2.3. Characterization of the liquid phase

In Ca-Pb-carbonates-sulphates and Ca-Pb-carbonates biogenic systems (Chapters 3 and 4) the chemical composition of the liquid phases was analyzed in order to quantify lead and calcium concentration in solution. In this thesis, the technique of induced coupled plasma mass spectroscopy was used to analayzed the aqueous solution. In addition, the pH evolution in the interaction experiments (chapter 3) was measured by a pH meter (pH Meter basic 20-CRISON).

2.3.1. Inductively Coupled Plasma Mass Spectroscopy (ICP-OES)

Inductively Coupled Plasma Mass Spectroscopy (ICP-OES) is an analytical technique used to determine and quantify in a sample most of the elements of the periodic table. It is based on the use of two methods, inductively coupled plasma and mass spectrometer, the first one generates ions and the second one separates and detects ions. The liquid sample is transformed into an aerosol through a nebulizer system by the action of argon (Ar) gas. Afterwards, this aerosol is ionized by applying an oscillating magnetic field induced by a high frequency current. The excited electrons of the ions resulting from this process emit light at specific wavelengths. The amount of light emitted is measured and used to calculate the concentration of the elements in the samples. Lead concentration was analyzed for the experiments included in chapter 3, with an Agilent MS 7700 spectrometer, and for the experiments in chapter 4 the liquid phase was analyzed using an Agilent Varian 700 ES spectrometer at the University of Bern, Switzerland.

2.4. Characterization of solid phases

Throughout this thesis, numerous techniques were used to characterize the solid samples. Before conducting the experiments, minerals and biominerals samples used as starting material were characterized by X-Ray Diffraction (XRD) (Chapters 3, 4 and 5), X-Ray Fluorescence (XRF) (Chapter 4), BET surface analysis (Chapter 5) and thermogravimetric analysis (TGA) (Chapter 4). After the completion of the experiments, reacted solid phases was characterized by XRD, their morphological characteristics were studied by scanning electron microscopy (SEM) and atomic force microscopy (AFM), and their chemical composition was analyzed using Raman spectroscopy. A brief description of each technique is described below.

2.4.1. X-Ray Diffraction (XRD)

X-ray diffraction (XRD) technique by powder method has been used to identify the crystalline mineral phases, both primary and secondary, involved in each system studied. In addition, in Chapters 4 and 5 the mineral phases were also quantified by performing Rietveld analysis of the diffractograms obtained by this technique. X-rays consist of electromagnetic radiation of high energy and small wavelength. A cathode ray tube generates X-rays that penetrates the solid sample and is diffracted by the atoms that compose the mineral. These diffracted X-rays are detected and processed. Each mineral has a set of unique d-spacings whereby samples can be compared to standard reference standards. All samples were ground in an agate mortar until obtain a homogenous powder. Diffraction data was collected by PANalytical Xpert Pro diffractometers using Cu Kα radiation (1.540598 Å). The range of 2θ angles as well as the step size varied for each system and are specified in the corresponding chapters.

2.4.2. Nitrogen physisorption (BET)

Chapter 4 studies Ca-,Pb- Biogenic carbonates system using two different biominerals with different textural and compositional characteristics. For this purpose, the textural characteristics of the biominerals were characterized by BET (Brunauer-Emmett-Teller) surface area analysis. The BET surface area was calculated by analysis of adsorption isotherms, obtained by physical adsorption of N_2 at -196°C in an ASAP 2020 volumetric adsorption system (Micrometrics).

2.4.3. Thermogravimetric analysis (TGA)

Thermogravimetric analysis quantifies mass variations as a function of time and temperature in a controlled atmosphere. This technique has been used to determine the average biopolymer content of the biominerals used in the

study of the Ca-, Pb-Biogenic carbonates system (Chapter 4). The analyses were carried out on a thermogravimetric analyzer that continuously measures the mass of the sample with increasing temperature from 25°C to 1000°C at a constant rate (5°/min). The analyses were conducted using the Mettler-Toledo TGA/SDTA851 thermogravimetric analyzer under oxygen atmosphere.

2.4.4. X-Ray Fluorescence (XRF)

X-ray fluorescence (XRF) is a spectroscopic technique used to determine the elemental chemical analysis of the samples used in the study of the Ca-,Pb-Biogenic carbonates system (Chapter 4). This technique uses the emission of secondary or fluorescent X-rays, which excite the atoms of the sample, so that each of them emits a characteristic energy. BRUKER S2 Ranger X-ray fluorescence spectrometer was used for these analyses

2.4.5. Raman Spectroscopy

One of the most specific molecular spectroscopic techniques for the determination of chemical composition is Raman spectroscopy. This technique is based on the interaction of light with matter (He-Ne laser, Ar laser, IR semiconductor laser, and diode laser). Light scattering is used to differente low-frequency modes such as vibrational and rotational modes, specific to each molecule. This technique was used in the Ca-Pb-carbonates and sulphates and Ca-phosphates-sulphates systems of Chapters 3 and 5, respectively.

Raman spectra were obtained with different equipment depending on the system studied. For the Ca-Pb-carbonates and sulphates system (Chapter 3) a microRaman BKTEK spectrophotometer equipped with an Ar laser, $\lambda = 532$ nm (green) was used. For the Ca-phosphates-sulphates system (Chapter 5), a JYVJobin Yvon equipment with a CDPS532-DPSS laser excitation source at 24.3

mW was used. This unit was connected to an Olympus BXFM-ILHS confocal microscope with a 100x objective.

2.4.6. Scanning Electron Microscopy (SEM)

Scanning electron microscopy (SEM) was used to acquire images of the crystals or crystalline aggregates formed during the experiments. This technique is based on the use of an electron beam, which scanning the surface of the sample. The electrons interact with atoms in the sample and a detector collects the amount of electrons sent to produce high-resolution images that allow to study the topography of the sample in detail and also its chemical composition. For the characterization of the samples, JEOL-6610LV scanning electron microscope with an energy dispersive X-ray coupled system (EDX, INCA Energy 350; Oxford Instruments) was used to obtain images and semi-quantitative analysis. All samples were imaged using secondary electrons and, in addition, the Ca-, Pb-Biogenic carbonates system was also imaged using backscattered electrons. All samples were coated with gold to make them conductive.

2.4.7. Atomic force microscopy (AFM)

Atomic force microscopy (AFM) is a technique that allows surface analysis of samples with nanometer or even atomic resolution. In contrast to scanning electron microscopy, it does not use electrons to generate images of the samples, but performs a piezoelectric scan of the surface, using a sharp tip located at the end of a flexible lever. The interaction between the tip and the sample surface is recorded by a photodiode detector that determines precise changes in oscillation and inclination of the tip. This technique allows the detailed study of the sample surface by accurately determining its topography. In this thesis, in situ AFM experiments were conducted with the Cypher ES©

atomic force microscope at the University of Bern. The images were recorded in tapping mode at 25°C using ultrahigh frequency tips (NanoWorld Arrow UHF-AuD). Measurements details are specified in chapter 4 (Ca-Pb-Biogenic carbonates System).

2.5. Data analysis

A series of scientific software were used to process the data, which are briefly described below.

X'Pert HighScore Plus: software used for the treatment of diffractograms obtained by X-ray diffraction. It was used for both the identification of mineral phases and Rietveld analysis.

Cypher Asylum (AMF): program used for processing images obtained by atomic force microscopy (AFM).

OriginPro 8: data analysis and graphical software. This program was used for all data processing, including graphics.

Crystal Maker: the projections of the crystalline structures were projected using this software, which allows the representation of crystalline morphologies.

PHREEQC Interactive: geochemical modeling program that can be used to perform calculations of speciation in aqueous solutions, saturation indices and kinetic aspects of dissolution reactions (Parkhurst and Appelo 1999). This software was used together with the minteq.dat and llnl.dat databases to model the aqueous solutions of the different systems studied in this thesis.

CHAPTER 3

Ca-Pb-Carbonates and Sulphates System

3. Ca-Pb-Carbonates-Sulphates System

3.1. Introduction

The quantity and the quality of available freshwater have been steadily declining over the last century in both industrialized and developing countries. Human activities like farming, mining, or manufacturing, which provoke the continuous rise of salinity and pollutant contents of freshwater in many sites worldwide overworld, are the main factors of this decline (Nriagu and Pacyna 1988; Zachara et al. 1991; Bradl 2005; Thevenon et al. 2011), as well as the adoption of new lifestyles by large groups of citizens in densely populated cities, which is responsible for the general increase of the drug and pharmaceutic contents in wastewaters. The current scenario of progressive climate warming, which sketches a future of groundwaters with increasing salinity, adds stress on the availability of clean fresh water supplies around the world (Khan et al. 2011).

Pb is a most hazardous heavy metal whose concentration in the atmosphere, soils, and waters underwent a striking worldwide increase during the 20th century associated with the development of the automobile industry and the generalized use of leaded gasolines until their banning in the 1980s (Hans von Storch 2004; Charlesworth et al. 2011). Other industrial activities like the production of ammunition, batteries, pigments, and certain glasses have also contributed anthropogenic Pb inputs to the hydrosphere and the biosphere (Chattopadhyay et al. 2003; Jang and Townsend 2003; Tukker et al. 2006; Obeng-Gyasi 2019; Hejami et al. 2020). Mining activities have contributed to the long-term release of Pb as a result of the interaction of large volumes of fine-grained Pb-ores exposed in tails with groundwaters and running waters (Oliver 1997; Audry et al. 2004; Mapanda et al. 2005; Zhuang et al. 2009; Khanam et al. 2020). Furthermore, most catastrophic emissions of Pb environments, which have

caused lasting damage in subaquatically and subaerially with great impact on soil fertility and productivity and wildlife diversity, have resulted from punctual wastewaters spills in mine sites and tails (Simón et al. 1999; Rodríguez et al. 2009; Li et al. 2014). Pb was the main component of plumbing instalments in worldwide households until the 1970s, after which the use of lead pipes rapidly declined in industrialized countries. Interestingly, Pb-related pollution of drinking water has become a hot topic in recent years as information on the relationship between the presence of lead-tainted water pipes in old buildings and high Pb contents being found in the blood and bones of children in deprived neighborhoods in industrialized countries has reached the news (Tukker et al. 2006; Laidlaw et al. 2016). Since Pb is potentially toxic to mammals, water pollution that results in excessive Pb intake often has dramatic impacts on human health, including long-lasting damage to the nervous, skeletal, circulatory, enzymatic, endocrine, and immune systems (Jung and Thornton 1997; Ryan et al. 2000; Tong et al. 2000; Zheng et al. 2007; Zhuang et al. 2009; Luo et al. 2012; Li et al. 2014). This damage is particularly dramatic in the case of sensitive populations, like children, pregnant women, and elderly people (Pirkle et al. 1998; Zheng et al. 2010; Njati and Maguta 2019; Piekut et al. 2019).

The bioavailability of dissolved Pb in natural environments is largely controlled by sorption processes that develop during the interaction between Pb-polluted waters and the surface of rock-forming minerals like calcite and gypsum, which are especially abundant in sedimentary basins as main constituents of limestones (calcite) and sulphate evaporitic deposits (gypsum) (Ma et al. 1993; Traina and Laperche 1999; Warren 2006). Sorption of pollutants by mineral surfaces can take place through different mechanisms, including adsorption, absorption, and surface precipitation (Sposito 1986; Brown et al. 1995a; Prieto et al. 2003; Pérez-Garrido et al. 2007). The first mechanism, adsorption, involves the bonding of the pollutant to the mineral surface by

chemical bonds that can be relatively strong, or through longer-range coulomb forces and/or hydrogen bonds. The second mechanism, absorption, requires the diffusion of the pollutant into the structure of the mineral. Absorption contribution to sorption is significant in the case of minerals like zeolites, whose structures contain large, interconnected channels that allow for ion exchange to occur at relevant rates (Dyer 1995). In contrast, under the temperature conditions reigning in surface and subsurface environments, the kinetics ion diffusion through carbonate and sulphate mineral structures is most sluggish and absorption contribution to sorption can be considered negligible. The third mechanism, surface precipitation, involves the co-precipitation of the pollutant which incorporates in the crystal structure of new mineral phase. This new phase forms through the chemical reaction between the pollutant and ions that are released to the fluid phase due to the dissolution of the primary mineral. This sorption mechanism commonly progresses by the development of coupled dissolution-crystallisation reactions. Coupled dissolution-crystallisation reactions are commonplace in surface and subsurface geological environments, where they affect primary mineral phases that can be highly soluble, like halite (NaCl), relatively soluble, like gypsum, or sparingly soluble (Putnis and Putnis 2007; Putnis 2009a; Pollok et al. 2011; Ruiz-Agudo et al. 2014), like leucite or wollastonite (Putnis et al. 2007; Ruiz-Agudo et al. 2012, 2016). Further evidence of the widespread nature of these reactions in natural environments have also been provided by a variety of macroscopic and microscopic experiments (Altree-Williams et al. 2015, 2019). In fact, coupled dissolution reactions that involve different sulphate and carbonate minerals are considered an effective long-term way of removing inorganic pollutants from natural water and wastewaters (Pina et al. 2000; Prieto et al. 2013; Wang et al. 2013; Morales et al. 2014) as well as reducing the increase atmospheric CO_2 (Sánchez-Pastor et al. 2007; Roncal-Herrero et al. 2017). Indeed, in situ AFM imaging has unraveled that coupled

dissolution–crystallisation reactions that involve calcite effectively remove pollutants like manganese (Pérez-Garrido et al. 2009), cadmium (Pérez-Garrido et al. 2007), lead (Di Lorenzo et al. 2020), phosphate (Wang et al. 2012a, 2012b), and chromate (Guren et al. 2020) from aqueous solutions. Similarly, coupled dissolution-crystallisation reactions that occur during gypsum-aqueous solution interaction can result in the sequestration of dissolved components like barium and strontium (Forjanes et al. 2020b), lead (Morales et al. 2013), arsenate (Rodríguez et al. 2008), phosphate (Pinto et al. 2009, 2010), and carbonate (Yu et al. 2019) through their immobilization in the structure of new phase.

Different authors have applied microscopic and macroscopic approaches to study the influence of the interaction of Pb-bearing fluids and common calcium-bearing carbonate and sulphate rock-forming minerals (namely, calcite, aragonite, gypsum, and anhydrite) in the fate of dissolved Pb in natural environments. This interaction has been addressed in numerous studies, most of which have been conducted at room temperature, using very fine-sized crystals (crystal size in the micrometer range), and considering circumneutral to slightly basic (pHi = 7–8) pHs as well as initial Pb ($[Pb_i]$) contents ≤ 1,000 ppm (Sturchio et al. 1997; Godelitsas et al. 2003; Elzinga et al. 2006; Rouff et al. 2006; Astilleros et al. 2010; Rangel-Porras et al. 2010; Morales et al. 2014). Some studies have assessed the long-term immobilization of Pb by calcium carbonate mineral surfaces conducting ageing experiments (Elzinga et al. 2006; Rouff et al. 2006). Recently, Di Lorenzo et al. (2019) conducted an in-depth analysis of the characteristics of Pb immobilization by calcite and aragonite surfaces.

Although gypsum and calcite often appear spatially and genetically associated in sedimentary basins, in our knowledge, all previous experimental studies of the interaction between Pb-bearing aqueous solutions and gypsum and calcite have been conducted considering these phases separately, forgetting

the fact that the dissolution of any of these Ca-bearing minerals can significantly alter physicochemical features of the aqueous solution like alkalinity, pH, or saturation state, thereby influencing the characteristics of the interaction of the fluid phase with the counterpart Ca-bearing mineral. Aiming to fill this gap, in this work we investigate the interaction of Pb-bearing aqueous solutions with gypsum and calcite, first separately and then simultaneously. We assess the degree of Pb removal from the liquid phase that is achieved depending on the solid phases involved in the interaction. Furthermore, in each case, we evaluate the relationship between the initial Pb concentration in the solution and the kinetics of the Pb removal. We focus our study on slightly acidic Pb-bearing aqueous solutions because acidic pHs are commonplace in running waters downstream Pb-bearing ore and mining sites. Our results evidence that more Pb becomes removed from the liquid phase when this simultaneously interacts with both gypsum and calcite than when the interaction only involves one of these phases. Apart from helping to better understand the fate of dissolved Pb in geological settings where sedimentary formations are predominant, taking this result into consideration might help to design more efficient strategies for decontaminating Pb-polluted waters through mineral coprecipitation processes.

3.2. Experimental Methods

Interaction experiments between gypsum and/or calcite natural crystals and Pb-bearing aqueous solutions (50 mL) equilibrated with atmospheric pCO_2 ($10^{-3.5}$ atm.) were conducted under ambient temperature conditions (~20–22°C). The Pb-aqueous solutions (1 and 10 mM) were prepared by dissolving reagent-grade $Pb(NO_3)_2$ (Panreac) in high purity deionized water (MiliQ) (18 MΩ cm). A set of experiments was carried out with 1 g of gypsum, calcite, or mixtures of gypsum and calcite (1:1) crystal grains with a relatively high size (average 3–4 mm) to avoid a fast dissolution of the primary minerals. To prepare these crystal

grains, large natural optically clear selenite-type gypsum crystals (Alameda de la Sagra, Toledo, Spain) and Iceland spar quality calcite crystals (Proaza, Asturias, Spain) were first crushed in an agate mortar, then sieved to the selected size range, and, finally, cleaned in an ethanol bath. Furthermore, the so-obtained crystal grains were inspected under a stereomicroscope Leica MZ75 (Leica microsystems) and impurity fragments were hand-picked and removed by using 50x magnification. Pb-bearing solutions and crystals were placed in a glass vessel. The system was then sealed with parafilm to avoid contact with the atmosphere and minimize evaporation. The aqueous solution was gently stirred (stirring rate < 60 rpm) along the duration of the experiment (from 5 min up to 96 h) by means of a magnetic stirrer. To avoid crystal fragmentation due to stirring-related impacts, a floating magnet was used. Additionally, further experiments carried out with mixtures of gypsum and calcite or with single calcite were made last, up to 7 days or 30 days, respectively, to assess the impact of long interaction times on Pb removal. Independent experimental runs were conducted for each initial physicochemical condition considered. Furthermore, experiments were run triplicate to confirm experimental reliability.

The pH of the Pb-bearing solutions was measured prior to the beginning of the experiments and immediately after the experiments were terminated using a digital pH-meter (pH Meter basic 20-CRISON). Initial pH values were 4.59 ± 0.05 for the solution with $[Pb]_i$ = 1 mM and pH = 4.42 ± 0.05 for the solution with $[Pb]_i$ = 10 mM. Samples of both the liquid and the solid phases were collected after experiments were terminated. The liquid phase was, then, first filtered through a 0.45 μm Millipore membrane and, afterwards, the concentrations of Pb and Ca were analyzed using an induced coupled plasma mass spectrometer (ICP-MS 7700 Agilent Technologies). The efficiency of the lead removal was expressed as the percentage of the initial concentration of Pb that had been eliminated from the solution ((($[Pb]_i$ - $[Pb]_f$)/$[Pb]_i$) x 100). The

evolution of physicochemical conditions in the system as the interaction between the lead-bearing aqueous solutions ($[Pb]_i$ = 10 mM and $[Pb]_i$ = 1 mM), equilibrated with atmospheric pCO_2 (SI_{CO2} = −3.3), and 200 mg of a calcite-gypsum mixture (50:50) progresses was modeled using the geochemical code PHREEQC (Parkhurst and Appelo 2013) and the minteq.dat database. The results of this modeling were used to interpret our observations.

The solid phase sample was immediately washed with ethanol and then dried overnight at room temperature. Afterwards, scanning electron microscope SEM, JEOL-6610LV (JEOL, Ltd., Akishima, Japan) imagining was used to identify dissolution features and newly formed phases on the surface of crystal grains. Energy-dispersive X-ray spectroscopy (EDX, INCA Energy 350; Oxford Instruments, Abingdon-on-Thames, UK) semiquantitative analyses on selected areas of the interacted samples provided information on the chemical composition of these newly formed phases. Raman spectra were collected from the surface of interacted crystals. Furthermore, in those experiments where precipitation from the bulk was observed, solutions were filtered after termination time and the recovered solids were also analyzed by Raman spectroscopy. All Raman spectra from 200 to 4000 cm^{-1} were obtained at room temperature on a microRaman BKTEK using as the excitation source the 532 nm line of an Ar ion laser and excitation times of 10 s. Powder X-ray diffraction (XRD) was used to identify the newly formed phases on the crystal surfaces and the precipitates from the bulk solution. Previously, interacted solid samples were powdered in an agate mortar. A PAN analytical X'Pert Pro diffractometer was used to collect the diffraction data from 5 to 80° 2θ using CuKα radiation with a step size of 0.02°. XRD patterns were processed with X'Pert HighScore Plus (PANalytical B.V.) software.

3.3. Results

The processes that take place during the interaction between Pb-bearing aqueous solutions and gypsum, calcite, or mixtures of gypsum and calcite crystals were studied by monitoring both chemical changes in the liquid phase and mineralogical changes in the solid phase in macroscopic batch experiments. Significant differences regarding the kinetics of both the dissolution of the primary phases and the precipitation of newly-formed Pb-bearing secondary phases are observed depending on (i) the initial Pb concentration ([Pb]i) and (ii) the solid phase(s) originally present in the system.

3.3.1. Chemical Evolution of the Liquid Phase

In all the experiments, the solution pH followed a similar evolution trend, which was characterized by a short initial period of marked pH increase that transitioned to an almost steady pH. This transition took place at different rates depending on the initial conditions, which determined that different final pHs were reached in the different experiments (Figure 3.1). Thus, when the Pb-bearing aqueous solution exclusively interacted with gypsum, the pH remained approximately constant (under the unavoidable analytical error), with values that were close to 5 along the whole duration of the experiments.

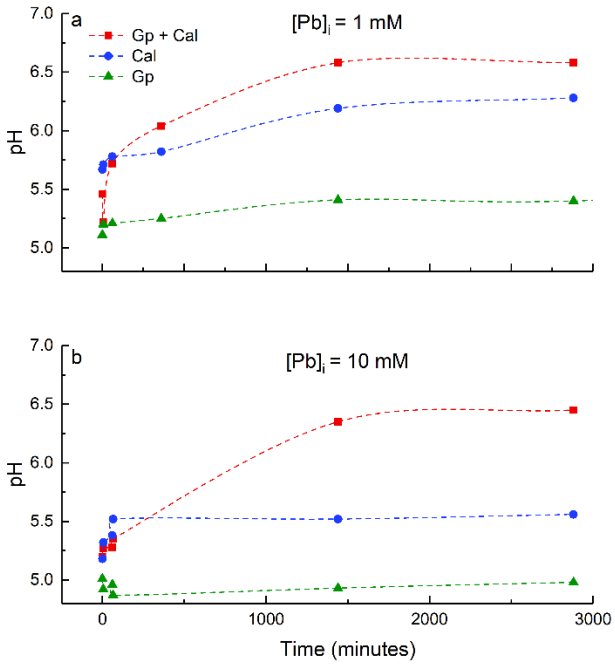

Figure 3.1. Evolution of the pH values during interaction of dissolved lead $[Pb]_i$ = 1 mM (a) and $[Pb]_i$ = 10 mM(b) with calcite (Cal), gypsum (Gp), and mixtures of both phases (Gp + Cal). The curves represent a modifier Bezier connection among the average values of three replicate experiments.

When the interaction took place with calcite, the initial pH increase was marked during the first minutes of the experiment. Afterwards, an asymptotic pH value (pHf = 5.6) was reached almost immediately when the interaction occurred with a solution with [Pb]i = 10 mM. In contrast, in the experiment where calcite crystals interacted with a solution with [Pb]i = 1 mM, the pH continued to slowly grow during the latest stages of the experiments, with the solution showing a pH_f = 6.3 at termination time (Figure 3.1).

The highest final pHs were found when Pb-bearing solutions simultaneously interacted with both gypsum and calcite crystals. In this case, an initial marked pH increase was also observed. This was followed by a steady slow pH increase to reach an asymptotic pH value ~24 h after the beginning of the experiment, with pH_f = 6.6 and 6.5 for solutions with $[Pb]_i$ = 1 and 10 mM, respectively.

Figures 3.2a and 3.3a depict the evolution of Ca concentration ([Ca]) along experiments. In all the cases, there was no Ca in the aqueous phase when experiments started ($[Ca]_i$ = 0). However, as experiments progressed, [Ca] underwent a progressive increase whose characteristics mainly depended on the mineral phase(s) involved in the interaction. Thus, when Pb-bearing aqueous solutions interacted with gypsum, [Ca] increased very rapidly to reach an asymptotic value after only 6 h interaction (see green line in Figures 3.2 and 3.3). This asymptotic [Ca] value was ~700 ppm in solutions with $[Pb]_i$ = 1 mM and 1000 ppm in solutions with $[Pb]_i$ = 10 mM.

When Pb-bearing aqueous solutions interacted with calcite crystals, [Ca] increased at a very slowly rate along the whole duration of the experiments to reach a value of ~45 ppm at termination time regardless of the $[Pb]_i$.

The evolution of [Ca] during the interaction with a 50:50 mixture of gypsum and calcite crystals closely resembled that observed during the interaction with only gypsum when $[Pb]_i$ = 1 mM, showing a very rapid initial [Ca] increase to reach a value close to 700 ppm after 6 h (Figure 3.3a). When $[Pb]_i$ = 10 mM, the interaction of the aqueous solution with gypsum and calcite led to a continuous [Ca] increase. This increase occurred faster during the first 6 h of the interaction to progressively slow down later on, leading to a [Ca] close to 1000 ppm at the experiment's termination time (48 h), without reaching a steady state (Figure 3.2a).

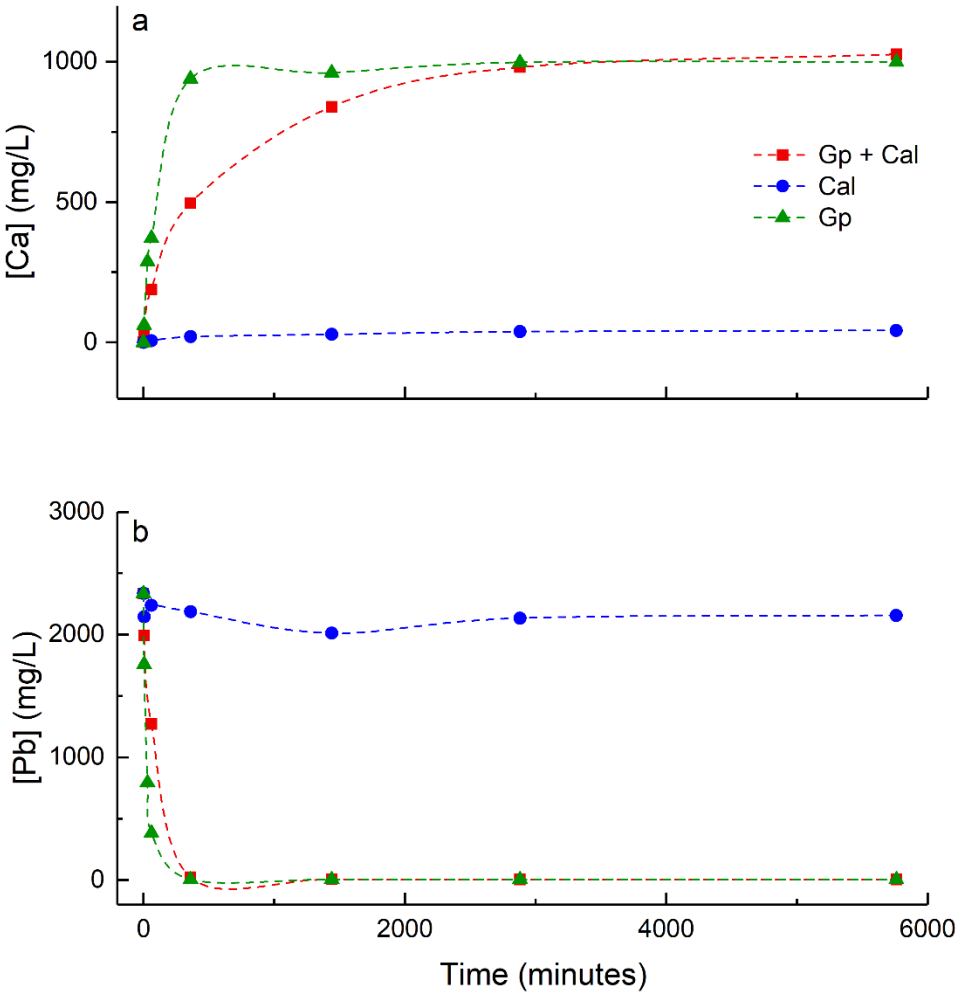

Figure 3.2. Evolution of Ca (a) and Pb (b) concentration as a function of time for interacton experiments carried out with [Pb]i = 10 mM. The drop in Pb concentratios (b) closely mirroris the release of Ca (a) to the aqueous solution when the latter interacts with gypsum (Gp). The interaction with calcite (Cal) leads to a very slow [Ca] increase (a) and [Pb] drop (b) in the aqueous solution. Finally, during the interacton wit mixtures of gypsum and calcite (Gp + Cal) [Ca] continues increase (a) after [Pb] drops to a steady value (b).

The evolution of [Pb] as the interaction progressed is depicted in Figures 3.2b and 3.3b. As can be seen, in all the experiments, a removal of Pb was observed, regardless of $[Pb]_i$ and the mineral phase(s) with which the solution interacted. However, the latter factor strongly influenced the extent of this removal. Thus, when the interaction took place with gypsum crystals, [Pb] rapidly dropped to reach a limit [Pb] value ~3–4 mg/L after 48 h regardless of

$[Pb]_i$. This limit value represented a Pb removal of ~98% for solutions with $[Pb]_i$ = 1 mM (Figure 3.3b) and ~99.8% for solutions with $[Pb]_i$ = 10 mM (Figure 3.2b). In contrast, when the interaction occurred with calcite crystals, both the characteristics of [Pb] evolution and the final concentration of Pb ($[Pb]_f$) in the solution strongly depended on $[Pb]_i$. Indeed, when the solution contained $[Pb]_i$ = 10 mM, its interaction with calcite resulted in a very limited Pb removal taking place during the experiment time framework. This Pb removal only reached 2132 ppm after 48 h of interaction and hardly increased with longer interaction times, reaching ~14% after 96 h, without showing further increase afterwards. Thus, even after 30 days of interaction the solution still contained $[Pb]_{30\ days}$ = 2012 mg/L (Figure 3.2b). When the aqueous solution contained a lower Pb concentration, $[Pb]_i$ = 1 mM, after 48 h of interaction with calcite crystal $[Pb]_{48h}$ = 34.2 mg/L, this meant that 84% of the Pb initially present in the solution had been removed. Further interaction resulted in further Pb removal, approaching 99% after 96 h ($[Pb]_{96h}$ = 2.4 mg/L) (Figure 3.3b), without reaching a limit [Pb].

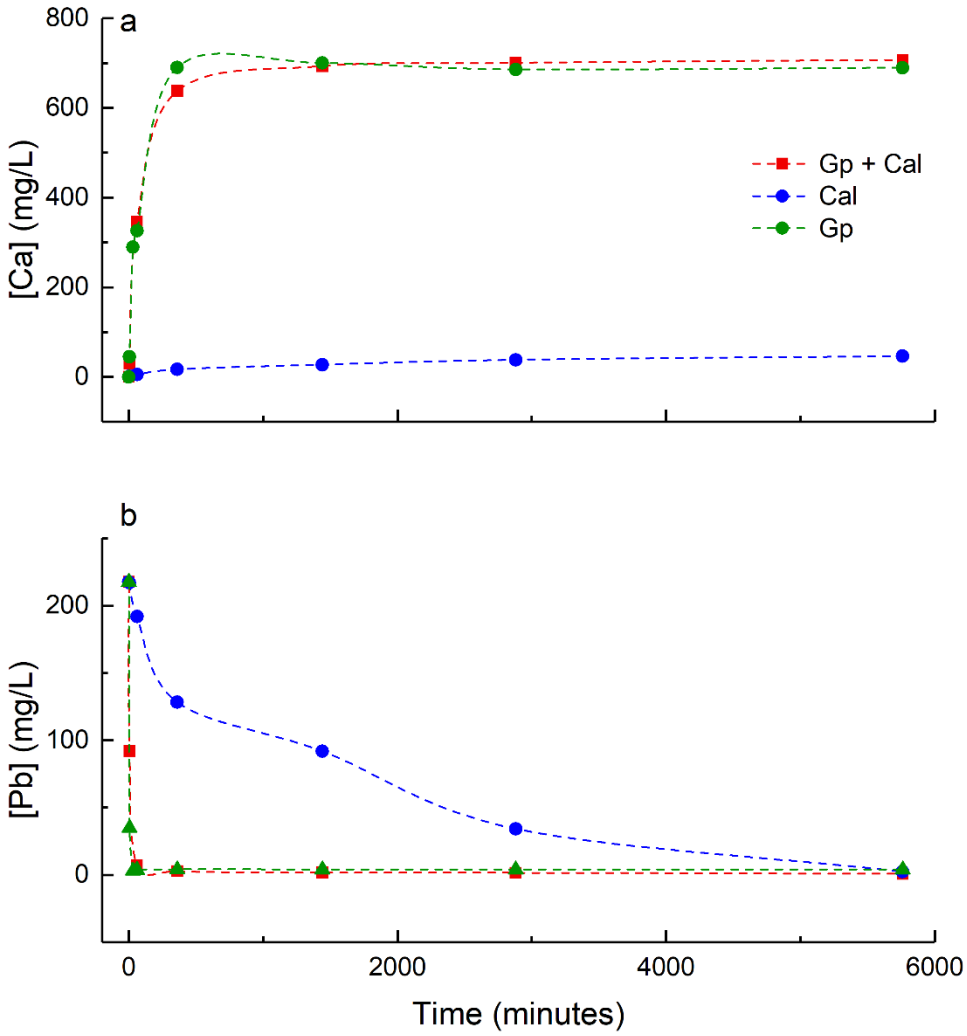

Figure 3.3. Evolution of Ca (a) and Pb (b) concentration as a function of time for interaction experiments carried out with $[Pb]_i$ = 1 mM. During the interaction with either gypsum (Gp) or mixtures of gypsum and calcite (Gp + Cal) the release of Ca (a) was closely mirrored by the removal of Pb (b) from the Pb-bearing solution. In contrast, during the interaction with calcite (Cal) [Ca] steadily increased at a very slow rate over the whole duration of the experiments (a), while [Pb] underwent a rapid drop during the first 48 h to continue slowly decreasing afterwards (b).

When the interaction of Pb-bearing aqueous solutions took place with mixtures of gypsum and calcite crystals, the characteristics of [Pb] evolution mirrored those observed during the interaction with only gypsum for both solutions with $[Pb]_i$ = 10 and 1 mM (Figures 3.2b and 3.3b). [Pb] underwent a very rapid drop during the first 24 h which resulted in a Pb removal of 99.3% from the solution with $[Pb]_i$ = 1mM and 99.8% from that with $[Pb]_i$ = 10 mM.

Further interaction led to a very slow increase in Pb removal. After 96 h, the solution with $[Pb]_i$ = 1 mM contained $[Pb]_{96h}$ = 0.7 mg/L, and this meant ~99.7% of its initial Pb content had been removed as result of the solution interaction with mixtures of gypsum and calcite. In the case of the solution with $[Pb]_i$ = 10 mM, a similar percentage of Pb removal (~99.9%) was reached after 7 days in contact with calcite crystals. Still, at this stage, the Pb content of the solution was relatively high ($[Pb]_{7d}$ = 1.9 mg/L).

3.3.2. Newly Formed Phases: Nature and Morphology

In all the interaction experiments, the formation of secondary phases was observed, regardless of $[Pb]_i$ and the solid phase(s) initially present in the system. When Pb-bearing aqueous solutions interacted with gypsum, a precipitate was observed to form in the bulk solution. Furthermore, tip imaging of the surface of interacted gypsum crystals also evidenced the formation of a precipitate (Figures 3.4a and 3.4b). Both precipitates were confirmed as anglesite ($PbSO_4$) by XRD and Raman analysis, respectively (Figures 3.5 and 3.6). The morphology of anglesite crystals formed on gypsum surfaces during the early stages of the interaction appeared elongated along the b-axis and showed a habit defined by flat surfaces that belonged to the pinacoid {001} and the rhombic prism {210}, as well as strongly stepped surfaces roughly parallel to (100) (Figure 3.4a). The latter surfaces appeared serrated and consisted of steps belonging to {210}. As the interaction progressed, anglesite crystals become lozenge-like, with their habit dominated by the pinacoid {001} and further bounded by much smaller {210} surfaces (Figure 3.4b).

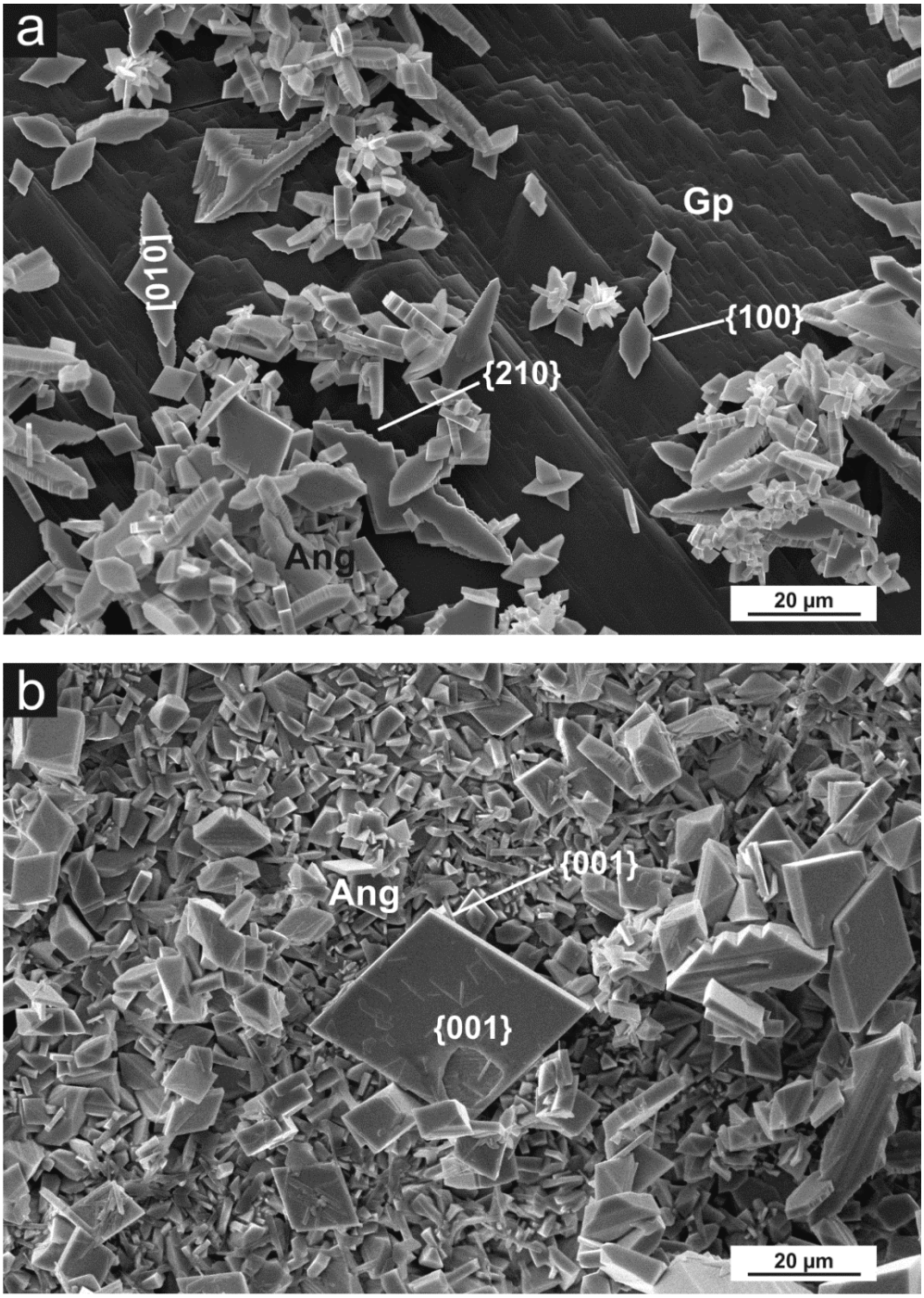

Figure 3.4. SEM micrographs of anglesite (Ang) formed on gypsum crystals (Gp) interacting with aqueous solutions with [Pb]i = 10mM. (a) After 5 min interaction, the development of dissolution features as well as the growth of anglesite crystals are observed on gypsum surfaces. Anglesite crystals initially growth elongated along the b-axis with a habit defined by flat surfaces that belong to the pinacoid {001}, the rhombic prism {210}, and stepped surfaces roughly parallel to (100). (b) After 24 h, gypsum surfaces become fully carpeted by anglesite crystals that show a habit dominated by platy faces belonging to the pinacoid {001} and smaller {210} forms.

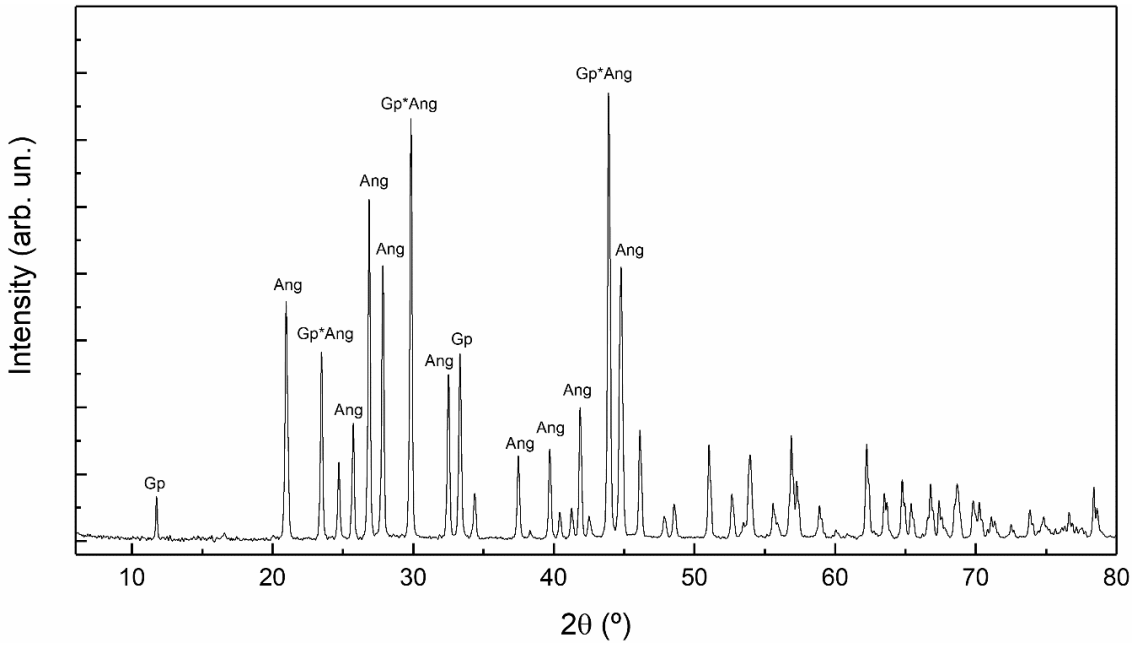

Figure 3.5. X-ray powder diffraction pattern of gypsum crystal interacting with a Pb-bearing solu-tions. All diffraction peaks can be assigned to gypsum (Gp) and anglesite (Ang).

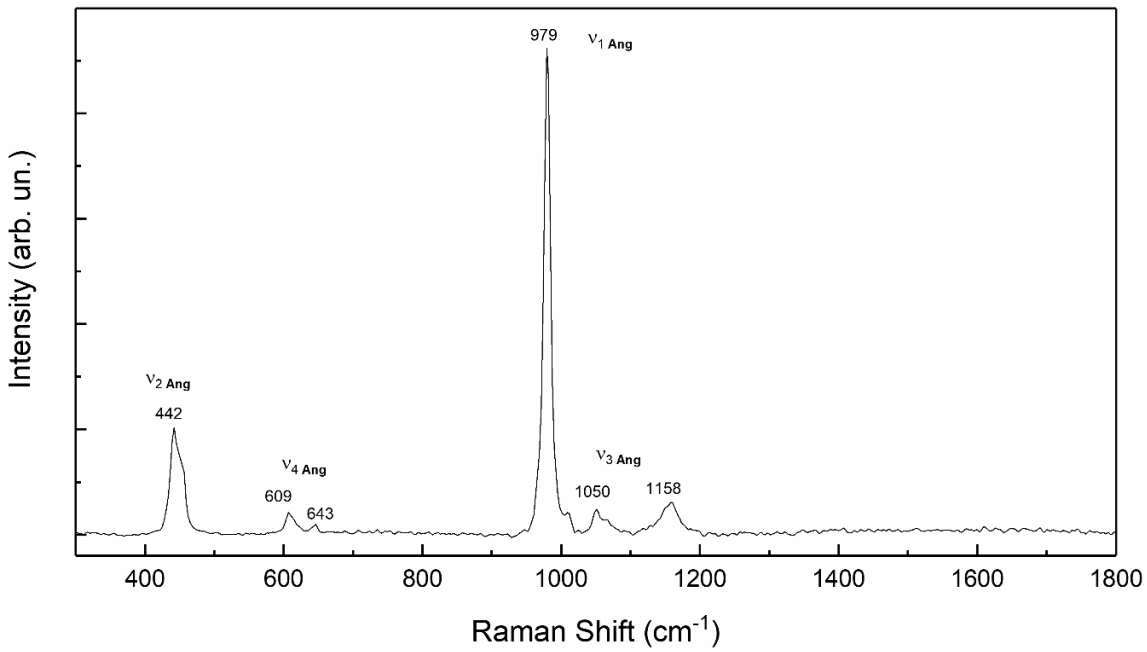

Figure 3.6. Raman spectra of the precipitate formed in the bulk of a Pb-bearing solution ([Pb]i = 10 mM) during its interaction with gypsum crystals. All bands can be assigned to the vibration modes of anglesite.

Different reaction pathways were observed during the interaction between Pb-bearing aqueous solutions and calcite crystals depending on $[Pb]_i$. When $[Pb]_i$ = 1 mM, SEM imaging calcite surfaces showed the formation of a precipitate that consisted of elongated prismatic crystals (Figure 3.7a). All peaks in the XRD pattern of these crystals matched well those of cerussite (PDF 5–417) (Figure 3.8a). A more complex precipitation behavior was observed when a solution with $[Pb]_i$ = 10 mM interacted with calcite. In this case, the precipitate that formed on the calcite surface consisted of two differently shaped types of crystals: Elongated prisms and hexagonal thin plates (Figure 3.7b). The X-ray diffraction pattern of this precipitate showed the main features characteristic of cerussite together to a small diffraction peak at 34.075 (2θ) whose location matched well that of the most important reflection (110) of hydrocerussite (PDF 13–131) (Figure 3.8b). Raman spectra of elongated prism-like crystals obtained in surface areas where they were the only newly formed phases showed the typical characteristics of cerussite (Figure 3.9). Taking into consideration the result of the X-ray diffraction analysis together with morphological criteria, the thin plate-like crystals were attributed to hydrocerussite.

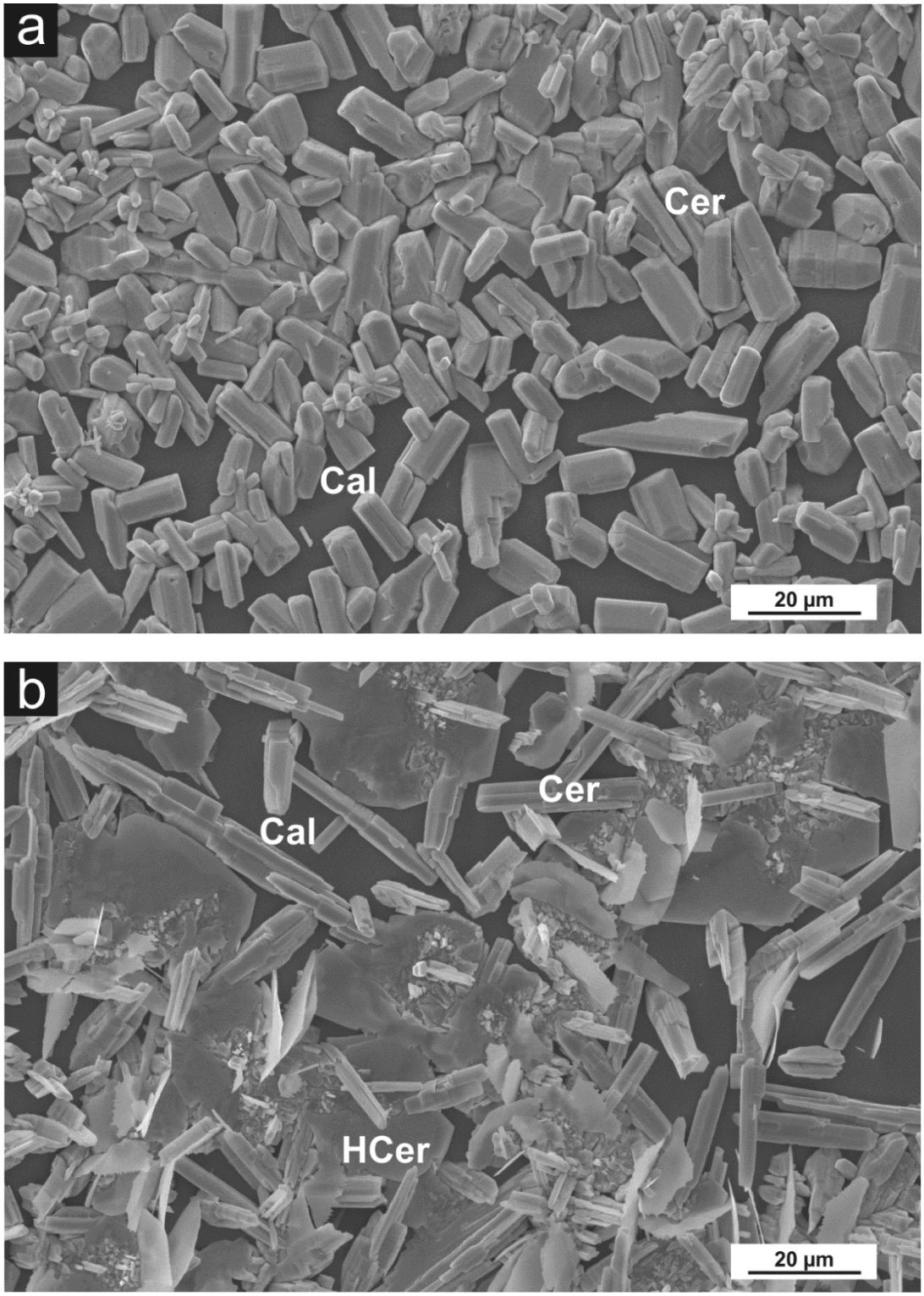

Figure 3.7. SEM micrographs of new phases formed after 24 h of interaction between Pb-bearing solutions and calcite crystals (Cal). (a) Cerussite (Cer) appears as prismatic crystals on calcite surface when calcite interacts with a solution with [Pb]i = 1 mM. (b) When the aqueous solution contains a higher Pb-bearing solution ([Pb]i = 10 mM), both prismatic cerussite (Cer) and hexag-onal plates of hydrocerussite (HCer) form on calcite surface.

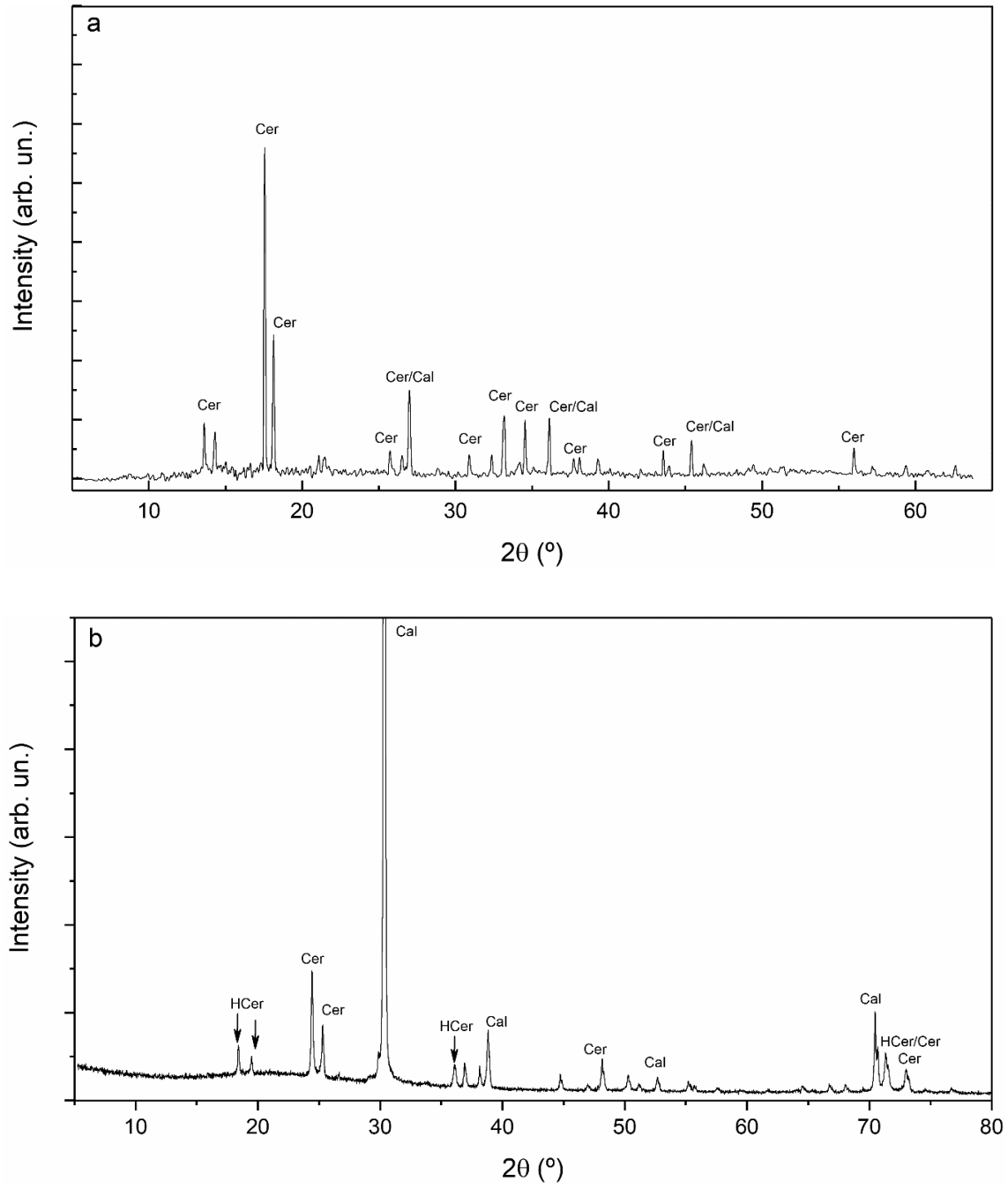

Figure 3.8. X-ray powder diffraction pattern of precipitates formed on calcite interacting with Pb-bearing solutions. (a) The main reflections of cerussite (Cer) are identified when the reaction takes places with a solution with [Pb]i = 1 mM. (b) Reflections that match well with hydrocerus-site (HCer) and cerussite (Cer) are identified in precipitates formed during the interaction be-tween calcite with solutions with [Pb]i = 10 mM.

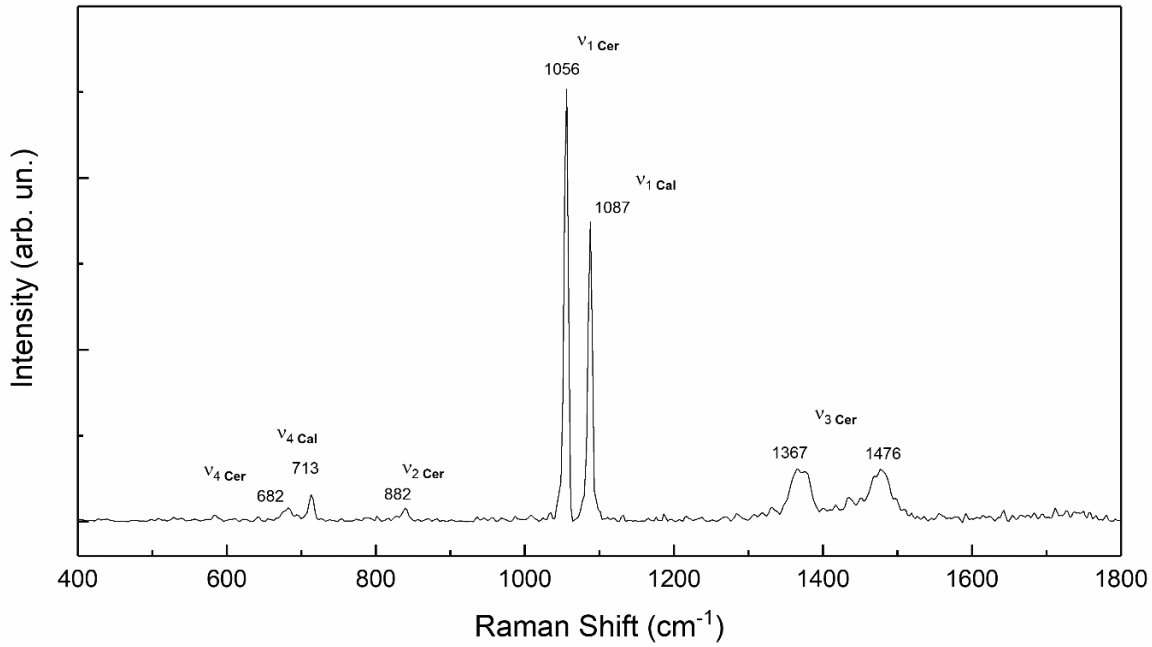

Figure 3.9. Raman spectra of the precipitate formed on a calcite crystal interacting with Pb-bearing solutions ([Pb]i = 1 mM). All bands can be assigned to vibration modes to either cerussite (Cer) or calcite (Cal).

Finally, an influence of $[Pb]_i$ in the nature of newly formed phases was also found during the interaction of Pb-bearing aqueous solutions with gypsum-calcite mixtures. This influence only regarded secondary phases that grew on the calcite surface, since anglesite was the only phase precipitated on gypsum surfaces regardless of $[Pb]_i$ (Figure 3.10). Thus, when $[Pb]_i$ = 1 mM (Figure 3.11 a), hydrocerussite formed on calcite surfaces. In contrast, the precipitate that formed when calcite interacted with a solution containing $[Pb]_i$ = 10 mM consisted of anglesite, hydrocerussite, and cerussite (Figure 3.11b). Furthermore, in the latter case, the relative abundance of these three phases changed as the reaction progressed: The precipitate mainly consisted of hydrocerussite, with a minor content of anglesite and a very minor content of cerussite during the first 5 min of the interaction. Afterwards, anglesite and hydrocerussite contents progressively decreased, and cerussite became the main component of the precipitate after 24 h. A detailed inspection of the distribution of the precipitate

on calcite surfaces evidenced a close spatial relationship between cerussite and hydrocerussite crystals, with most crystals of the former phase growing on the surface of hydrocerussite plates (Figure 3.11b). No morphological differences were observed between anglesite, cerussite, or hydrocerussite precipitated during the interaction of Pb-bearing solutions with gypsum-calcite mixtures or with gypsum or calcite crystals independently. It is worth noting that only anglesite crystals were observed to precipitate from the bulk solution when gypsum-calcite mixtures were used, regardless of $[Pb]_i$.

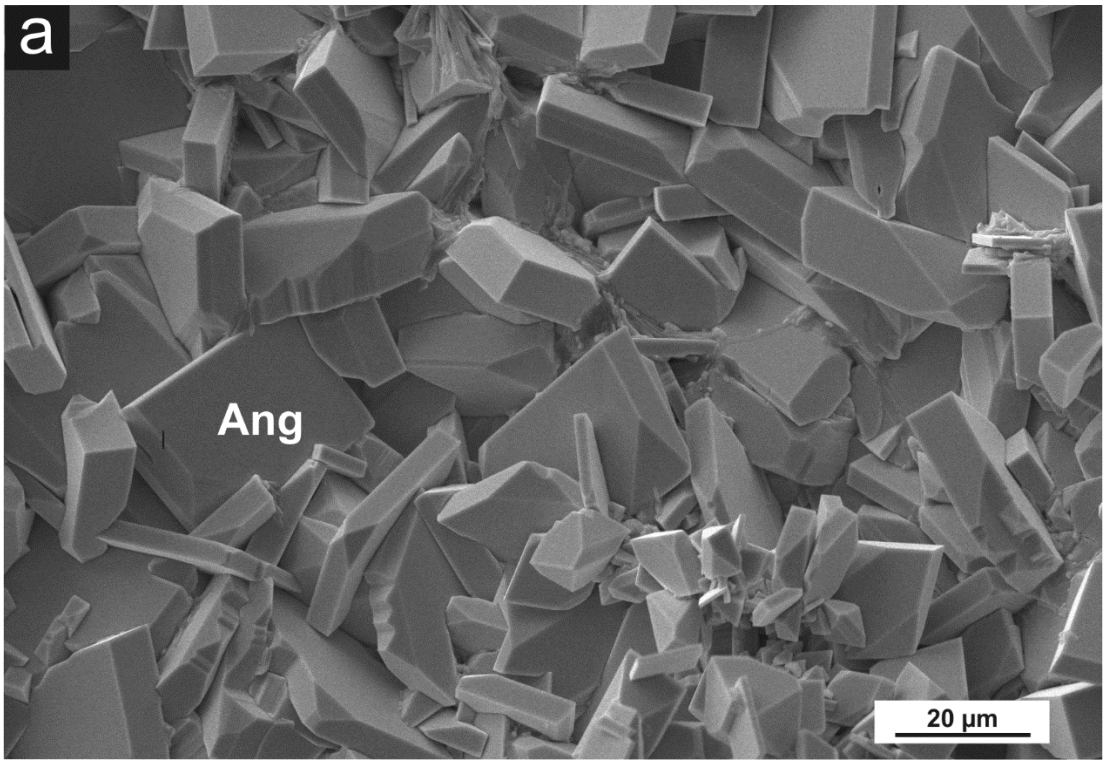

Figure 3.10. SEM micrographs of phases newly formed after 24 h of interaction between Pb-bearing solutions and mixtures of gypsum and calcite. A continuous layer of anglesite crystals (Ang) carpet gypsum surfaces interacting with solutions with [Pb]i = 10 mM.

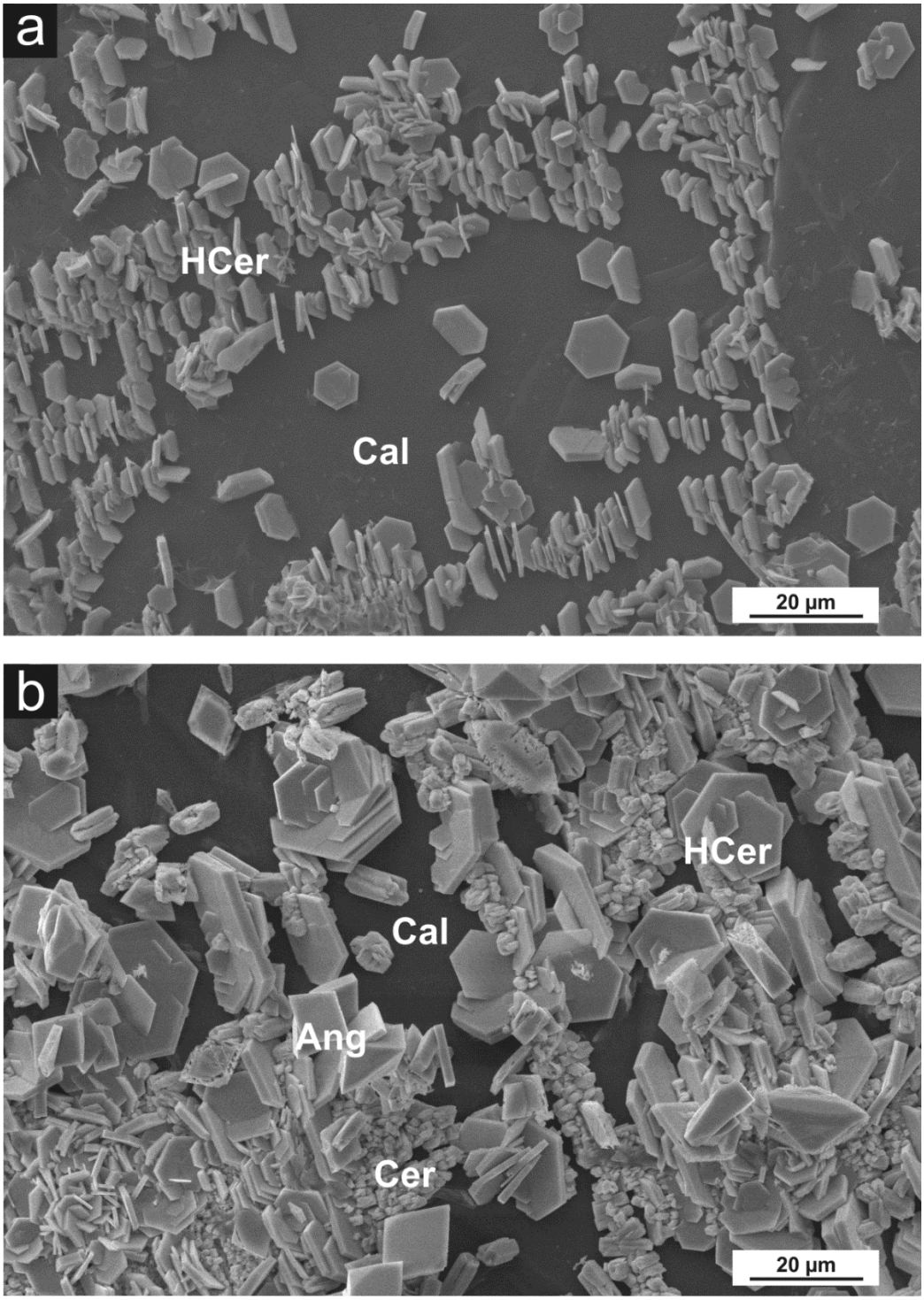

Figure 3.11. SEM micrographs of phases newly formed after 24 h of interaction between Pb-bearing solutions and mixtures of gypsum and calcite. (a) The sur-face of calcite crystals (Cal) interacting with solutions with $[Pb]_i$ *= 1 mM appears covered by discontinuous patches consisting of hydrocerussite (HCer). (b) The surface of calcite crystal interacting with solutions with* $[Pb]_i$ *= 10 mM appears covered by a discon-tinuous layer of closely intergrown hydrocerussite (HCer) plates and cerussite (Cer) prismatic crystals. A small number of anglesite (Ang) crystals can also be observed scattered on the sur-face.*

3.4. Discussion

3.4.1. Effectiveness of Gypsum as Pb Scavenger

As explained above, the interaction of aqueous solutions bearing Pb ($[Pb]_i \leq 2300$ mg/L) with gypsum crystals resulted in a fast and significant removal of Pb from the fluid, with $[Pb]_{48h}$ ~3 mg/L regardless of the value of $[Pb]_i$. Astilleros et al. (2010) and Morales et al. (2014) reported similar [Pb] drops in solutions that initially contained 1000 mg/L Pb after they interacted gypsum or anhydrite, respectively. According to these authors, [Pb] dropped due to the development of a dissolution-crystallisation process. Dissolution-crystallisation reactions have been invoked by different authors as the main mechanism responsible for the removal of different dissolved components from aqueous solutions interacting with gypsum crystals (Rodríguez et al. 2008; Astilleros et al. 2010).

This process started as soon as a Pb-bearing aqueous solution that was undersaturated with respect to either gypsum or anhydrite entered in contact with crystals of any of these phases. The dissolution of a calcium sulphate mineral, either gypsum, anhydrite, or the hemihydrated bassanite, released Ca^{2+} and SO_4^{-2} ions to the Pb-bearing liquid phase, whose supersaturation with respect to anglesite ($PbSO_4$) progressively increased. Eventually, the supersaturation threshold that allowed for the formation of anglesite nuclei was overcome and anglesite precipitated after reaction times shorter than 5 min regardless of the $[Pb]_i$ concentration (Astilleros et al. 2010). The precipitation of anglesite removed both SO_4^{-2} and Pb^{2+} ions from the aqueous solution and promoted further dissolution of the calcium sulphate phase. Further release of Ca^{2+} and SO_4^{-2} ions to the fluid promoted further anglesite precipitation, defining of a dissolution-precipitation loop that was operative to remove Pb from the

aqueous phase as long as the balance between calcium sulphate crystal dissolution and anglesite precipitation kept the system undersaturated with respect to the former phase and supersaturated with respect to the latter. The progress of the dissolution-precipitation reactions did not induce significant changes in the aqueous solutions pH. The final $[Pb]_f$ = 3 mg/L detected in the experiments by Astilleros et al. (2010) and Morales et al. (2014) as well as in this work derived from the solution being simultaneously equilibrated with anglesite and the initially present calcium sulphate phase. This value was directly related to anglesite solubility and, consequently, it represented the minimum [Pb] that could be achieved when anglesite precipitation was the main mechanism scavenging Pb from a Pb-bearing solution. This minimum [Pb] value (3 mg/L) was still 300 times too high to meet standard potability requirements for drinking water (10 μg/L), according to the World Health Organization and the European Community directive (Gray 2008). Therefore, although effective to rapidly remove large Pb amounts from aqueous solutions, the dissolution-crystallisation reaction that operated during the interaction of Pb-bearing solutions with gypsum (and other calcium sulphate rock-forming minerals) could only be considered as an initial step in a strategy for the decontamination of highly polluted waters, which would need to be implemented together with complementary Pb-uptake mechanisms if aimed at the production of drinking water, or even for treating mildly Pb-contaminated waters.

3.4.2. Effectiveness of Calcite as Pb Scavenger

Pb removal during the interaction of Pb-bearing aqueous solutions with calcite crystals occurred at a very slow rate compared to that observed when the interaction took place with gypsum. Thus, while in the latter case $[Pb]_{48h}$ approached 3 mg/L, a slower Pb-removal rate during the interaction with calcite resulted in $[Pb]_{48h}$ values that were well above 2000 and 100 mg/L for solutions

with $[Pb]_i$ = 10 and $[Pb]_i$ = 1 mM, respectively. Moreover, after 96 h of interaction with calcite, [Pb] still remained above 2000 mg/L in solutions with $[Pb]_i$ = 10 mM ($[Pb]_{96h}$ = 2155 mg/L), although it dropped to values below 3 mg/L in solutions with $[Pb]_i$ = 1 mM ($[Pb]_{96h}$ = 2.4 mg/L). The presence of cerussite and hydrocerussite crystals carpeting the surface of calcite crystals (Figures 3.7a and 3.7b) supported a dissolution-precipitation process as the main mechanism responsible for Pb removal during this interaction. As explained in the introduction section, dissolution-precipitation was the main operating mechanism that led to effective removal of a variety of dissolved pollutants from aqueous solutions interacting with calcite (Pérez-Garrido et al. 2007; Di Lorenzo et al. 2020; Guren et al. 2020). The dissolution-precipitation process that operated during the interaction of Pb-bearing solutions and calcite had similar characteristics to those of the gypsum dissolution-anglesite precipitation one described in Section 3.4.1. In contact with Pb-bearing aqueous solutions, calcite crystals underwent dissolution that resulted in the release of Ca^{2+} and CO_3^{-2} ions to the liquid. As the concentration of the released CO_3^{-2} ions mounted, the pH of the solution increased. Both factors determined that the threshold supersaturation for the nucleation of lead carbonate phases was rapidly overcome in the solution. At this point, a calcite dissolution-lead carbonate(s) precipitation feedback loop was established. This loop-operated pH evolved differently in solutions with different $[Pb]_i$, reflecting differences in the balance between the amount of CO_3^{-2} ions that were released to the liquid phase through calcite dissolution and the amount of both CO_3^{-2} and Pb^{2+} ions that became removed from it by precipitation of lead carbonates. In the case of calcite interaction with a solution with $[Pb]_i$ = 10 mM, higher supersaturation with respect to lead carbonates was reached, which resulted in a larger amount of lead carbonate precipitation and, consequently, larger depletion of CO_3^{2-} from the solution than would occur during the interaction of calcite with a solution with

$[Pb]_i$ = 1 mM. This larger CO_3^{2-} depletion from solutions with $[Pb]_i$ = 10 mM could explain that after an initial increase, pH rapidly reached a steady state value around 5.5. In contrast, the smaller CO_3^{2-} removal during the interaction of calcite with solutions with $[Pb]_i$ = 1 mM explained that the pH continued to slowly grow to approach values around 6.3 at the later stages of the interaction. The removal from the solution of

CO_3^{2-} ions was associated with the removal of the acidic Pb^{2+}, which added up to the explain the pH evolution in the latter. The impact of Pb^{2+} removal on the pH evolution was much less significant in solutions ($[Pb]_i$ = 10 mM) because in this case, the lead concentration remained very high during the whole duration of the experiments. Di Lorenzo et al. (2019) pointed out that a small increase in the pH of a solution bearing both lead and carbonate ions translated into a much higher increase of the solution supersaturation with respect to hydrocerussite than with respect to cerussite. According to this, one would expect that hydrocerussite was formed in experiments conducted with an aqueous solution with $[Pb]_i$ = 1 mM. However, this was not the case. The formation of hydrocerussite together with cerussite was observed when calcite interacted with solutions with $[Pb]_i$ = 10 mM. However, despite the higher pH increase undergone by solutions with $[Pb]_i$ = 1 mM during the interaction, only cerussite formed in this case. A plausible explanation for this was that most Pb removal from solutions with $[Pb]_i$ = 1 mM took place during the first 24 h of interaction, while pH solutions values remained below 6.

The kinetics of Pb removal is defined by the balance between the rate of the two reactions involved in the calcite dissolution-lead carbonate(s) precipitation loop. Both cerussite and hydrocerussite are very sparingly soluble phases ($pK_{cerussite}$ = −13.13; $pK_{hydrocerussite}$ = −17.46) (Parkhurst and Appelo 2013), which means that higher departures from equilibrium can result in the system

during the interaction with calcite than during the interaction with gypsum (Prieto et al. 1993, 1994). In other words, the release of the same amount of Pb^{2+} ions to the solution led to far larger supersaturation changes with respect to lead carbonates than with respect to anglesite. However, in the time scale of the experiments in this work, precipitation of anglesite more efficiently removed Pb from a Pb-bearing solution interacting with gypsum than the formation of cerussite and hydrocerussite did when this solution interacted with calcite. Reaching slightly larger Pb removals through lead carbonate precipitation requires far longer interactions of Pb-bearing solutions with calcite. The comparison of the variation of [Ca] in Pb-bearing solutions during their interaction with gypsum or calcite illustrates the overwhelming difference between gypsum and calcite dissolution rates (Figures 3.2a and 3.3a), which has been contrasted by numerous macroscopic and microscopic studies (Godelitsas et al. 2003; Elzinga et al. 2006; Astilleros et al. 2010; Yuan et al. 2016; Di Lorenzo et al. 2019). Calcite dissolves much more slowly than gypsum. Consequently, the release of carbonate ions to the liquid phase that resulted from calcite dissolution took place much more slowly than the release of sulphate ions due to the dissolution of gypsum, which completely overbalanced the faster Pb-removal that could be expected from the precipitation of more insoluble phases like cerussite and hydrocerussite compared to the precipitation of anglesite. Nevertheless, it is interesting to note that during the experiments of interaction between Pb-solutions and calcite crystals in the work, more Pb^{2+} was removed from the solution than Ca^{2+} was released to it. Since calcite dissolution was congruent, this unbalance could imply that there was some CO_2 atmospheric input leading to the formation of lead carbonate phase(s) and/or other Pb-uptake mechanisms than coprecipitation, such as Pb absorption and adsorption on calcite surfaces, were also operating and contributing to the net Pb removal.

From the results in this work, a scarce effectiveness of the interaction with calcite crystals to remove Pb from Pb-bearing aqueous solutions can be concluded. This contrasts with the conclusions reported by Godelitsas et al. (2003). These authors reported a drop of the Pb concentration of solutions bearing 10 to 1000 mg/L Pb to values below the experimental detection limit after 16 h of interaction with calcite crystals. The size of the calcite crystals used in both studies might be in the basis of the very different conclusions reached in both works. Godelitsas et al. (2003) conducted interaction experiments with 100–200 micrometer-sized calcite crystals. Calcite crystals in this work were 3–4 mm-sized. The larger crystal surface area exposed to the interaction with the Pb-bearing aqueous solution of the former may have resulted in a significantly faster release of calcium and carbonate ions to the liquid phase, which would have allowed for a faster mounting of the supersaturation of the Pb-bearing solution with respect to lead carbonate phases. This faster supersaturation rate and reached supersaturation actual value could have facilitated the formation of significantly larger amounts of cerussite precipitates and, thereby, larger Pb-removals than observed in this work. Moreover, the larger surface area of smaller-sized crystals could also have provided more sites for other sorption mechanisms to operate. These other sorption mechanisms could have further contributed to the larger balance of scavenged Pb reported by Godelitsas et al. (2003).

3.4.3. Effectiveness of Gypsum + Calcite as Pb Scavenger

Regardless of $[Pb]_i$, the interaction of Pb-bearing aqueous solutions with gypsum and calcite mixtures rapidly resulted to drops in [Pb] that closely paralleled those observed when the interaction took place only with gypsum (Figures 3.2b and 3.3b). In the latter experiments, a [Pb] ~3 mg/L was reached after 48 h interaction regardless of $[Pb]_i$. In the case of calcite-gypsum mixtures,

the same [Pb] was also reached after 48 h for solutions with $[Pb]_i$ = 1 mM and after 96 h when $[Pb]_i$ = 10 mM.

However, the interaction with calcite-gypsum mixtures resulted in larger Pb removals than those attained in experiments using only gypsum (and, obviously, using only calcite) when longer interactions were considered. The minimum [Pb] reached through the interaction with gypsum and calcite mixtures in the time set of experiments in this work was 1.9 mg/L in a solution with $[Pb]_i$ = 10 mM, 0.7 mg/L in a solution with $[Pb]_i$ = 1 mM, and after 7 days' interaction. The acidic conditions (pH < 5.6) at the beginning of all the experiments promoted the dissolution of the pristine minerals. Gypsum dissolution was a transport-controlled reaction (Berner 1980) which occurred at a significantly faster rate than the dissolution of calcite. This fact together with the relatively high solubility of gypsum explained that anglesite precipitation not only took place on gypsum surfaces but also occurred on calcite surfaces and in the bulk solution. Thus, the presence of anglesite crystals on the surface of both interacted gypsum and calcite crystals, together with the similarity between the [Pb] evolution curves in these experiments and those conducted with only gypsum crystals, supported the interpretation that the precipitation of anglesite was main reaction responsible for the fast [Pb] drop to approach [Pb] ~3 mg/L, during the first 48 and 96 h in solutions with $[Pb]_i$ = 1 and 10 mM, respectively. However, as these Pb-bearing solutions became equilibrated with gypsum and anglesite, anglesite precipitation could no longer occur. Further Pb removal mainly took place due to the precipitation of lead carbonates, most likely in the boundary layer around calcite crystals since these phases were only observed to form on calcite surfaces. During the interaction with gypsum and calcite mixtures, a similar pH evolution was observed in both Pb-bearing aqueous solutions; that with $[Pb]_i$ = 1 mM and that with $[Pb]_i$ = 10 mM (Figure 3.1). Furthermore, in both cases pH values above 6 were reached after relatively short

reactions times. This explained the formation of hydrocerussite on calcite surfaces regardless of $[Pb]_i$. This phase was not observed to form from solutions with $[Pb]_i$ = 1 mM that interacted only with calcite, whose pH remained below 6 at the beginning of the experiment, as discussed in Section 3.4.2. Once lead carbonate precipitation became the main Pb removal operating mechanism, Pb removal slowed down. This slowdown was observed at latter stages of the interaction, when the slow calcite dissolution became the rate limiting process defining the kinetics of the calcite dissolution-lead carbonate precipitation feedback loop. This slowdown that occurred was more marked and occurred earlier when gypsum and calcite mixtures interacted with solutions with $[Pb]_i$ = 10 mM. A possible explanation for this slowdown could relate to significant Pb adsorption taking place on calcite surfaces that resulted in calcite dissolution inhibition.

CHAPTER 4

Ca-Pb-Biogenic Carbonates System

4. Ca-Pb-Biogenic Carbonates System

4.1. Introduction

The volume of soils and groundwater contaminated by heavy metals due to industrial activities such as pharmacy, nuclear, chemical and battery manufacturing steadily has increased over the past century (Hassaan et al. 2016). Moreover, water pollution by heavy metals in abandoned mines and accidental spillages has generated important environmental damages and threatened drinking water supplies in numerous countries around the world (Tong et al. 2000; Li et al. 2014). In recent years, a variety of methods such as coagulation and flocculation, electrocoagulation, electrolysis and electro-deionization has been applied to decontaminating heavy metal-polluted waters (Johnson et al. 2008; Al Aji et al. 2012; Peng et al. 2014; Lu et al. 2015). Most of these methods are efficient, but they also are costly energy, which makes them unfeasible for the economies of those countries with the most important problems of heavy metal contamination. In this scenario, the design of cheap, efficient strategies for decontaminating heavy metal polluted water is essential (Oller et al. 2011; Howells et al. 2013; Crini and Lichtfouse 2019; Guo et al. 2021).

Among heavy metals, lead is one of the most hazardous for the environment and poses the most serious risks to human health as it can damage the circulatory, nervous, endocrine and immune systems of the human body (Zhuang et al. 2009; Li et al. 2014). Furthermore, due to its mutagenic, teratogenic and carcinogenic potential, Pb is especially dangerous for vulnerable groups, such as children, pregnant women and the elderly (Jung and Thornton 1997; Ryan et al. 2000; Tong et al. 2000; Zheng et al. 2007, 2010; Luo et al. 2012; Hassaan et al. 2016; Piekut et al. 2019). It has been demonstrated that the mobility of Pb in the environment can be controlled by its interactions with mineral surfaces

through different sorption mechanisms (absorption, adsorption, and surface precipitation) (Fulghum et al. 1988; Sturchio et al. 1997; Godelitsas et al. 2003; Rouff et al. 2004, 2005, 2006; Elzinga et al. 2006; Astilleros et al. 2010; Morales et al. 2014; Yuan et al. 2018; Di Lorenzo et al. 2019; Roza Llera et al. 2021; Fiorito et al. 2022). Different authors have demonstrated that the interaction between Pb polluted waters and calcium carbonate polymorphs calcite and aragonite leads to the precipitation of Pb – carbonate and Pb removal from the liquid phase (Godelitsas et al. 2003; Du et al. 2011; Zhou et al. 2017; Yuan et al. 2018; Di Lorenzo et al. 2019, 2020; Roza Llera et al. 2021). Most of these studies have been conducted using calcite and aragonite samples of abiogenic origin (Stipp et al. 1997; Chada et al. 2005; Elzinga et al. 2006; Pérez-Garrido et al. 2007, 2009; Yuan et al. 2016). Despite obtaining very promising results, few studies have been focused on exploring the potential of biogenic $CaCO_3$ materials (BIO-$CaCO_3$ hereafter) as heavy metal scavenger (Köhler et al. 2007; Alidoust et al. 2015; Zhou et al. 2017). Recent studies show that BIO-$CaCO_3$, such as marine shells, eggshells, sepia cuttlebone, etc., widely outperform inorganic $CaCO_3$ taking up heavy metals from polluted waters with triple efficiency (Zhou et al. 2017; Lee et al. 2018; Nkutha et al. 2021). The fact that main waste products of the mariculture industry like shells of bivalves or cuttlebones of cephalopods are BIO-$CaCO_3$ of problematic disposal strengthens the interest of using these materials as toxic elements scavengers. Up to now, only a small fraction of these wastes are being recycled in the production of fertilisers and as animal food additives (Arvanitoyannis and Kassaveti 2008). It is, therefore, worth exploring the heavy metal decontamination strategies based on the use of readily available BIO-$CaCO_3$.

Most biogenic calcium carbonates are hierarchically-structured composite materials that comprise two intimately interlinked components: pliant polymers (up to 10 wt%) and hard, brittle minerals (≥ 90 wt%)

(Lowenstam and Weiner 1989). The mineral component mainly consists of nanoparticulate calcite and/or aragonite, which appear arranged in mineral units with definite textures and microstructures (Berman et al. 1993; Weiner and Dove 2003; Checa et al. 2007, 2016, 2018; Lee et al. 2008; Harper et al. 2009; Kim et al. 2016). The biopolymers are complex assemblies of polysaccharides, proteins, glycoproteins and glycosaminoglycans, which form a network of fibrils surrounding BIO-$CaCO_3$ mineral units. The texture and microstructure of biominerals as well as the composition and distribution of its biopolymers are species-specific and can even vary between different parts of the hard tissue (Addadi and Weiner 1992; Checa et al. 2016).

In this work we study the uptake of Pb^{2+} by the surface of two highly BIO-$CaCO_3$ materials, the shell of the bivalve *Chlamys opercularis (Aequipecten opercularis)*, which is composed of calcite (BIO-CAL), and the cuttlebone of the cephalopod *Sepia officinalis,* which is composed of aragonite (BIO-ARG). Both species are popular seafoods whose hard tissues constitute important waste products from fishery, aquaculture and canning industries. *Chlamys opercularis (Aequipecten opercularis)* is an important fishery in North-Atlantic European countries, including UK, Ireland, France, Norway, and Spain, where annual landings are well over 30,000 tons (Duncan et al. 2016). Similarly, *Sepia officinalis* is among the commercially most important species of cephalopod, constituting an appreciated fishery resource in Northeast Atlantic and Mediterranean waters (Belcari et al. 2002; Royer et al. 2006). Total annual landings of *Sepia officinalis* in the English Channel between 2015 and 2020 ranged from 8.9-12.6 to thousand metric tons (Laptikhovsky et al. 2023).

Aiming to evaluate the efficiency of Pb uptake by BIO-$CaCO_3$ materials, we conducted batch experiments in which micrometer-sized fragments of the bivalve shell and the cephalopod cuttlebone were interacting with an acidic

solution containing Pb. The X-ray diffraction and scanning electron microscopy analysis of the interacted samples allowed characterization of the nature and distribution of newly formed phases. *In situ* atomic force microscopy (AFM) observations of the BIO-ARG surface nanotopograhy in contact with water and a Pb-bearing aqueous solution provided information about the surface evolution in the course of Pb-carbonate precipitation. The results of Pb^{2+} uptake by BIO-CAL and BIO-ARG reported herein are compared to previously published data on Pb^{2+} sorption on the surface of geologic calcite and aragonite crystals. Differences in the Pb^{2+} scavenging capacity of BIO-CAL, BIO-ARG and abiogenic carbonate minerals are interpreted on the basis of structural considerations, thermodynamic solubility, surface reactivity and dissolution kinetics. The conclusions derived from this work provide clues that might help to optimise the use of BIO-$CaCO_3$ material for remediation of water contaminated with heavy metals within the framework of a circular economy that promotes the recycling of waste materials, allowing for a reduction in the extraction of natural resources.

4.2. Experimental section

4.2.1. Materials

Two different calcium carbonate hard tissues composed of calcite (BIO-CAL) and aragonite (BIO-ARG) were selected for this study: the calcitic shell of the scallop *Chlamys opercularis (Aequipecten opercularis)* and the aragonitic cuttlebone of the cephalopod *Sepia officinalis.* The microstructure of these biogenic materials is quite different: like other bivalves, the shell of scallop consists of three superposed layers built up of long, tabular, lath-like calcite crystals defining a foliated microstructure (Popov 1986; Checa et al. 2016, 2019). Mineral units in the shell *Chlamys opercularis (Aequipecten opercularis)* are encased

by very thin (20 - 50 nm) organic membranes and occlude finer fibril networks of biopolymers (Checa et al. 2019). Sepia cuttlebone is an oval, flattened endoskeleton, whose main structural elements are septa and walls/pillars (Griesshaber et al. 2023). These elements are arranged in a carpark structure that comprise chambers enclosed by septa and internally subdivided by walls/pillars (Florek et al. 2009; Checa et al. 2015). The crystal units that built up Sepia cuttlebone are encased by biopolymer membranes (Figure 4.1), which can be as thick as 500 nm, and occlude fine, foam-like networks of fibrils (Griesshaber et al. 2023). Samples of both skeletons were collected from the Cantabrian Sea (North Spain) (Figure 4.2). X-ray Fluorescence (XRF) (Bruker S2 Ranger) shows that both mineral components both BIO-CAL and BIO-CAL are almost pure $CaCO_3$, with minor amounts of Mg and Sr (0.12 wt.% Mg and 0.17 wt.% Sr in BIO-CAL and 0.13 wt.% Mg and 0.17 wt.% Sr BIO-ARG). Each sample was ground using an agate mortar and sieved to separate the selected grain size fraction $125 < ø < 200$ μm. Powdered samples were then cleaned by immersing them in technical grade ethanol (94% isopropanol) in an ultrasonic bath during 10 min. This procedure was repeated three times. Afterward, samples were washed with high purity deionized water ($ϱ > 18$ MΩ·cm) and then dried for 12 h in an oven at 105°C.

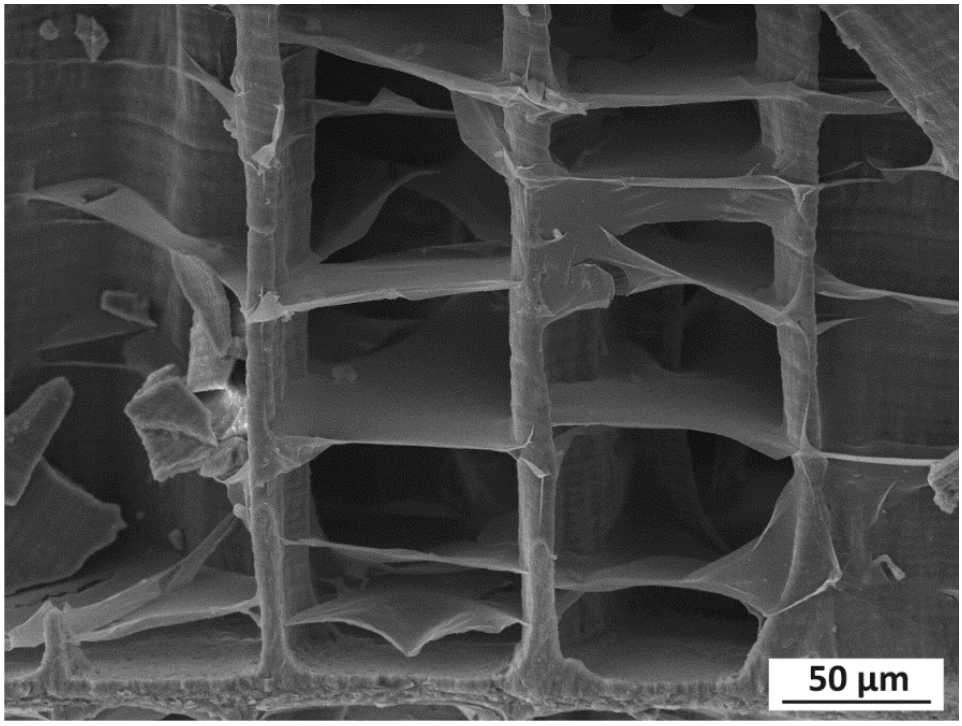

Figure 4.1. SEM micrograph from a fragment of Sepia officinalis cuttlebone showing the biopolymer membranes encasing the crystal units that built up Sepia cuttlebone.

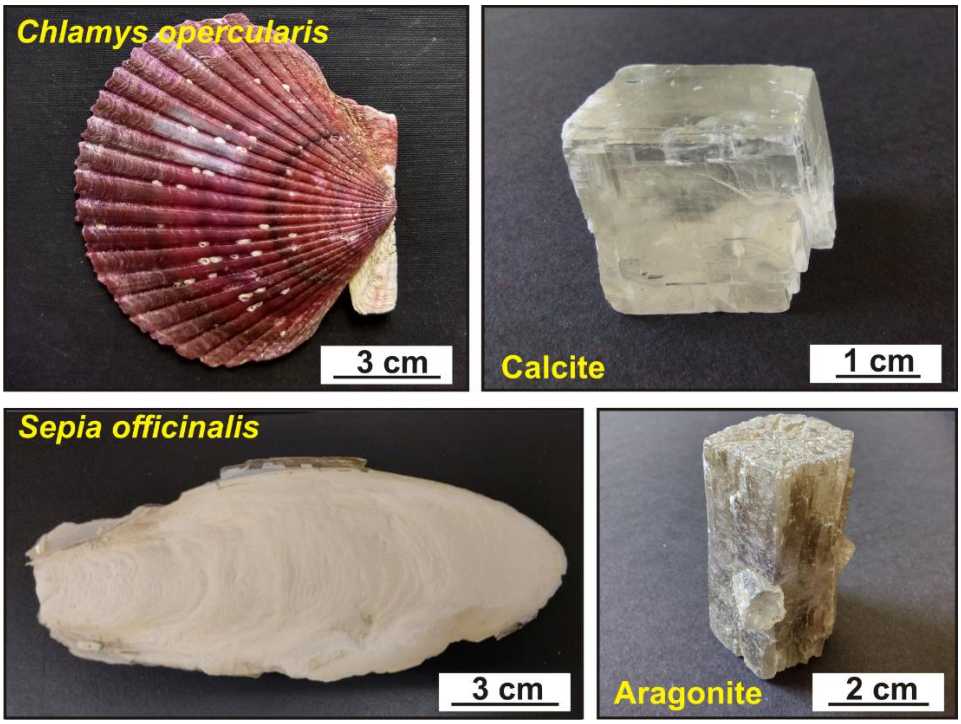

Figure 4.2. Overview images of biominerals used for the interaction experiments and the inorganics minerals used to compare the lead removal efficiency of Pb-bearing aqueous solutions. Images were taken prior to grinding.

The specific surface area of the biocarbonate samples was determined by measuring the N_2 adsorption isotherms. These measurements were conducted at −196°C in an automatic apparatus (Micrometrics ASAP 2020). Prior to the adsorption measurements, the samples were outgassed in situ under vacuum overnight at 90°C. It is controversial that this type of measurement is adequate to estimate specific surface areas in systems where organics are present (Saidian et al. 2016). In the particular case of biocarbonates, different authors have pointed out that N_2 adsorption isotherm measurements are likely to be influenced by specific biocarbonate microarchitectures and lead to overestimated reactive surface areas (Keir 1980; Walter and Morse 1984; Cubillas et al. 2005; Subhas et al. 2018). This inference has been proved for being wrong for biocarbonates like the shells of benthonic foraminifera (Subhas et al. 2018). To evaluate the possible contribution of the biopolymers that resulted in an overestimation of the specific surface areas of BIO-CAL and BIO-ARG, N_2 adsorption isotherm measurements were conducted on both, pristine samples and samples thermally treated (2 h at 350°C in an oxygen atmosphere) to remove most of their biopolymers. The specific surface areas (S_{BET}) thus determined were 28.59 ± 0.26 and 30.85 ± 0.23 m^2/g for pristine and thermally treated BIO-CAL, respectively. In the case of pristine and thermally treated BIO-ARG, the determined S_{BET} values were 27.49 ± 0.13 and 29.58 0.18 m^2/g, respectively. The similarity of the S_{BET} of the pristine samples and the thermally treated ones indicates that the presence of the polymeric component in does not lead to an overestimation of the specific area of the pristine samples. The slightly higher surface area of the thermally treated samples can be explained by the generation of porosity during biopolymer degradation (Forjanes et al. 2022). Part of this porosity can also be destroyed during the thermal treatment due to recrystallization and abutting of the crystal units. The average biopolymer contents of BIO-ARG and BIO-CAL samples, as determined by

thermogravimetric analysis (TGA) in a Mettler Toledo TGA/SDTA 851 thermal analyzer in an oxygen atmosphere, are 9.8 and 1.7 wt.%, respectively. These values are in good agreement with previously reported organic contents for *Sepia officinalis* cuttlebone (9.8 wt.%; (Florek et al. 2009)) and scallop shells (1.3 wt.%; (Lagos et al. 2021)).

4.2.2. Batch Experiments

Interaction experiments were carried out at 23°C and atmospheric pressure by placing 200 mg of each powdered pristine hard tissue (BIO-CAL or BIO-ARG) into beakers containing 100 mL of Pb-bearing solution ($[Pb]_{aq}$= 10 mM) and a floating magnet. The Pb- bearing aqueous solution was prepared by dissolving reagent grade $Pb(NO_3)_2$ (Sigma Aldrich) in ultrapure deionized water. Borosilicate glassware (VWR) was used to perform all the experiments. Beakers were sealed (V_{total} = 150 mL) with Parafilm to avoid water evaporation during experiments. A suspension of skeleton fragments in Pb-bearing solution was stirred at 300 rpm with a multiposition magnetic stirring plate during the entire duration of experiments lasting for 4 h, 1, 2, 3, 5, 7 and 10 days. Independent experimental runs were conducted for both biogenic materials. Experimental runs were duplicated to confirm experimental reliability and to determine the standard deviations. After the end of each experiment the solution was filtered under low vacuum using 0.45 μm Nitrocellulose filters (Millipore, Ø = 0.45 μm). Recovered solids were then dried at room temperature and stored in plastic Petri dishes containing a filter for gravimetric analysis to decrease the relative humidity. This experimental procedure has been previously used by the authors to study Pb sorption by purely inorganic $CaCO_3$ (calcite and aragonite). Therefore, the kinetic data obtained in the current study allow for a fully consistent comparison with those derived from our previous work (Di Lorenzo et al. 2019).

4.2.3. Analytical Methods

The mineralogy of both, pristine and reacted skeletons was characterized by X-ray powder diffraction (XRD) using a PANalytical Xpert Pro equipped with a Cu X-ray source (working at 40 kV and 40 mA) and a zero silicon holder. X-ray patterns were recorded between 5° and 70° 2θ, with a step range of 0.017° and a measured time per step of 80 s. XRD patterns were used to identify and semiquantify (Rietveld refinements) the phases with X'Pert HighScore Plus (PANalytical B.V., Erie, PA, USA) software. The diffraction patterns were compared to standard mineral files for calcite (PDF 05-0586), aragonite (PDF 41-1475), cerussite (PDF 47-1734) and hydrocerussite (PDF 13-0131). Reacted samples were further analysed by scanning electron microscopy (SEM). Backscattered electron (BSE) and Secondary electron (SE) images were taken on polished gold-coated cross sections of epoxy embedded samples using a JEOL-6610LV microscope equipped with Energy-dispersive X-ray spectroscopy (EDX, INCA Energy 350). The pH of the initial Pb-bearing solutions (4.3 ± 0.05) was measured using a Thermo Scientific (Tokyo, Japan) Orion Versa Star Pro system. Finally, the total concentration of lead (Pb) and calcium (Ca) in the liquid samples was analysed by inductively coupled plasma optical emission spectrometry (ICP-OES) (Agilent Varian, 700 ES).

4.2.4. In Situ AFM Observations

The interaction between millimeter-sized fragments (~ 2 × 2 × 2 mm) of *Sepia officinalis* and 10 mM Pb-bearing aqueous solutions was studied at the nanoscale with a Cypher ES© atomic force microscope. The images were recorded in tapping mode at 25°C using ultrahigh frequency tips (NanoWorld Arrow UHF-AuD). The topographies of the mineral surface were acquired with a line-scanning rate of 1.8 Hz during and after the injection of the solutions. The only mathematical treatment applied to the images was a zero-order flattening

executed by the default software of the Cypher Asylum. Individual representative samples were carefully prepared for the experiments by cutting the initial bigger specimens with a stainless steel blade. Samples were stuck on a magnetic holder (Ted Pella) using an adhesive for microscopy, Leit-C©. The samples were initially observed in ultrapure water for 2 h. After locating a suitable surface with optimal scanning parameters, the Pb-bearing solution was injected into the AFM cell and the interaction process was observed continuously up to 7 hours. To confirm the reproducibility of the observations, different locations on the same crystal have been observed before concluding each experiment. The entire experimental procedure has been replicated two times. Profile measurements were made with the open source software Gwyddion 2.59 (Nečas and Klapetek 2012).

4.3. Results

4.3.1. Biomaterials Interacting with a Pb-bearing Aqueous Solution

XRD confirmed that the only mineral components present in the pristine samples of *Chlamys opercularis (Aequipecten opercularis)* shell (BIO-CAL) and *Sepia officinalis* cuttlebone (BIO-ARG) are calcite and aragonite, respectively. The interaction between Pb-bearing aqueous solutions and grains of biogenic materials (BIO-CAL and BIO-ARG) was studied by characterizing mineralogical changes in the reacted samples compared to the pristine ones as well as chemical changes in the liquid phase as the reaction proceeds in batch experiments.

The X-ray diffraction patterns shown in Figure 4.3 correspond to BIO-CAL and BIO-ARG samples after interaction times in contact with Pb-bearing aqueous solution. In addition to the characteristic diffraction peaks of calcite (BIO-CAL) and aragonite (BIO-ARG), the diffractograms of both biogenic materials (Figure 4.3a, 4.3b) show new slightly broad peaks at $2\theta = 24.90°$ and

25.59° shortly after the beginning of the interaction (4 h). These new peaks can be attributed to cerussite. With the interaction time, an increase in the relative intensities of the cerussite peaks was also observed. The peak position remained unchanged during the experiment, although the cerussite peaks became narrower with time. The results of XRD Rietveld analysis indicate that after 4 h contact time with the Pb-bearing solution BIO-CAL and BIO-ARG samples contain 5.3 and 6.0 mol % cerussite, respectively. After 3 days, cerussite content goes up to 23.7 mol % in reacted BIO-CAL and 34.2 mol % in reacted BIO-ARG. Finally, after 10 days of interaction, reacted BIO-CAL and BIO-ARG samples contain 44.2 and 32.6 mol % cerussite, respectively. The results indicate fast initial precipitation of cerussite in the presence of BIO-ARG, followed by a stagnation of reaction rate. On the contrary, steady cerussite precipitation leading to a larger reaction yield after long interaction times is observed in experiments with BIO-CAL samples.

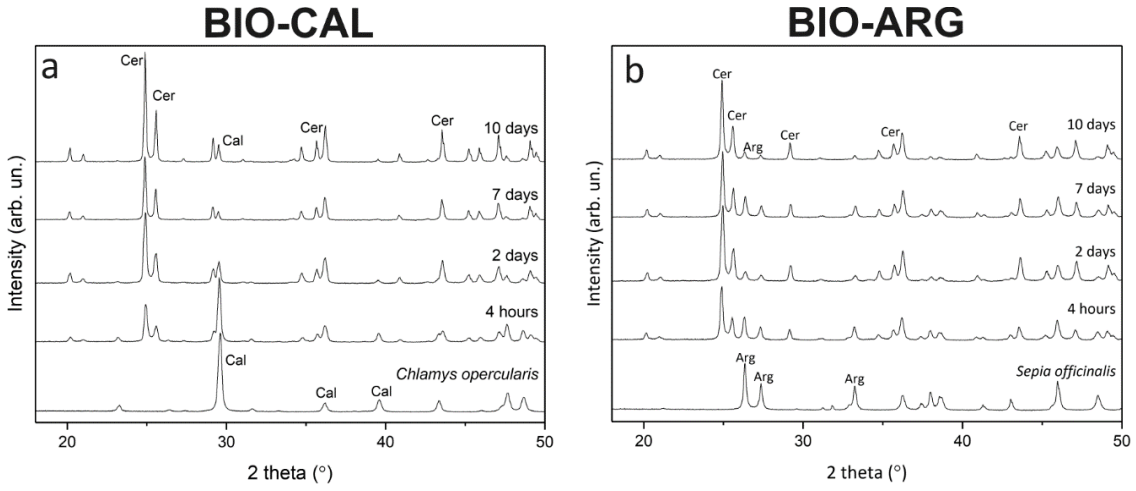

Figure 4.3. X-ray diffraction patterns of Chlamys opercularis (Aequipecten opercularis) (BIO-CAL) (a) and Sepia officinalis (BIO-ARG) crystals (b) after different times of interaction with a 10 mM Pb-bearing aqueous solution.

Backscattered electron microscopy imaging of cross-cut sections of reacted BIO-CAL and BIO-ARG samples shows that these samples consist of a

large dark core surrounded by a bright rim (Figure 4.4). The transition between the rim and the core is sharp and no significant gap is observed at the rim-core interface. The EDX analysis of cores and rims in both types of samples yield highly homogeneous compositions that are consistent with the cores composed of a $CaCO_3$ polymorph and the bright rims consisting of cerussite. In the case of reacted BIO-CAL samples, cerussite rims are initially thin (thickness ~ 3 ± 0.9 μm; interaction time = 4 h) and very patchy but become thicker (thickness ~ 8 ± 2 μm; interaction time = 7 days) and less patchy as the interaction progresses (Figures 3 a-c). Moreover, cerussite crystals in the rim can reach sizes as large as 10 μm and develop euhedral morphology after 7 days of interaction (see, for example, crystals at the top left corner in Figure 4.5a. However, a continuous cerussite layer around the calcite core fails to form, leaving small domains of surface of BIO-CAL sample grains uncovered by cerussite, even after long interaction times (Figures 4.4c and 4.5). In contrast, cerussite rims formed around aragonite cores in reacted BIO-ARG appear as continuous layers that resemble the original shape of the pristine samples after short interaction times (Figure 4.4b). An increase in the rim thickness with the interaction time is also observed in this case. Rims are ~ 5 ± 0.9 and ~ 8 ± 0.6 μm thick after 4 h and 7 days of interaction, respectively (Figures 4.4 b-d). Rims in BIO-ARG samples consist of smaller cerussite crystals compared with the ones observed in reacted BIO-CAL sample rims (Figure 4.5b).

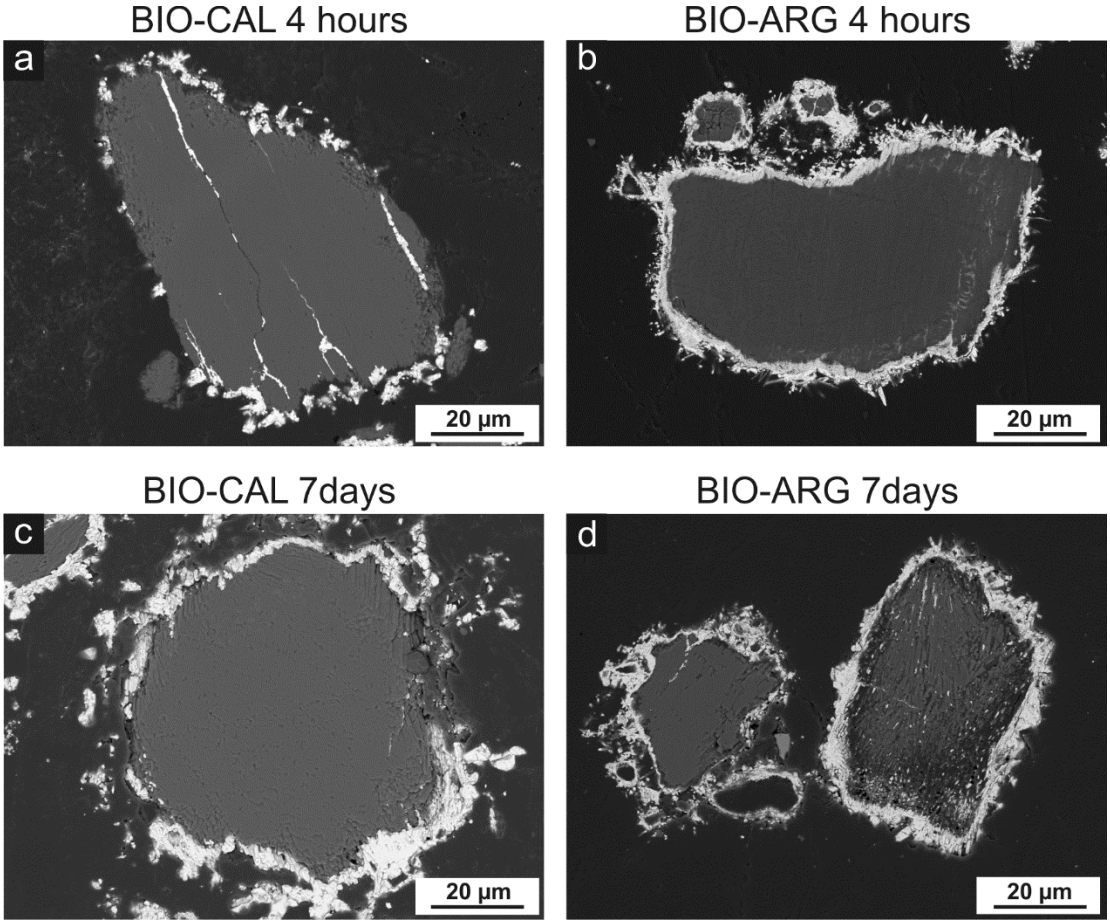

Figure 4.4. SEM micrographs of the cross-section of BIO-CAL and BIO-ARG samples reacted with 10 mM $Pb(NO_3)_2$ aqueous solution at different interaction times.

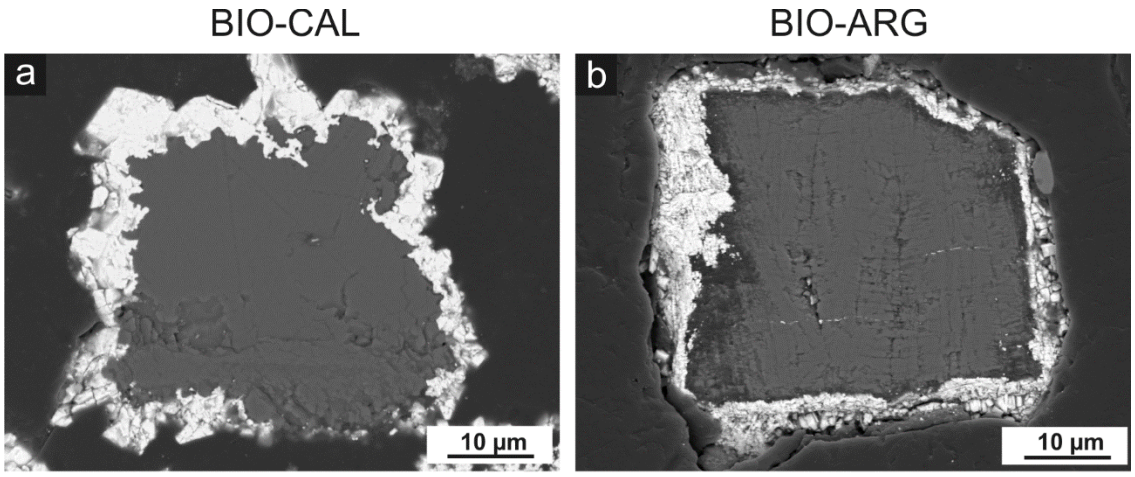

Figure 4.5 BSE-SEM micrographs of cross-sections of reacted crystals after 7 days of interaction with Pb-bearing aqueous solutions: (a) The BIO-CAL core is rounded by an incomplete layer of cerussite crystals showing euhedral morphology. (b) The BIO-ARG surface is completely covered by cerussite crystals showing sizes lower than those observed in BIO-CAL.

The compositional evolution of the aqueous phase during the interaction between the Pb-bearing aqueous solutions and the BIO-CAL or BIO-ARG samples is monitored by ICP-OES analysis. Plots of Ca and Pb concentrations against interaction time are shown in Figure 4.6. As can be seen, the Pb concentration in the aqueous solution undergoes an early rapid drop (during the first 4 h) followed by a slower decrease, regardless of the material used in the interaction experiments. The total Ca + Pb concentrations remain nearly unchanged. Thus, the observed decrease in the Pb concentration is reciprocally correlated with an increase in the Ca concentration. A closer inspection of the data plotted in Figures 4.6a and 4.6b reveals some differences in the removal rate of Pb from the liquid phase depending on the type of biogenic materials used in the experiments. In experiments conducted using BIO-ARG samples, the Pb concentration drops very fast during the first 4 h and reachs ~ 4 mmol/L. At longer interaction time, the rate of Pb precipitation slows down. The Pb-concentration reaches values around 2 mmol/L after 48 h and approximately 1 mmol/L at the end of the experiment after 10 days (Figure 4.6b). In experiments

conducted with BIO-CAL samples, the Pb concentration drops at a significantly slower rate. After 4 h of interaction Pb concentration in solution reaches a value of ~ 8 mmol/L. Afterward, the rate of Pb concentration decreases slows down but less strongly compared to the corresponding experiments with BIO-ARG. Pb reaches a value of ~ 1 mmol/L after 48 h and is ~ 3 µmol/L after 10 days (Figure 4.6a). Therefore, during the first 4 h of interaction, BIO-ARG surface appears as a more efficient Pb scavenger, which takes up ~ 79 % of the initially dissolved Pb, whereas BIO-CAL takes up only ~ 50 % in the same interaction period. The Pb uptake efficiency is inverted at longer interaction times. After 10 days of interaction ~ 99.9 % of dissolved Pb has been scavenged from the solution by BIO-CAL and only ~ 90 % by BIO-ARG. The observed differences in the amounts of Pb removed from the solution, estimated by the ICP analysis of the aqueous solution correlate with the thickness of cerussite layers formed around the grains of carbonates. Longer interaction times result in thicker cerussite rims.

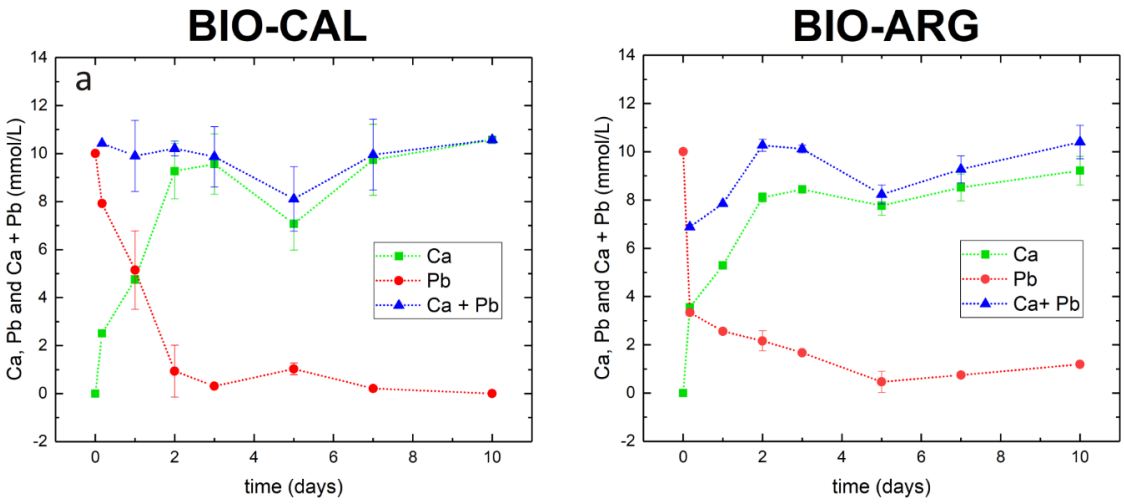

Figure 4.6. Evolution of Pb and Ca concentrations as a function of time for interaction experiments carried out with [Pb]i = 10 mM obtained by ICP-OES. (a) Chlamys opercularis (Aequipecten opercularis) (BIO-CAL) and (b) Sepia officinalis (BIO-ARG).

4.3.2. Surface Reaction with AFM

The interaction between BIO-ARG surfaces and the Pb-bearing aqueous solution leading to the precipitation of $PbCO_3$ was in-situ monitored by AFM. In Figures 4.7 a-f a sequence of height-channel images shows the evolution of Sepia Officinalis surface in contact with Pb aqueous solution at different reaction times. Figure 6a shows the typical nanogranular appearance of *Sepia officinalis* cuttlebone surface prior to the beginning of the interaction. As soon as the Pb-bearing solution is injected into the AFM cell, the formation of nuclei of a new phase on the biomineral surface is observed (Figure 4.7b). As the Pb-bearing solution-biomineral surface interaction progresses to the newly formed nuclei rapidly grow and coalesce (Figure 6c) to form a layer that completely carpets the biomineral surface after interaction times as short as 25 min (Figure 4.7d). After 2 h of interaction, newly formed crystals in this layer exceed 2 μm and appear to be strongly coaligned (Figure 4.7d).

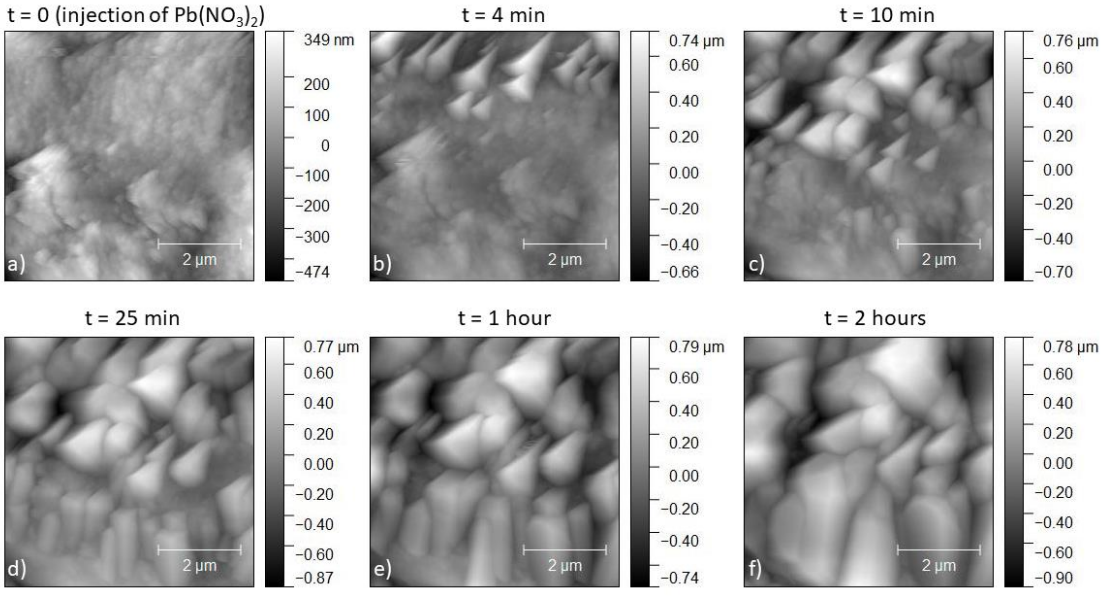

Figure 4.7. AFM images showing the evolution of the cuttlebone surface after injection of 10 mM ($Pb(NO_3)_2$ at different reaction times.

SEM images in Figures 4.8 a-c show a *Sepia officinalis* cuttlebone sample after 7 h of interaction with the Pb-bearing solution. It is worth noting that the carpark structure characteristic of the pristine biomaterial, with evenly spaced platforms interconnected by pillars, is preserved throughout the interaction (Figures 4.8 a-b). Inspection of this structure under higher magnification shows that elongated prismatic crystals of a newly formed crystals reacted with the *Sepia officinalis* cuttlebone. These crystals appear arranged with the prism length approximately perpendicular to platform surfaces in the cuttlebone carpark structure (Figure 4.8c). Cerussite crystals formed on the surface of cuttlebone pillars show features and orientations identical to as those in the platforms. In situ AFM imaging of the surface of septa and pillars of reacted cuttlebone (reaction time = 7h) confirms that crystals of the new phase grow aligned to each other (Figures 4.8 d-f).

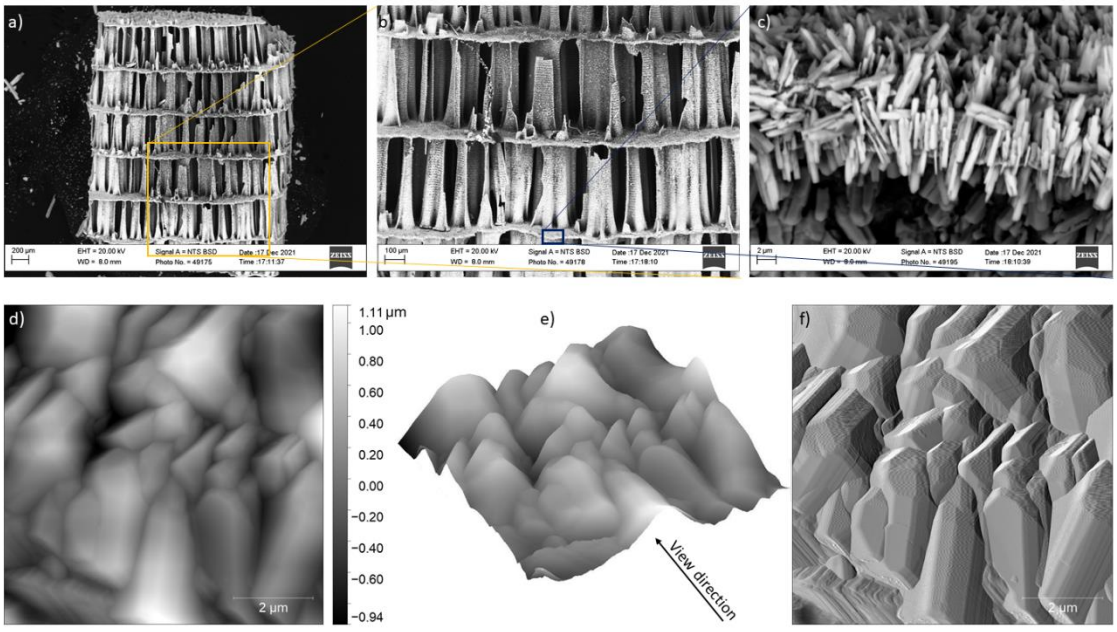

Figure 4.8. Characterization of the BIO-ARG surface at nanoscales: (a-c) BSE-SEM micrographs recorded ex situ at the end of AFM flow-through experiments (t = 7 h): (a-b) the pristine biomineral structure is preserved and (c) the newly formed crystals appear as elongated prisms that grow near perpendicular to platforms surface. AFM images of height channel (d-e) and amplitude channel (f) show that the cerussite crystals grow co-aligned on Sepia officinalis surfaces.

4.4. Discussion

4.4.1. Removal of Dissolved Pb by Biogenic Calcium Carbonates: Efficiency and Mechanisms

Figure 4.9 illustrates the variation of Pb taken up as a function of time during the interaction of a solution containing 10 mM Pb with (i) fragments of the biogenic carbonates *Chlamys opercularis (Aequipecten opercularis)* shell (BIO-CAL) (pink rhombus) and *Sepia officinalis* cuttlebone (BIO-ARG) (blue triangles) (this work) and (ii) equally-sized fragments of abiogenic calcite and aragonite crystals (Di Lorenzo et al. 2019). As can be seen, both biogenic carbonates remove Pb from the aqueous phase at a much faster rate than their geological counterparts. The total amount of Pb removed at termination time is overwhelmingly higher when experiments are conducted using biomineral fragments: resulting in the removal of up to 99.9 and 90.0 mol % of the initial dissolved lead by BIO-CAL and BIO-ARG respectively. Only Godelitsas et al. (2003) have reported similarly high Pb removal efficiency in the experiments conducted with calcium carbonate mineral of geological origin whose grain size and surface area were similar to those of the samples in this study . However, it is worth mentioning that in the experiments conducted by Godelitsas et al. (2003) the initial concentration of dissolved Pb was significantly lower (5 mM) and the solid/liquid ratio (0.01g/mL) was significantly higher than in the experiments in this study, which were conducted using the exact same conditions as Di Lorenzo et al. (2019).

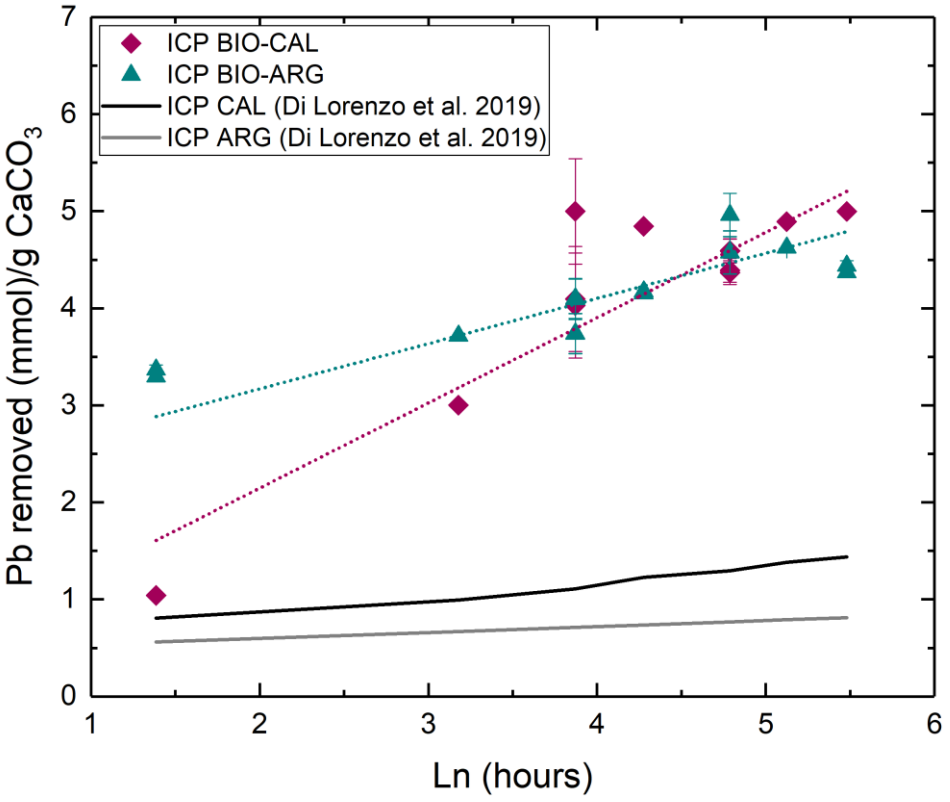

Figure 4.9. Plot of Pb uptake by BIO-CAL and BIO-ARG against interaction time (in logarithmic units). Data of Pb uptake by geological calcite and aragonite (Di Lorenzo et al. 2019) are also plotted for comparison. Note that Pb uptake data are mass-normalized.

Three main mechanisms can be responsible for the removal of heavy metals from aqueous solutions by mineral surfaces: (i) formation of chemical bonds that can be strong (chemisorption) or weak (nonspecific adsorption), (ii) solid solution formation through solid state in- and out- diffusion ions in the near surface region, and (iii) through precipitation of secondary minerals (Sposito 1986; Brown et al. 1995b; Godelitsas and Astilleros 2010). Pb sorption mechanisms at the abiogenic calcite or aragonite – aqueous solution interface have extensively been studied combining multiscale approaches, (Fulghum et al. 1988; Sturchio et al. 1997; Godelitsas et al. 2003; Rouff et al. 2004, 2005, 2006; Elzinga et al. 2006; Yuan et al. 2018; Di Lorenzo et al. 2019; Roza Llera et al. 2021; Fiorito et al. 2022). There is a consensus that the interaction of Pb-bearing aqueous solutions with geological calcite or aragonite Pb leads to the surface

precipitation of lead carbonates (cerussite and hydrocerussite). Potential Pb absorption into the calcite or aragonite crystal lattice is negligible due to the extremely low solid state diffusion rate under ambient condition, which is confirmed with transmission electron microscopy observation of the interfaces (Dyer 1995; Di Lorenzo et al. 2020). Moreover, spectroscopic analyses have confirmed that surface adsorption of Pb onto calcite and aragonite crystals is only relevant at the very early stages of the mineral-fluid interaction process or in a very diluted solution (Godelitsas et al. 2003). The larger surface area of calcium carbonate biogenic carbonates compared with their inorganic counterparts may be one of the factors that explain the higher uptake of Pb by the former. However, the chemical analyses of the fluid during its interaction with BIO-CAL and BIO-ARG samples show that the decreases in the Pb concentration is coupled to the increase in Ca concentration. This observation indicates that Pb precipitation is coupled with the dissolution of the biogenic calcium carbonate as previously reported in the studies with inorganic calcium carbonate phases (Godelitsas et al. 2003). This interpretation is in good agreement with SEM observations showing the formation of new crystalline phases growing on the surface of BIO-CAL and BIO-ARG samples soon after the beginning of the interaction (Figures 4.4 and 4.5). EDX analyses of these crystals showed that they contain Pb. However, the amount of removed Pb estimated from the chemical analysis of the aqueous solution (Figure 4.6) can include a contribution that does not correspond to cerussite precipitation but to Pb adsorption by biopolymers exposed on biocarbonates surfaces. Furthermore, XRD analysis of interacted samples confirm that they consist of a mixture of the initial calcium carbonate phase and secondary cerussite (Figure 4.3). The Pb removal estimated from XRD analyses of interacted biominerals confirms higher effectiveness of both biominerals (3.25 mmol cerussite / g BIO-ARG and 4.68 mmol cerussite/g BIO-CAL) than those previously reported for

geocarbonates (1.33 mmol cerussite/g aragonite and 1.58 mmol cerussite/g calcite) (Di Lorenzo et al. 2019). Future works will investigate the contribution of biopolymers to the Pb-removal.

4.4.2. Reaction Paths and Physicochemical Evolution of the System

Experimental results show that the interaction of a Pb-bearing aqueous solution with BIO-CAL and BIO-ARG leads to surface precipitation of cerussite crystals. At the same time, dissolution of biogenic carbonates Ca^{2+} and CO_3^{2-} ions is released to the fluid. The reaction between the released CO_3^{2-} ions and the dissolved Pb^{2+} ions may result in the formation of cerussite crystals as soon as supersaturation for the formation of this phase is attained. This dissolution-precipitation reaction can be described as:

$$CaCO_3 + Pb^{2+}{}_{(aq)} = PbCO_{3_{(s)}} + Ca^{2+}{}_{(aq)} \quad (1)$$

The equilibrium constants for aragonite and calcite in reaction (1) are slightly different:

$$K = \frac{\{Ca^{2+}\}\cdot\{CO_3^{2-}\}}{\{Pb^{2+}\}\cdot\{CO_3^{2-}\}} = \frac{K_{sp}(aragonite)}{K_{sp}(cerussite)} = \frac{10^{-8.34}}{10^{-13.13}} = 10^{4.79} \quad \text{ARG experiments} \quad (2)$$

$$K = \frac{\{Ca^{2+}\}\cdot\{CO_3^{2-}\}}{\{Pb^{2+}\}\cdot\{CO_3^{2-}\}} = \frac{K_{sp}(calcite)}{K_{sp}(cerussite)} = \frac{10^{-8.47}}{10^{-13.13}} = 10^{4.66} \quad \text{CAL experiments} \quad (3)$$

The terms in brackets represent the activities of the aqueous ions. The equilibrium constants for aragonite ($K_{sp}= 10^{-8.34}$), calcite ($K_{sp}= 10^{-8.47}$) and cerussite ($K_{sp}= 10^{-13.13}$) have been taken from the llnl.dat database, included in the geochemical code PHREEQC (Parkhurst and Appelo 1999). Aragonite is slightly more soluble than calcite and both calcite and aragonite are more than 4 orders of magnitude more soluble than cerussite.

The large solubility difference between both calcium carbonate polymorphs and cerussite explains that as soon as the former phases start to dissolve, the fluid becomes supersaturated with respect to cerussite. Considering the $CaCO_3$-$PbCO_3$ system as a mechanical mixture of pure end-members (Di Lorenzo et al. 2020), the equilibrium constant of reaction 1 can be defined as the ratio between the solubility product of each involved calcium carbonate phase and that of cerussite, as described by expressions 2 and 3. It is important to note that the equilibrium constants for aragonite and calcite have been defined without taking into consideration whether these phases have an inorganic or a biogenic origin. As explained in Introduction section, biocarbonates are composite materials that consist of two intimately interlinked phases, biopolymers and calcium carbonate minerals with mesocrystalline architectures (Weiner and Dove 2003). In both calcite and aragonite biomaterials, networks of biopolymer fibrils are occluded within the mineral component. Different authors have studied the effect of these intracrystalline organic molecules on the structure of biocalcites, bioaragonites and biomimetic calcium carbonates (Pokroy et al. 2004, 2006b, 2006a, 2006c). Pokroy et al. (2006b) concluded that this occlusion induces anisotropic lattice distortions in biocarbonates of the mollusk phylum. These authors found that intracrystalline organic inclusions cause an increase in the a- and c-lattice parameters and decrease in the b-lattice parameter of bioaragonite, while they promote the increase in both the a- and c-lattice parameters in biocalcite. Similar lattice distortions have been observed in crystals formed in the presence of organic macromolecules and biopolymers extracted from calcium carbonate hard tissue shells (Herman et al. 1988; Aizenberg et al. 1997; Metzler et al. 2010; Różycka et al. 2019; Lang et al. 2020). Seknazi and Pokroy (2018) have established that high lattice strain in biocarbonates arises from the structural mismatch at interfaces between biopolymers and mineral phases. The existence of biopolymer

occlusion-related lattice strain increases the free energy of biogenic calcium carbonates compared to that of their abiogenic counterparts. Consequently, their solubility is also increased (Lippmann 1977; Plummer and Busenberg 1987; Astilleros et al. 2003; Prieto 2009; Forjanes et al. 2022). Biocarbonates commonly incorporate small amounts of ionic impurities. As explained in Introduction section, both BIO-CAL and BIO-ARG contain minor amounts of Mg and Sr, most likely as isomorphic substitutions in the lattice of their mineral component. These deviations from the composition of each $CaCO_3$ counterpart end-member further contribute to the increase in BIO-CAL and BIO-ARG solubility (Lippmann 1980, 1991; Plummer and Busenberg 1987; Astilleros et al. 2003; Prieto 2009). Moreover, biocarbonates are nanoparticulate, polycrystalline materials. It is well known that crystal size influences solubility and smaller crystals are less stable than larger ones (Baronnet 1982; Kile et al. 2000; Noguera et al. 2006; Vetter et al. 2013). All these factors result in a larger negative Gibbs free energy change involved in reaction 1 for BIO-CAL and BIO-ARG, which makes it more likely to proceed further above the limits observed for purely inorganic materials.

4.4.3. Lead Scavenging Capacity of Calcium Carbonate Biomaterials: BIO-Carbonate versus GEO-Carbonates.

The higher solubilities of biocalcite and bioaragonite compared to their abiogenic counterparts may also contribute, to some extent, to their enhanced Pb-scavenging capacity. Since larger amount of biogenic calcium carbonate can be dissolved, the fluid becomes more supersaturated with respect to cerussite and, consequently, a larger amount of this phase will precipitate. As soon as the dissolution-precipitation feedback loop is established, the process will progress leading to the precipitation of larger amounts of cerussite as long as the loop continues to operate.

It is worth noting to note that the biopolymeric component of biomaterials comprises both water-soluble and -insoluble macromolecules (Weiner and Traub 1984; Goffredo et al. 2011; Sancho-Tomás et al. 2013). During the interaction of Pb-bearing aqueous solutions with biocalcite and bioaragonite, it can be expected that small amount of the soluble macromolecules exposed on the surface of the biocarbonate will be released to the fluid phase as the calcium carbonate dissolution-cerusite precipitation reaction progresses. Dissolved macromolecules are complex mixtures that may influence the kinetics of the reaction through their functional groups. However, it was experimentally assessed that organic ligands play a minor role in the dissolution of calcite (Oelkers et al. 2011). Their effect only becomes appreciable for concentrations of organics in the range of 10^{-2} mol/kg, which result in an increase of calcite dissolution rate of around 2.5 times). In the case of the biocarbonates used in this work, BIO-ARG shows the higher content of biopolymers (9.2 wt%), which mostly consist of chitin (Malferrari et al. 2013). Assuming the organic matter to be entirely composed of the most abundant component, the chitin $(C_8H_{13}O_5N)n$, and this polysaccharide to completely depolymerize into monomeric units, the concentration of dissolved chitin would be around 0.8×10^{-4} mol/kg, negligible compared to the concentration of divalent metals in the aqueous solution at any interaction time ($[Pb^{2+}] + [Ca^{2+}] = 0.01$ mol/kg. Since a monomer of chitin only contains one carbonyl group and at least two molecules of chitin will be needed to chelate a dissolved divalent ion, under the most favorable conditions, the maximum amount of aqueous cations that could be complexed would be below 4 % of those available. Finally, the nanocrystalline nature of biogenic calcium carbonates grants them significantly larger specific surface areas than shown by their inorganic equivalents. Thus, the specific surface areas of BIO-CAL and BIO-ARG are 28.6 and 27.5 m^2/g, respectively. These values largely exceed those published for inorganic calcite (4.65 m^2/g) and aragonite (6.8 m^2/g) samples

within the same size range (Di Lorenzo et al. 2019). A larger specific surface area can translate into a larger reactive surface, which, in turn, results in a faster dissolution of biocarbonates compared to the geological counterparts. Indeed, the measured dissolution rates of BIO-CAL and BIO-ARG in pure water are 1.33 x 10^{-12} and 1.38 x 10-^{12} (mol cm^{-2} sec^{-1}), respectively. In equivalent experiments, Di Lorenzo et al. (2021) determined dissolution rates for 6.45 x 10^{-13} (mol cm^{-2} sec^{-1}) for geological calcite and 5 x 15 10^{-13} (mol cm^{-2} sec^{-1}) for geological aragonite. This means that BIO-CAL and BIO-ARG dissolve around 2 and 2.7 times faster than their geological counterparts, respectively. As a consequence, a coupled faster precipitation of cerussite could be expected. Furthermore, the availability of a larger reactive area also provides more space for cerussite nucleation, facilitating the removal of higher amounts of Pb from the fluid. Moreover, it cannot be discarded that dissolved macromolecules may play a role in promoting cerussite nucleation. The formation of porosity is a common process that occurs during interface-coupled dissolution-crystallisation reactions. This porosity can have two origins, the first of which is shared with inorganic samples: (i) porosity generated during interface coupled dissolution-crystallisation reactions to balance negative molar volume and/or solubility changes involved in the reaction and (ii) porosity that results from the dissolution/degradation of biopolymers occluded in the biomineral. The first type of porosity cannot form during the transformation of calcium biocarbonate into cerussite because the molar volume change is positive and large enough that it counterbalances the negative solubility change, regardless of the calcium carbonate polymorph considered. In the time length of the experiments conducted, the second type of porosity can form only through the dissolution of water soluble biopolymeric components exposed on the surface of the biomineral to interaction with the aqueous solution. Not all biopolymers are soluble and biopolymer degradation is a very slow process at low temperatures (Gaffey 1988; Gaffey et al. 1991;

Forjanes et al. 2022). Since biocarbonate dissolution and cerussite precipitation are concomitant processes, the impact of this newly formed porosity through biopolymer dissolution on the overall Pb-scavenging process will largely be modulated by the characteristics of the precipitated cerussite layer.

4.4.4. Lead Scavenging Capacity of Biogenic Calcium Carbonates: BIO-CAL versus BIO-ARG.

Despite the close similarity of the thermodynamic driving force controlling the dissolution-crystallisation reaction for BIO-CAL and BIO-ARG, the experimental results indicate the differences in the time dependent reaction yield. Figure 4.10 shows the time evolution of the cation activity ratio, $\{Ca^{2+}\}/\{Pb^{2+}\}$, calculated using the PHREEQC code and the results of ICP-OES analysis of the fluid phase (Figure 4.10). After 4 h of interaction $\{Ca^{2+}\}/\{Pb^{2+}\}$ ratios are 0.4 for BIO-CAL and 1.2 for BIO-ARG, reaching after 10 days of interaction maximum values of 3952 and 21 for BIO-CAL and BIO-ARG, respectively. At this point, the system is not yet in equilibrium with the actual phase assemblage, since according to expressions 2 and 3, for this to be the case the values of ionic activity ratio should be 61660 and 45709, respectively. The precipitated cerussite partially passivates the surface of both calcium carbonate biomaterials, preventing the system from reaching full thermodynamic equilibrium. Thus, only a partial equilibrium is established. In any case, it is worth noting that the maximum values for $\{Ca^{2+}\}/\{Pb^{2+}\}$ ratio observed in the experiments by far exceed the values previously obtained in analogous study with inorganic carbonates ($\{Ca^{2+}\}/\{Pb^{2+}\} \sim 0.5$) (Di Lorenzo et al. 2019), which is in agreement with the much higher lead scavenging capacity of biocarbonates.

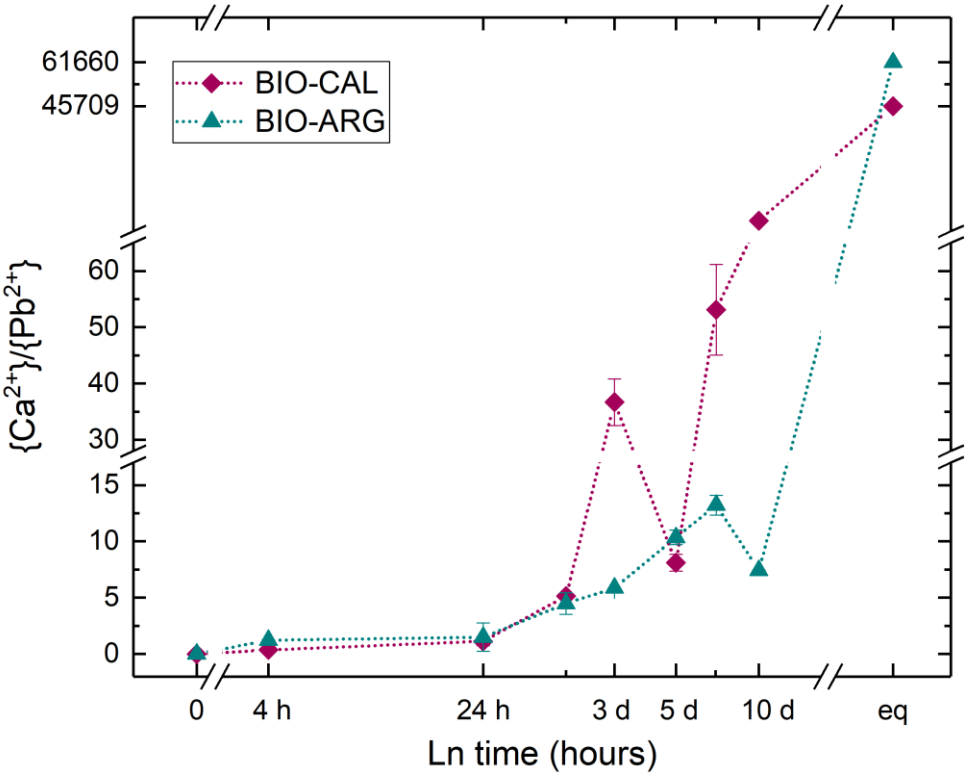

Figure 4.10. Variation of the Ca2+ and Pb^{2+} aqueous ion activity ratio in batch experiments.

The saturation indexes with respect to the involved calcium carbonate phases are calculated as a function of the amount of inorganic carbon, following the expression:

$$SI = \log(\Omega) = \log\frac{IAP}{K_{sp}} \qquad (5)$$

where IAP is the product of ion activities in the aqueous solution and K_{sp} is the thermodynamic solubility product of the solid phase. Because the acidic pH of the solutions makes it impossible to determine the amount of total dissolved carbon by alkalinity titration, the total carbon was considered as a variable in the description of the evolution of saturation indexes during the interaction process. The saturation in the system is expressed as a function of total carbon considering the range $1 < C_{tot} < 10^{-7}$ M. This broad interval enables a reliable evaluation of the partial equilibrium between the phases involved (Figure 4.11) as seen in the previous study by (Di Lorenzo et al. 2019). Thus, Figure 4.11 shows

the evolution of the saturation indexes with respect to cerussite, calcite and aragonite. After 4 h, calcite and aragonite are undersaturated for any $C_{tot} < 1$ and therefore they are dissolving. The minimum amount of carbon released is $10^{-5.6}$ M because the formation of cerussite crystals was identified already at this stage by XRD and therefore cerussite must be supersaturated. A comparison of the different approach toward the thermodynamic equilibrium depending on BIO-CAL and BIO-ARG, in the period ot 4 h to 10 days, is presented in Figure 4.11. The global equilibrium condition would require that the lines describing cerussite and $CaCO_3$ meet at the value corresponding to the equilibrium carbon concentration, which is directly related to the equilibrium pH and partial pressure of CO_2. In the system with BIO-ARG, the concentration of total carbon that could maintain supersaturation with respect to cerussite is achieved with similar carbonate concentration for 4h and 10 days. Consequently, the growth of the initially formed cerussite crystals is hindered by the lack of carbon supply from BIO-ARG. The epitactic growth of the product on the surface of the substrate leads BIO-ARG in a condition of partial equilibrium where there is no direct interface between the solvent and the substrate. On the contrary, in the system with BIO-CAL, a significant increase in the carbonate concentration is required to maintain supersaturation with respect to cerussite between 4h and 10 days ($C^{IV} = 10^{-5.6}$ and $C^{IV} = 10^{-2}$ respectively) (Figure 4.11). This demonstrates that under such a condition that a direct contact between the substrate and the solution can be maintained during the progress of the reaction, the formation of cerussite continues even after a significant reduction of the driving force proportional to the distance between cerussite and calcite lines in Figure 4.11. Obviously, this simulation considers that the main lead removal mechanism would be the precipitation of lead carbonates, although the contribution of other sorption reactions such as Pb adsorption on biopolymers cannot be ruled out.

The study of the role of biopolymers in the dissolution-precipitation reaction loop process is beyond the scope of this work.

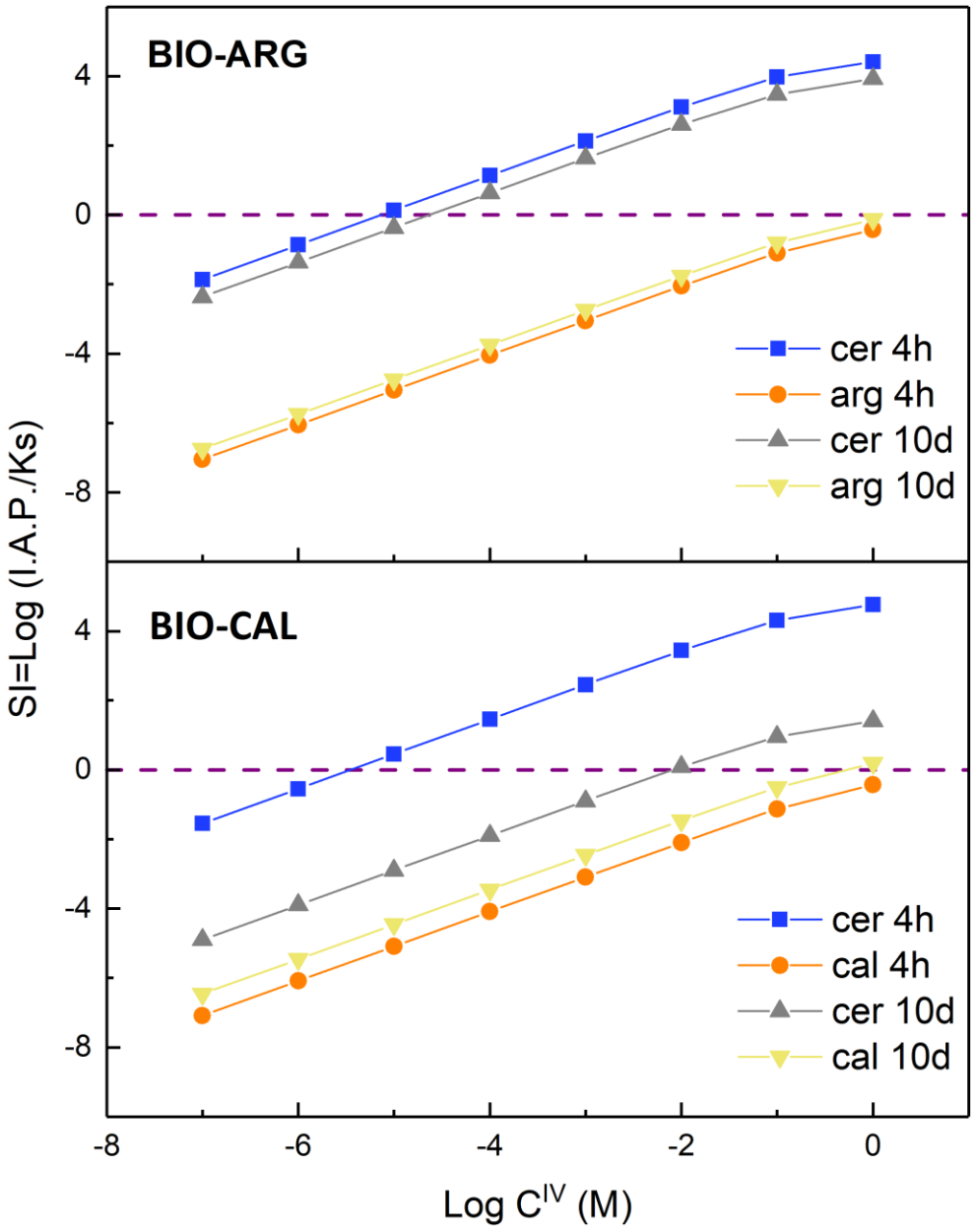

Figure 4.11. Evolution of the saturation index values of calcite, aragonite and cerussite during batch experiments (all curves are calculated for pH = 5.4) as a function of total inorganic carbon concentration in log10 units for different interaction times. The equilibrium conditions (SI= 0) are marked by discontinuous lines.

Despite the fact that both BIO-CAL and BIO-ARG strongly outperform their geological counterparts, they are not equally effective at scavenging Pb

from polluted aqueous solutions. Moreover, their Pb removal capacity differently evolves as the dissolution-crystallisation reaction proceeds. As can be seen in Figure 4.6, BIO-ARG shows a quick initial Pb uptake but its Pb removal capacity rapidly decays with the interaction time. In contrast, BIO-CAL steadily uptakes Pb up to 48 h of reaction. This Pb uptake capacity slowly declines afterward. BIO-CAL's Pb removal capacity outperforms that of BIO-ARG for longer interaction times. Figure 4.9 shows the ICP-OES results normalized for the total moles of cations in solution (n_{M2+} = 1 mmol). In this way the progress of the reaction can follow considering the amount of dissolved $CaCO_3$ or the amount of precipitated cerussite. As can be seen, when the total amount of cerussite precipitated during the experiment is considered, BIO-CAL is an overall better Pb-scavenging material than BIO-ARG (Figure 4.9). This conclusion is in good agreement with the results reported by different authors who compared the Pb-scavenging performance of calcite and aragonite of geological origin (Godelitsas et al. 2003; Du et al. 2011; Zhou et al. 2017; Di Lorenzo et al. 2019, 2020).

All previous studies have concluded that a significantly higher cerussite yield results from the interaction of Pb-bearing solutions with calcite than with aragonite. The main reason underlying this different behavior of the system studies is the structural epitaxy between aragonite and cerussite and the structural mismatch between calcite and cerussite. By combining BSE-SEM and TEM analyses, Di Lorenzo et al. (2020) demonstrated that cerussite grows on geological aragonite showing a strong preferential orientation, with both phases sharing a coherent interface. These authors interpreted that the geological aragonite surface act as a template that catalyzes the heterogeneous epitactic nucleation of cerussite crystals. The lower energy barrier associated with epitactic nucleation compared to both homogeneous nucleation and a growth on structurally incompatible template surface explains this catalytic effect of the

aragonite substrate. A fast formation and growth of numerous oriented cerussite crystals on the surface of BIO-ARG can also explain the high initial Pb uptake capacity of this material. As can be seen in Figure 4.8c, cerussite crystals appear highly coaligned with their length perpendicularly oriented to *Sepia officinalis* septa. Moreover, AFM observations also support an oriented growth of cerussite crystals on BIO-ARG surfaces, at least at early stages of the dissolution-crystallisation reaction (4.7 b-f). A recent in-depth study of *Sepia officinalis* cuttlebone microstructure using Electron Backscattered Diffraction (EBSD) has shown that in all its structural elements, septa as well as pillars/walls, the c-axis of their constituting aragonite crystal subunits are arranged perpendicularly to their surface and rotates with the surface curvature (Griesshaber et al. 2023). Moreover, Griesshaber et al. (2023) also concluded that biopolymer components of *Sepia officinalis* cuttletbone consist of a mixture of chitin-protein, which is arranged as cholesteric liquid crystals in both, the foam-like network occluded within aragonite crystal units and the membranes that envelop these units. Moreover, these authors interpret that the fabric arrangements of the biopolymer guide the organization of the mineral component in both, septa and walls/pillars. The observed arrangement of cerussite crystals, with their length perpendicularly oriented to the BIO-ARG surface, consistis of cerussite nucleation being epitactic and aragonite crystals in the substrate and cerussite crystals in the overgrowth sharing the orientation of their *c*-axes (Figure 4.12). Moreover, a guiding effect of BIO-ARG biopolymers cannot be discarded on the nucleation of cerussite crystals. The later rapid decline of BIO-ARG Pb uptake capacity can be explained as due to the coalescence of cerussite crystals as their epitactic growth progresses, accompanied by competitive growth that further promotes cerussite crystals coorientation, which results in the formation of a continuous porosity-free cerussite layer that carpets the BIO-ARG substrate. This interpretation is in good agreement with SEM observations showing that BIO-

ARG cores appear almost completely coated by neo-formed cerussite rims after only 4 h of reaction (Figure 4.4b). Cerussite rims only undergo slight thickening during the interval between 4 h and 10 days of interaction with the Pb bearing solution. This is indicative of a highly effective armoring of BIO-ARG substrates by cerussite rims, which prevents further interaction with the Pb-bearing solution and results in a virtually complete stoppage of Pb removal (Figure 4.6).

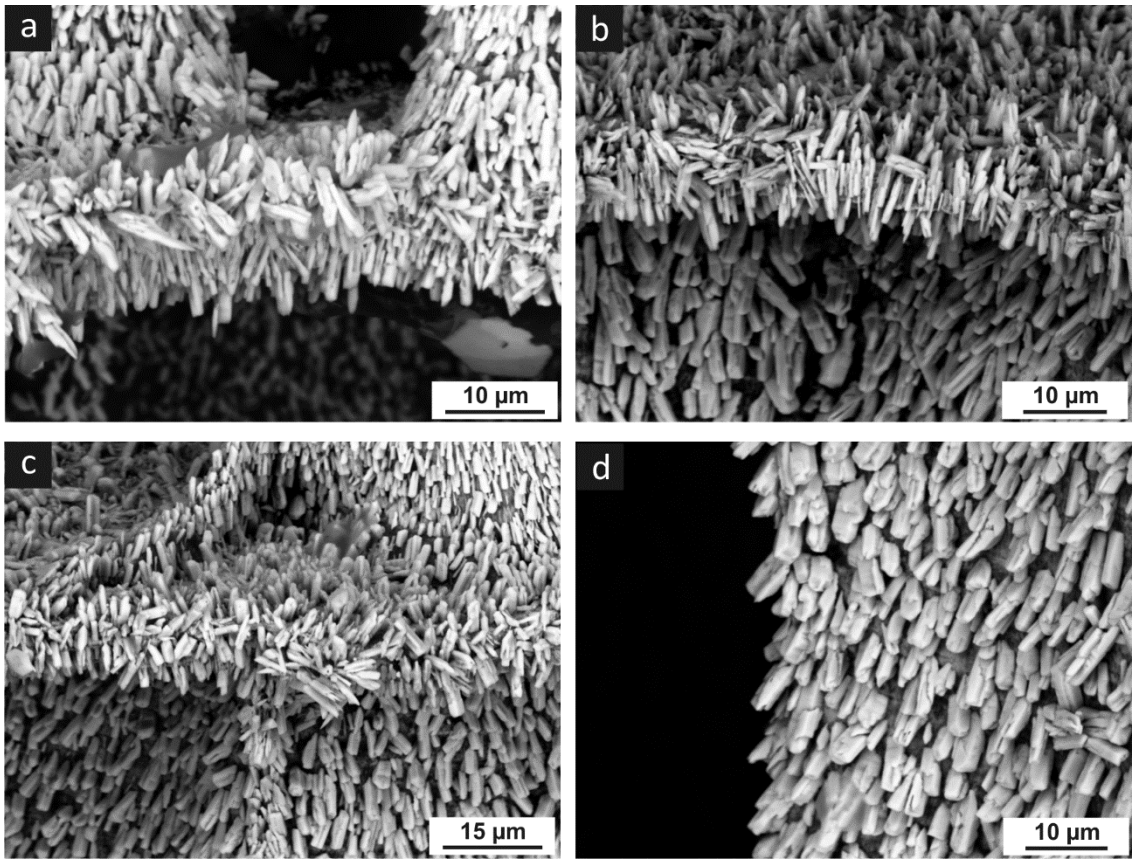

Figure 4.12: SEM micrographs depicting the cerussite crystals covering the BIO-ARG surface. As can be observed, a high co-orientation of cerussite crystals overgrown on cuttlebone septa (a, b, c) and pillars (d) as well as the approximately perpendicular orientation of these crystals with respect to the BIO-ARG surface.

Most studies of cerussite precipitation on a geological calcite substrate concur that no epitactic relationships are observed between the two phases and cerussite crystals grow randomly oriented (Chada et al. 2005; Yuan et al. 2018; Di Lorenzo et al. 2019, 2020). Even if a calcite substrate provides a site for

cerussite heterogeneous nucleation thereby reducing the free energy barrier for cerussite nucleation compared to that for nucleation in the bulk, cerussite nucleation will take place at a slower rate on a calcite substrate than on an aragonite one. This explains that geological calcite, as reported by previous studies, as well as BIO-CAL, as shown here, less efficiently removes Pb at an early stage of the replacement reaction than their respective aragonite counterparts do. Indeed, as can be observed in Figure 3, after 4 h interaction with the Pb-bearing solution, few crystals have formed on the BIO-CAL surface, most of which remains available for interaction with the substrate. The percentage of the BIO-CAL reactive surface that remains uncoated by cerussite crystals decreases as the reaction progresses. The lattice mismatch between cerussite and calcite determines that most Pb removal progresses through the growth of the first formed cerussite crystals rather than through the nucleation of new cerussite crystals on the yet uncoated BIO-CAL surface areas. Thus, as can be seen in Figures 4.4c and 4.5a, even after 7 days of reaction, although patches consisting of large cerussite crystals coat most of the BIO-CAL surface, these patches do not constitute a continuous layer, leaving areas of the BIO-CAL surface uncoated and available for continuing interactiion with the aqueous phase. Moreover, because cerussite patches consist of randomly oriented crystals, they contain a certain volume of intra-crystal pores, some of which are open and connect the cerussite-BIO-CAL interface with the bulk solution (Yuan et al. 2018).

The importance of the existence or absence of epitactic relationships between crystal phases to predict the likelihood of a dissolution-crystallisation reaction resulting in large pollutant uptake yields has been highlighted by the results of numerous previous studies (Godelitsas et al. 2003; Prieto et al. 2003; Cubillas et al. 2005; Pérez-Garrido et al. 2007; Rodríguez-Blanco et al. 2007; Pinto et al. 2009; Astilleros et al. 2010; Morales et al. 2014). As a rule, the existence of a

good matching between crystal structures facilitates the epitaxial growth of a pollutant bearing precipitate on the surface of the primary one and results in a fast initial pollutant uptake. However, it also results in a rapid decrease in the primary phase reactive surface and, consequently, a fast drop in its pollutant uptake capacity. Conversely, the absence of epitaxial relationships between the primary phase and the precipitate commonly guarantees a slower decrease in the substrate reactive surface area. Consequently, the dissolution-crystallisation reaction can be sustained for a longer period, giving rise to larger precipitate yields and pollutant uptake. It appears that this rule also applies to biocarbonates as the epitactic growth of cerussite on the surface of BIO-ARG strongly limits its long-term efficiency as a Pb scavenger while the formation of randomly oriented cerussite crystals on the BIO-CAL surface favors its persistent Pb scavenging activity.

CHAPTER 5

Ca-Phosphate-Sulphate System

5. Ca-Phosphates-Sulphates System

5.1. Introduction

Mineral replacements are common processes in sedimentary, diagenetic, metamorphic, and metasomatic environments, where they take place mediated by a fluid that facilitates the dissolution of the primary mineral and the concomitant precipitation of the secondary one(s). The coupling through the interface of the dissolution and precipitation rates allows for the preservation of original shape and volume of the primary mineral (Putnis 2002, 2009b; Putnis and Putnis 2007; Pollok et al. 2011; Ruiz-Agudo et al. 2014). Moreover, when the dissolution of the latter is the rate-limiting step of the interface coupled dissolution-precipitation reaction (ICDP), original microscopic, and even nanoscopic, features also are accurately preserved during the replacement (Xia et al. 2009; Ruiz-Agudo et al. 2014; Altree-Williams et al. 2015). The progress of ICDP reactions requires a continuous communication between the interface, where the reaction takes place, and the bulk fluid. This communication is ensured by the formation of a network of porosity and/or fractures during the mineral replacement. This network facilitates mass transport to and from the interfacial fluid (Zhao et al. 2009; Jonas et al. 2013; Ruiz-Agudo et al. 2014; Putnis 2015).

In this work we describe the replacement of anhydrite by mixtures of two calcium phosphate phases, β-tricalcium phosphate (β-$Ca_3(PO_4)_2$) (β-TCP) and hydroxyapatite ($Ca_5(PO_4)_3(OH)$) (Hap) through a ICDP mediated by an aqueous fluid containing phosphorous (P). Anhydrite is a rock-forming mineral common in sedimentary basins, where it appears as a major component of evaporites as well as forming nodules and cements in sandstones, limestones and dolostones (Murray 1964; Rahimpour-Bonab et al. 2010; Olivarius et al.

2015). Anhydrite also forms massive accumulations in modern submarine hydrothermal vents (Kuhn et al. 2003). Apatite ($Ca_5(PO_4)_3(OH,Cl,F)$) is the main source of phosphorous, an element that is scarce in the Earth's crust but has great economic interest in the fertiliser industry (Filippelli 2002). Phosphorous is an essential macronutrient for biota as well as a pollutant which in excess causes eutrophication of water bodies, contributes to the growth of toxigenic algae, and boosts the development of potentially pathogenic microbes in the water column and in soils (Mallin and Cahoon 2020). The structural characteristics of apatite make it a relevant phase for immobilizing and storing of radioactive and other pollutant elements (Rakovan and Reeder 1996; Ewing and Wang 2002; Mavropoulos et al. 2002).

There is abundant evidence that mineral replacement reactions play an important role in controlling the fate of a variety of pollutants in soils and sedimentary basins (Pinto et al. 2009, 2012; Wang et al. 2012a, 2015; Hövelmann and Putnis 2016; Callagon et al. 2017; Di Lorenzo et al. 2019; Roza Llera et al. 2021). Anhydrite is highly reactive to dissolved ions. Thus, cycles of anhydrite dissolution/precipitation influence the fate of trace elements (Sr, Y, REE) in hydrothermal systems. Moreover, anhydrite surfaces effectively remove metal pollutants from aqueous solutions through coprecipitation phenomena (Morales et al. 2014; Forjanes et al. 2020b, 2020a). Pollution of running waters and aquifers by phosphorous currently is widespread due to the extensive use of ammonium phosphate as a fertiliser in intensive agriculture (Smith 2003; Wei and Bailey 2021). Understanding the processes that result from the interaction of phosphorous containing waters with common sedimentary rock-forming minerals can help to mitigate the effects of phosphorous pollution in sedimentary basins.

Moreover, apatite is a main constituent of sedimentary phosphorites (Bentor 1980; Sheldon 1981; Hughes et al. 1989; Knudsen and Gunter 2002). Baturin (1989) reported on the diagenetic origin of some apatite accumulations and connected their formation to changes in the chemistry of pore waters due to organic matter decay and sulphate reduction. The concentration of phosphorous in diagenetic fluids in pores can reach values up to 8-9 mg/L, according to Sheldon (1981). Filippelli (2002) and Dzombak and Sheldon (2020) have reported that P concentrations in young soils can reach values as high as 5340 mg/L, highlighting the potential importance of P fluxes from soils to rivers in the current scenario of climate change. In contact with the surface of sediment particles, these high concentrations are sufficient to guarantee the precipitation of apatite, which opens the question of the role that interface coupled dissolution-precipitation reactions (ICDP) may play in the formation of diagenetic apatite. It has been experimentally demonstrated that the interaction of phosphate-bearing fluids with other sedimentary rock-forming minerals like aragonite and calcite results in their replacement by aggregates of apatite crystals (Kasioptas et al. 2010, 2011; Jonas et al. 2013; Reinares-Fisac et al. 2017).

The purpose of the present work is to study the interaction of a P-bearing aqueous solution with anhydrite single crystals. The main goal is to determine the kinetics and mechanisms of anhydrite replacement by calcium phosphate at temperatures between 120°C and 200°C. Two calcium phosphate phases, β-TCP (β-$Ca_3(PO_4)_2$) and Hap ($Ca_5(PO_4)_3(OH)$), formed during this replacement, which were identified by Raman spectroscopy and X-ray powder diffraction (XRD). The amount of each phase as a function of temperature and reaction time was calculated by conducting the Rietveld analysis of the X-ray diffraction (XRD) patterns. This information was applied to determine the kinetics of the process. The textural relationships and the crystal habit of the product phases were studied by scanning electron microscopy (SEM). The influence of the

transformation of β-TCP into Hap, which occurs concomitantly to the progress of the replacement, as well as the specific morphological and textural features of both calcium phosphates in the overall kinetics of the replacement reaction, was considered.

5.2. Materials and methods

5.2.1. Hydrothermal experiments

Hydrothermal interaction experiments were performed by reacting anhydrite single crystals with a 2M $(NH_4)_2HPO_4$ aqueous solution at different reaction times (1 h to 5 days) and temperatures (120, 150, 180 and 200°C) under autogenous pressure. The P concentration in the aqueous solution is around 10 times higher than that reported in young soils (Filippelli 2002; Dzombak and Sheldon 2020). Anhydrite single crystals from Naica mine (Chihuahua, México) were used in all experiments. X-ray fluorescence spectroscopic analysis confirmed them as highly, with less than 0.4 wt% foreign elements and Sr as the major impurity. The anhydrite crystals were cleaved along {100}, {010} and {001} using a sharps stainless-steel knife edge to obtain similarly sized (about 3 x 3 x 3 mm) anhydrite subsamples. Prior to their use in the experiments, these subsamples were cleaned in an ethanol bath to remove surface impurities and then left to dry overnight in a desiccator at room temperature. Four anhydrite subsamples (average weight ≃ 250 ± 1mg) were used in each experiment, and the volume of the solution (~4mL) was adjusted to guarantee a solid-to-liquid ratio of 0.06 g/mL. Anhydrite subsamples were placed together with the P-bearing aqueous solution in pre-heated individual stainless-steel Teflon-lined autoclaves (2.5 Ø x 10 cm). Within the autoclave, all four anhydrite subsamples laid with one of their surfaces in contact with the bottom of the reactor, while their other five surfaces were directly exposed to the interaction with the P-bearing solution.

The crystallographic orientation of the laying surface was not taken into consideration when setting the different experimental runs. The P-bearing aqueous solution was prepared by dissolving reagent-grade $(NH_4)_2HPO_4$ (Acros Organics) in high purity deionized water (MilliQ) (18 MΩ cm). The pH of the fluid was measured prior to and after reaction by using a pH Meter basic 20-CRISON. Experiments were run triplicated to confirm reproducibility. The aqueous solutions were modeled using the geochemical code PHREEQC (Parkhurst and Appelo 1999) and llnl.dat database to calculate saturation indexes (SI) with respect to relevant solid phases at the beginning of the experiments.

After reaction, the autoclaves were removed from the oven. To accelerate their cooling to room temperature (25°C) a flow of compressed air was applied during 20 min. The reaction time does not comprise this cooling period. Afterwards, the product samples were removed from the solution, washed with distilled water, and dried overnight at 30°C in a thermostatic chamber. Two of the four product samples from each experiment were powdered in an agate mortar and used for powder X-ray diffraction (XRD) analyses. The other two product samples were crosscut using a steel cutter and used for Raman spectroscopy and scanning electron microscopy (SEM) imaging analyses.

5.2.2. Analytical methods

Diffraction patterns of powdered product samples were measured at room temperature with a PANalytical Xpert Pro diffractometer, using a CuKα1 radiation. XRD data were collected in the range 7–90° 2θ with a step size of 0.001° and a dwell time of 1 s per step. Samples were hold in thin-walled glass capillaries to minimize preferential orientation effects. General peak matching runs were conducted for the diffraction patterns of product samples. These runs confirmed that in all diffraction patterns all peaks could be assigned to anhydrite

(PDF 98-900-1234) and/or Hap (PDF 98-006-8592) and β-TCP (PDF 00-009-0169). Furthermore, anhydrite, Hap and β-TCP fractions in the reacted samples were determined by performing Rietveld refinement analyses using the X'Pert HighScore Plus (Version 3.0) software package from PANalytical. The aforementioned structural models were used as references.

Crosscut reacted samples were gold-coated and imagined using a JEOL-6610LV microscope equipped with Energy-dispersive X-ray spectroscopy (EDX, INCA Energy 350). The contrast resulting from the different composition of reacted and unreacted areas provided information on the progresses of the anhydrite-(P)-bearing fluid interaction. Secondary electron images of the external surfaces of the reacted solid samples were also obtained.

Raman spectra were collected from freshly crosscut sections of the reacted subsamples. Raman spectroscopy was performed by means of a labRam HRU using JYVJobin Yvon equipment with an excitation source laser CDPS532-DPSS at 24.3 mW and excitation times of 10 s. This equipment was connected to a confocal microscope Olympus BXFM-ILHS with a 100x objective.

5.2.3. Kinetic analysis

We assume that the isothermal kinetics of the anhydrite phosphation reaction can be described by the Avrami equation (Eq.1):

$$y_{CaP} = 1 - e^{-(kt)^n} \qquad (1)$$

where y_{CaP} corresponds to the fraction of calcium phosphate formed (y_{Anh}= 1-y_{CaP}), this is the extent of the phosphation reaction, t (hours) represents the reaction time, k is the Avrami rate constant (hour^{-1}) and n is the Avrami exponent. By linearizing the Avrami equation taking twice natural logarithms the following expression is obtained:

$$ln(-\ ln\ (1 - y_{CaP}))\ = nlnk + nlnt \qquad (2)$$

The Avrami equation has successfully been used to describe the kinetics of a variety of dissolution, crystallisation, transformation, and mineral replacement processes (Lasaga 1998; Xia et al. 2009; Kasioptas et al. 2010; Altree-Williams et al. 2017; Pedrosa et al. 2017). If a reaction follows the Avrami equation, different isokinetic curves will have the same n value. Moreover, their plot as ln(-ln(1-y_{CaP})) against ln *t* (Hancock-Sharp plot) will show approximately equal gradients (Hancock and Sharp 1972). Changes in the value of *n* are indicative of changes in the mechanisms of the reaction. If the activation energy of the reaction is constant, the Hancock-Sharp plot will yield a straight line, whose slope corresponds to the value of *n* and from whose intercept with the y-axis the rate constant *k* can be estimated. Deviations from linearity of the Hancock-Sharp plot indicate that the reaction equation differs from the Avrami one.

The rate constant *k* of most reactions shows a dependence of temperature that follows an Arrhenius type equation:

$$k = A \cdot e^{\frac{-Ea}{R \cdot T}} \qquad (3)$$

where *A* is a frequency factor, R is the gas constant, T is the temperature of the experiment (Kelvin) and E_a is the empirical activation energy. Taking logarithm, the equation 4 is obtained:

$$\ln k = \ln A - E_a/RT \qquad (4)$$

If A and E_a are constant, the plot of ln*k* versus 1/T is a straight line whose slope is E_a/R and its intercept with the y-axis is ln*A*. Thus, the value of E_a can be estimated using the rate constants *k* derived from the Hancock-Sharp plots of a set of isothermal runs.

Commonly the empirical activation energy sums up contributions of different events involved in the reaction (dissolution of primary phases, mass transfer through interfaces, ion dehydration, nucleation and growth of secondary phases, etc). Moreover, the method described above fails to reveal changes in the activation energy that occur as the reaction progresses. It is possible to derive information on the evolution of the empirical activation energy E_a along the reaction by rewriting equation 1 and calculating the time required to achieve the transformation of a given fraction of the primary phase, in this case, anhydrite, into the secondary phase(s), in this case, Hap and β–TCP or a mixture of both phases, according to equation 5:

$$t_Y \propto k^{-1} \propto A^{-1} e^{\frac{E_a}{RT}} \quad (5)$$

where t_Y is the time for a given fraction to transform. This approach is described as the isoconversional method or the time to a given fraction method (Putnis 1992).

Taking logarithms, equation 5 can be rearranged as:

$$\ln t_Y = \text{const} - \ln A + E_a/RT \quad (6)$$

Empirical activation energies can be derived by plotting ln t_Y versus 1/T. If there is no change in the reaction mechanism as the reaction progresses, all plots will have similar gradients and, consequently, E_a will have a constant value, regardless of the given fraction transformed. On the contrary, changes in plot slopes are indicative of different mechanisms operating at different stages of the reaction, each one characterised by a different E_a.

5.3. Results

5.3.1. Reaction Pathway and Textural Features

The hydrothermal interaction of anhydrite single crystals with a phosphate-bearing aqueous solution (2M $(NH_4)_2HPO_4$) results in their partial to total transformation into Hap ($Ca_5(PO_4)_3(OH)$). Hydroxyapatite can be accompanied by varying amounts of β-TCP (β-$Ca_3(PO_4)_2$) depending on the temperature and duration of the interaction. During the transformation, the pH of the solutions progressively decreases from an initial value of 8.1 (1) to 6.8 (1) at experiment termination time. Figure 1a depicts the XRD patterns from subsamples reacted during 6 to 72 h at 120°C. All the diffraction patterns show sharp peaks that can be assigned to anhydrite and/or the calcium phosphate phases Hap and β–TCP. Although the XRD patterns of other calcium phosphates like whitlockite ($Ca_{18}(Mg,Fe)_2H_2PO_4)_{14}$) show similar features as the pattern of β–TCP (Gopal and Calvo 1972; Jonas et al. 2014), the formation of any amount of the former phase is disregarded, since the pristine anhydrite is highly pure and the aqueous phase contains no dissolved Fe and Mg. The intensity of anhydrite peaks progressively decreases with the reaction time. Anhydrite peaks are absent in the pattern corresponding to a reaction time of 72 h. Conversely, the intensity of peaks assigned to Hap progressively increases with time. Peaks assigned to β-TCP show a more complex evolution: their intensity initially grows to latter decrease. In all the experiments, regardless of the reaction temperature, Hap rapidly becomes the main constituent of the transformed fraction. For example, in experiments conducted at 120°C, the transformed fraction contains ~ 20 wt% Hap after 12 h, 37 wt% Hap after 24 h and 73 wt% Hap after 48 h (Figure 5.1b). In experiments conducted at temperatures ≥ 200°C, Hap becomes the only solid phase present in the system after 10 h since the beginning of the experiment. In addition, longer experiments were carried out at temperatures below 180°C, once the anhydrite had been completely replaced, to observe the evolution of the β-TCP and Hap phases. The results of these experiments indicated that the amount of β-TCP continued to decrease with time (Figure 5.2).

After 5 days interaction at 120ºC, reacted samples consist of 7.2% β-TCP and 92.8 anhydrite. The Raman spectra collected on crosscut sections of reacted anhydrite subsamples indicate that all transformed rims exclusively consist of calcium phosphate phases in good agreement with the conclusions of XRD analyses. Figure 2 shows SEM images and Raman spectra taken on crosscut sections of anhydrite reacted with the P-bearing fluid at 150°C during 12 h (Figures 5.3a-5.3d) and 24 h (Figures 5.3e-5.3h). The spectrum in Figure 5.3a shows the main vibration bands of SO_4^{2-} in anhydrite: a symmetric stretching (v_1) band at 1019 cm^{-1}, three asymmetric stretching (v_3) bands at 1113 cm^{-1}, 1131 cm^{-1} and 1160 cm^{-1}, two symmetric bending (v_2) bands at 416 cm^{-1} and 502 cm^{-1}, and three asymmetric bending (v_4) bands at 610 cm^{-1}, 627 cm^{-1} and 678 cm^{-1}. Raman spectra collected from transformed regions of samples reacted during 12 h (Figure 5.3c) and 24 h (Figures 5.3e and 5.3g) show bands that can be assigned to Hap: the symmetric stretching (v_1), the symmetric bending (v_2) and the asymmetric bending (v_4) vibration modes of PO_4^{3-} are located at 961 cm^{-1}, 432 cm^{-1} and 588 cm^{-1}, respectively. The presence of a minor broad band around 880 cm^{-1} (Figures 5.3c and 5.3e) that can be attributed to the P-OH stretching is also consistent with Hap (Penel et al. 1998). Moreover, a triplet at 1007, 1045 and 1075 cm^{-1}, corresponds to the PO_4^{3-}asymmetric stretching (v_3) as well as a band at 3571 cm^{-1} can be assigned to the OH-stretching (Figure 5.3). In addition, a broad band near 946–949cm^{-1} assigned to the symmetric stretching (v1) (Jonas et al. 2014; Pedrosa et al. 2016) indicates the presence of β-TCP in the core of the sample reacted during for 24 h (Figure 5.3e). The absence of bands around 925 cm^{-1} (v1 mode) in all Raman spectra, confirms that whitlockite is not present in the system at any stage, in good agreement with the results of XRD analyses that only identify two calcium phosphate phases (β-TCP and Hap).

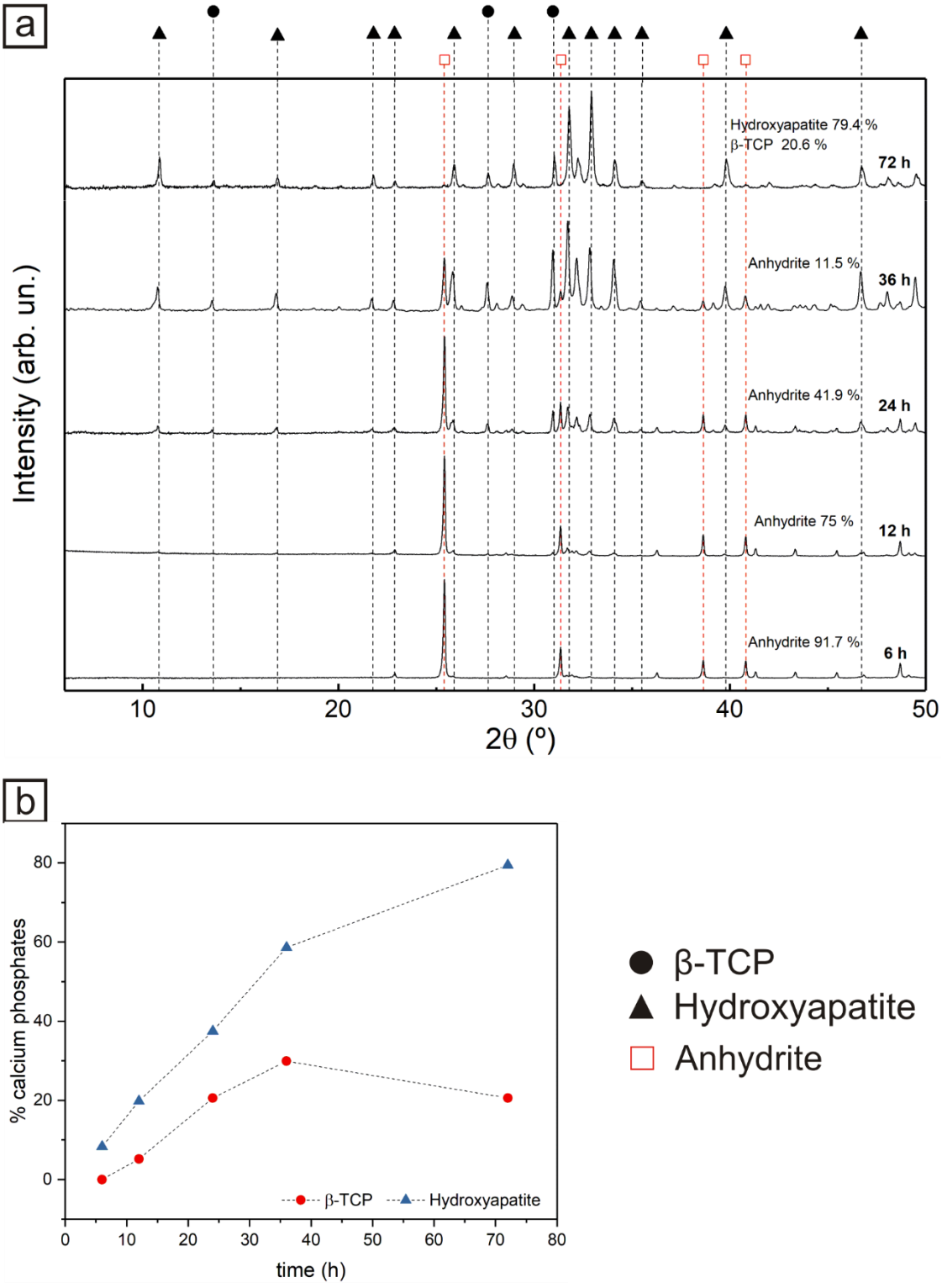

Figure 5.1. (a) X-ray powder diffraction patterns showing the mineralogical evolution of the replacement of anhydrite by calcium phosphates after hydrothermal interaction experiments carried out at 120°C at different reaction times. The reflections of anhydrite, hydroxyapatite and β –TCP were marked with squares, triangles and circles, respectively. (b) Percent calcium phosphates, calculated by Rietveld refinement, against reaction time.

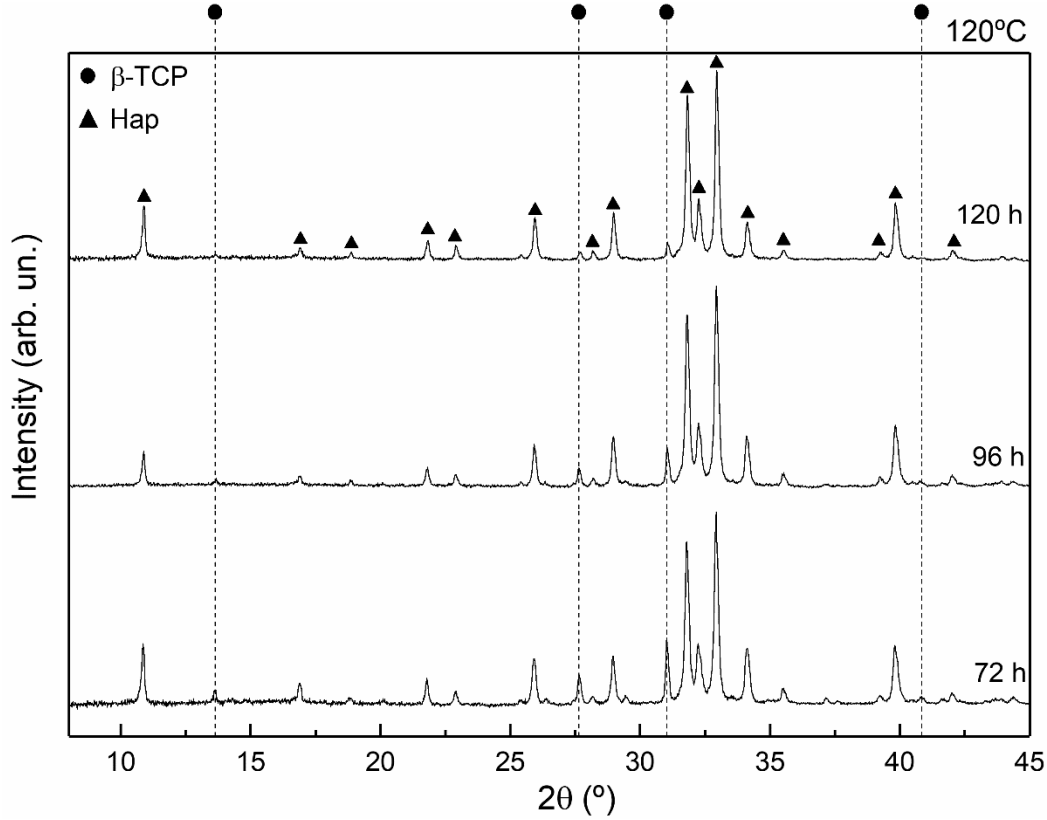

Figure 5.2 X-ray powder diffraction patterns showing the mineralogical evolution after complete replacement of anhydrite at 120 °C. The amount of β-TCP continues to decrease with time.

The main PO_4^{3-} vibrational mode (ν1) in β-TCP, which is located at 971cm^{-1}, is not apparent in any of the Raman spectra, most likely due to overlapping with the main band in the spectra of Hap (PO_4^{3-} ν1 at 961 cm^{-1}). No bands that can be attributed to β-TCP are present in areas close to the surface of the anhydrite sample reacted during 24 h (Figure 5.3g). In summary, XRD and Raman results corroborate that the transformed samples consist of mixtures of Hap and β-TCP at early stages of the replacement reaction. At T ≥ 180°C, hydroxyapatite/β-tricalcium phosphate ratio rapidly increases, and hydroxyapatite is the only phase in fully replaced samples. At T < 180°C hydroxyapatite/β-tricalcium phosphate ratio increases slowly. Furthermore, reacted samples still contain significant amounts of β-tricalcium phosphate even after full replacement of anhydrite is reached.

The anhydrite by calcium phosphate replacement initiates at the surface of the anhydrite subsamples and advances inwards, defining a sharp reaction front (Figures 5.3b and 5.3d). This front defines the interface between a shell-like transformed rim and the unreacted anhydrite core (Figures 5.3d). Figure 5.4a shows the contact between the transformed rim and the unreacted anhydrite core. As can be seen, the rim mainly consists of needle-like crystals arranged in fan-like bunches that appear oriented roughly perpendicular to the surface of the anhydrite core, and a smaller amount of euhedral rhombohedron-shaped crystals (Figure 5.4a). Based on Raman spectroscopy analysis and the known crystal morphology of calcium phosphates, we interpret the needle-like crystals as Hap (Zhu et al. 2008; Kasioptas et al. 2010; Yang et al. 2014; Li et al. 2016) and the euhedral rhombohedron-shaped ones as β –TCP (Roy and Linnehan 1974). Closer inspection of the latter evidences the presence on their surfaces of dissolution pits and nanometric Hap crystals that appear to grow in close spatial relation with the dissolution pits (Figure 5.4b).

Regardless the reaction temperature, the replacement reaction takes place with preservation of both the volume and external shape of the anhydrite crystals and results in the formation of calcium phosphate pseudomorphs. The pseudomorphs obtained in series of isothermal experiments were crosscut and SEM imaged. Figure 5.5 depicts SEM microphotographs of samples reacted during 12 h at 120°C (a), 150°C (b), 180°C (c) and 200°C (d). The transformed rim undergoes progressive thickening with increasing reaction time. The anhydrite core concomitantly shrinks. It is important to note that, before full anhydrite replacement is reached, the thickness of the transformed rim can significantly vary within each crosscut section, as is apparent in Figures 5.5a-5.5c. Differences in rim thickness, measured from opposite sides of a subsample along the same crystallographic direction, reflect the reduced exposure of the subsample surface that lies in contact with the reactor bottom to the interaction with the fluid.

Differences in rim thickness measured along different crystallographic directions reflect the different reactivity of anhydrite cleavage surfaces.

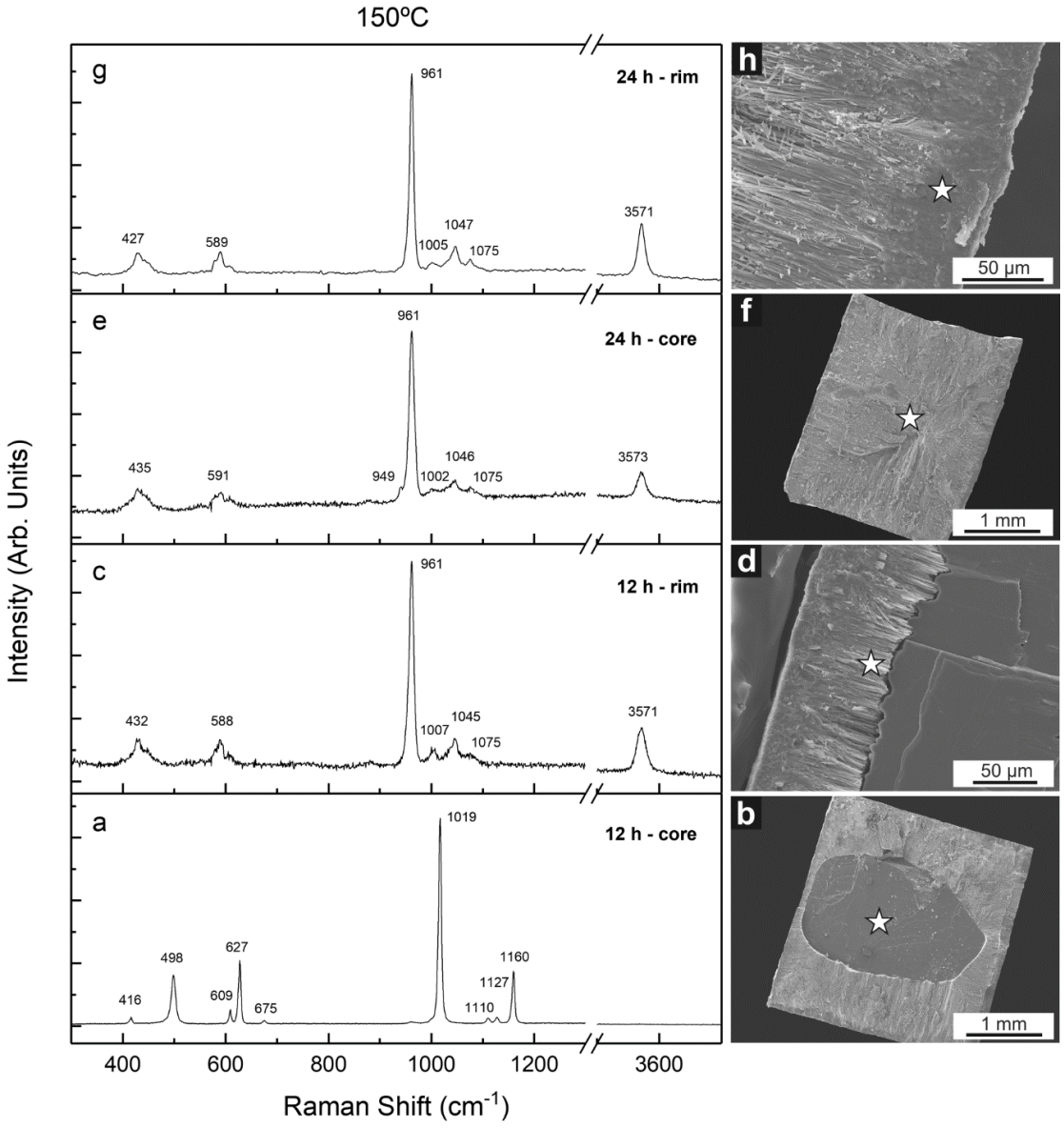

Figure 5.3. Raman spectra and SEM images of cross-section of partially replaced anhydrite samples for 12 h and 24 h at 150°C. The main vibrational bands of SO42- identified (a) in the core of anhydrite sample reacted (b) match well with anhydrite. The main vibrational bands of PO43- (c, e and g) identified in the rim (d and h) and core (f) of reacted samples corresponds to hydroxyapatite. The broad band at 949 cm-1 and the presence of the band at 1045 cm-1 (d) are characteristic of β-TCP. SEM micrographs of the reacted samples show the position where the spectra were measured.

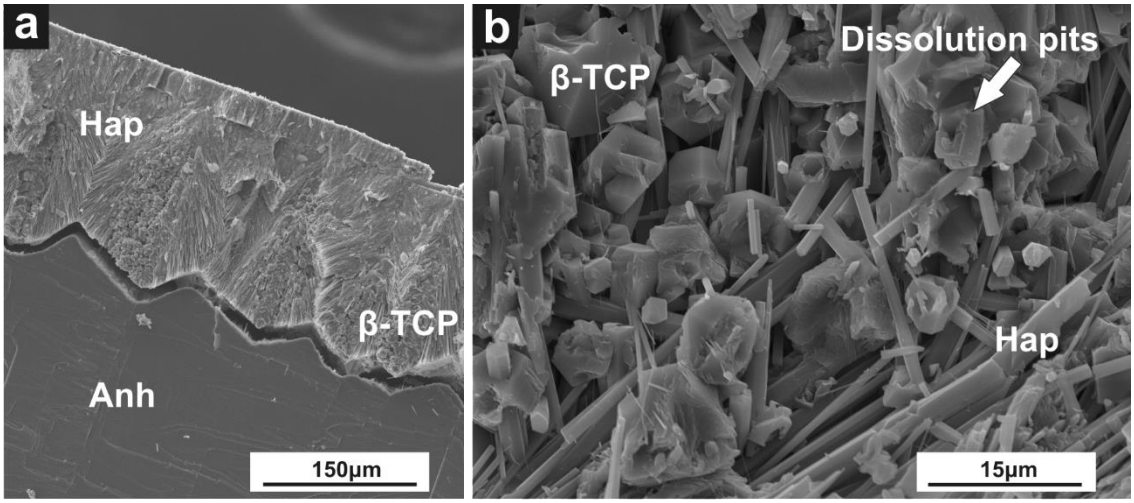

Figure 5.4. SEM micrographs of anhydrite (Anh) reacted with 2M (NH4)2HPO4 aqueous solution at different temperatures and reaction times. (a) After 3 h at 150°C a cross cut section image shows the unreacted anhydrite core and the two calcium phosphates that can be distinguished, β-tricalcium phosphate (β -TCP) and hydroxyapatite (Hap). Hydroxyapatite is clearly more abundant and is growing in elongated hexagonal needle-like crystals that are arranged perpendicular to the unreacted anhydrite core and β-TCP shows an euhedral habit. (b) At higher temperatures and shorter reaction times (200°C and 2 h), β –TCP appears with dissolution features and at the same time the development of smaller and thinner hydroxyapatite crystals from β –TCP faces.

As can be seen, the reaction front advances faster with increasing temperature. Thus, after 12 h of reaction, in samples reacted at 120°C and 150°C and 180°C, the average transformed rim thickness was 250, 550 and 1500 µm, respectively (Figures 5.5a-5.5c). After 12 h reaction, no unreacted core is observed in the crosscut sections of samples from experiments conducted at 200°C reacted (Figure 5.5d). This is consistent with the results of both, X-ray diffraction and Raman spectroscopy analyses, which also support the complete replacement of anhydrite by calcium phosphate phases in samples reacted 12 h at 200°C.

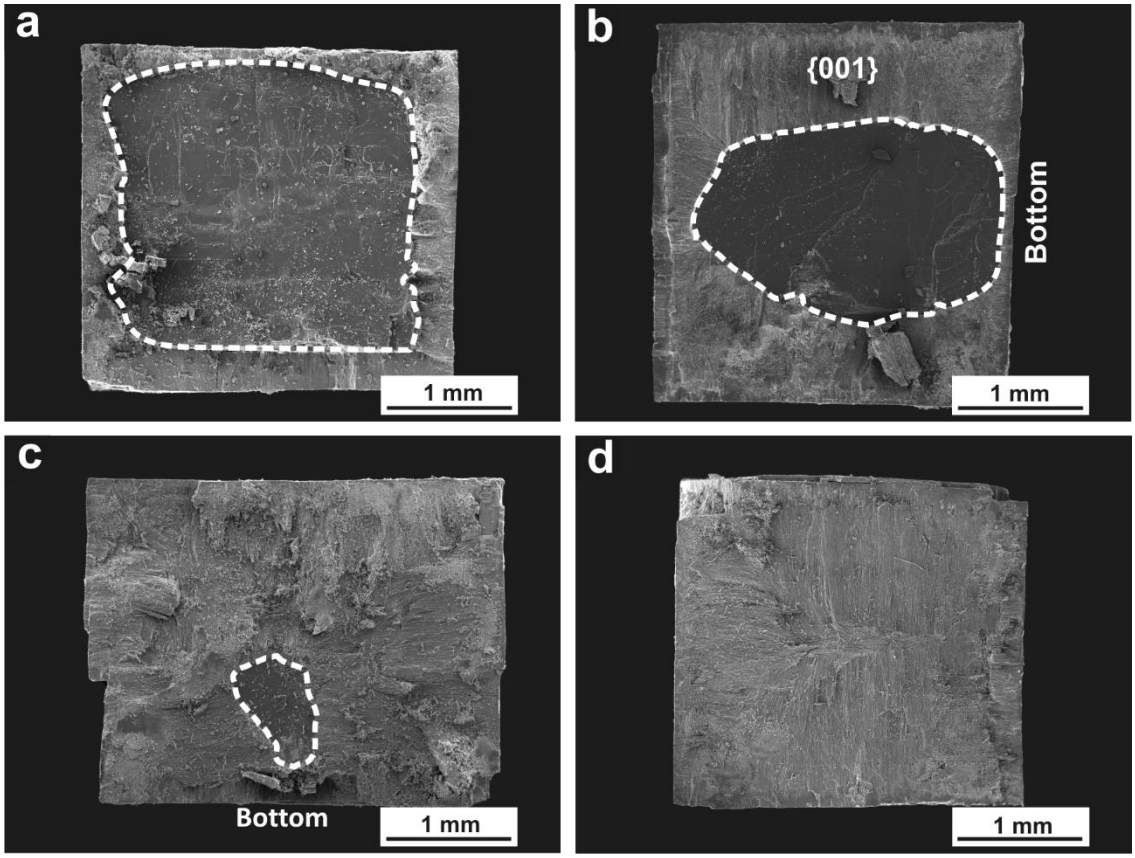

Figure 5.5. SEM micrographs of cross-sections surfaces showing the anhydrite replacement by calcium phosphates after 12 h of reaction at temperatures of 120 (a), 150 (b), 180 (c) and 200 (d).

5.3.2. Kinetics of the replacement reaction

Several sets of hydrothermal interaction experiments were conducted to derive information on the kinetics of the replacement of anhydrite single crystals by calcium phosphate crystal aggregates. Table 1 summarises the fraction of anhydrite, Hap and β-TCP, as determined from the Rietveld refinements of X-ray powder diffraction patterns of samples interacted with the phosphate-bearing aqueous solution at temperatures between 120°C and 200°C during times that varied between 2 and 72 h. In Figure 5.6, the fraction of sample transformed into calcium phosphate phases (y_{CaP}) is plotted against the reaction time (t) for each isothermal experiment. Figure 5.7 shows the temperature dependence of the anhydrite-by- calcium phosphate reaction, evidenced in the

Hancock-Sharp plots derived by fitting the linearized Avrami expression (equation 2) to the experimental data. All fitted lines are approximately parallels. The Avrami parameters calculated for each set of isothermal data are also shown in Figure 5.7. The activation energy can be obtained by plotting the slopes of the linear regressions in Figure 5.7 against reciprocal temperature in an Arrhenius plot (Figure 5.8. The rate constant (*k*) clearly increases with temperature and the linear regression yields an empirical activation energy, *Ea* of 40.2 ± 1.9 kJ/mol.

Alternatively, empirical activation energies can also be determined by using the isoconversional method. *Ea* values were calculated for three different fractions of anhydrite replacement by calcium phosphate, 0.40, 0.60, and 0.80 (Figure 5.9). In all cases, the data are well described by linear correlations and show closely parallel trends. The empirical *Ea* values yielded from these fittings slightly decreases, from 40.4 ± 2.3 to 39.3 ± 2.3 $kJ \cdot mol^{-1}$, as the replaced fraction increases from 40 to 80%.

120°C				150°C				180°C				200°C			
t (h)	% Anh	% β-TCP	% Hap	t (h)	% Anh	% β-TCP	% Hap	t (h)	% Anh	% β-TCP	% Hap	t (h)	% Anh	% β-TCP	% Hap
6	91.7		8.3	3	78.5	3.2	18.3	2	73.5	12.9	13.6	2	58.8	27.1	14.1
12	75	5.2	19.8	6	48.4	20.4	31.3	4	40.3	21.9	37.9	4	26.8	6.6	66.7
24	41.9	20.6	37.5	8	41	22.5	36.5	6	20	16.7	63.3	6	8.9	4.4	86.7
36	11.5	29.9	58.6	12	19.8	21.1	59.2	8	8.2	7.7	84.2	10	0	0	100
48	9.5	17.2	73.3	20	0	13.5	86.5	10	6.1	3.9	90				
72		20.6	79.4					12	4.1	2	93.9				
								14	0	0	100				

Table 5.1. Calculated transformation (% calcium phosphates) calculates by Rietveld refinement of X-ray diffraction patterns during hydrothermal experiment.

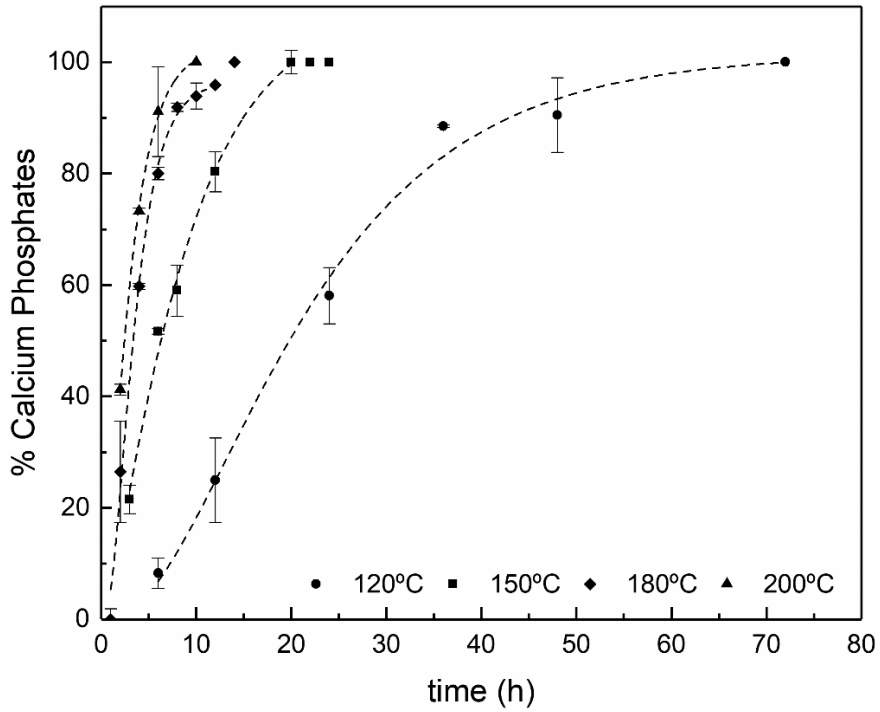

Figure 5.6. Fraction of calcium phosphates replacing anhydrite crystals against the reaction time for each isothermal experiments. The lines are fitted to the Chapman equation.

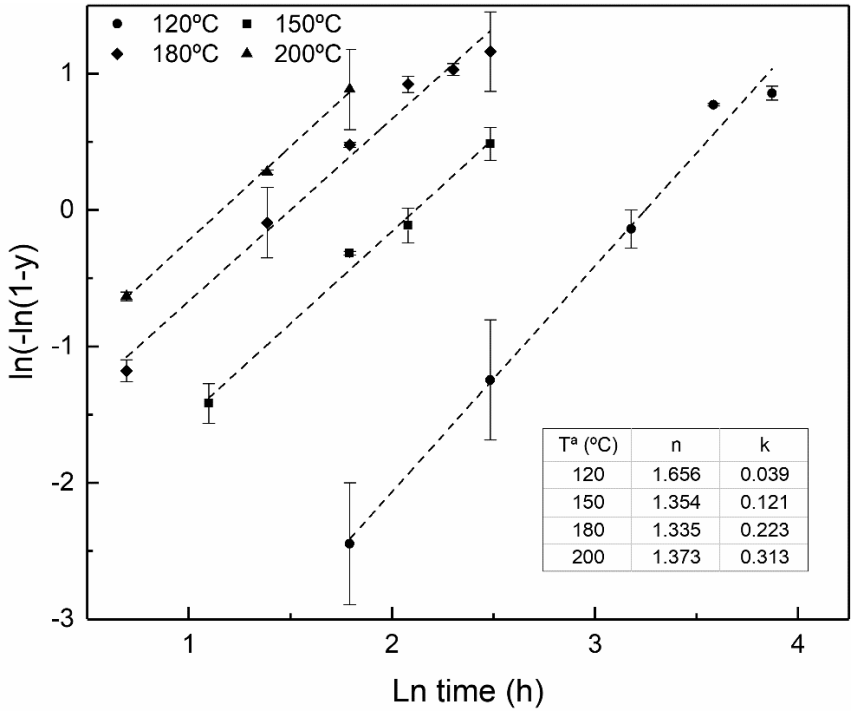

Figure 5.7. Plot of the calcium phosphates transformed fraction (y) versus time. From the slope and the intercept, Avrami rate low parameters (n and k) are determined.

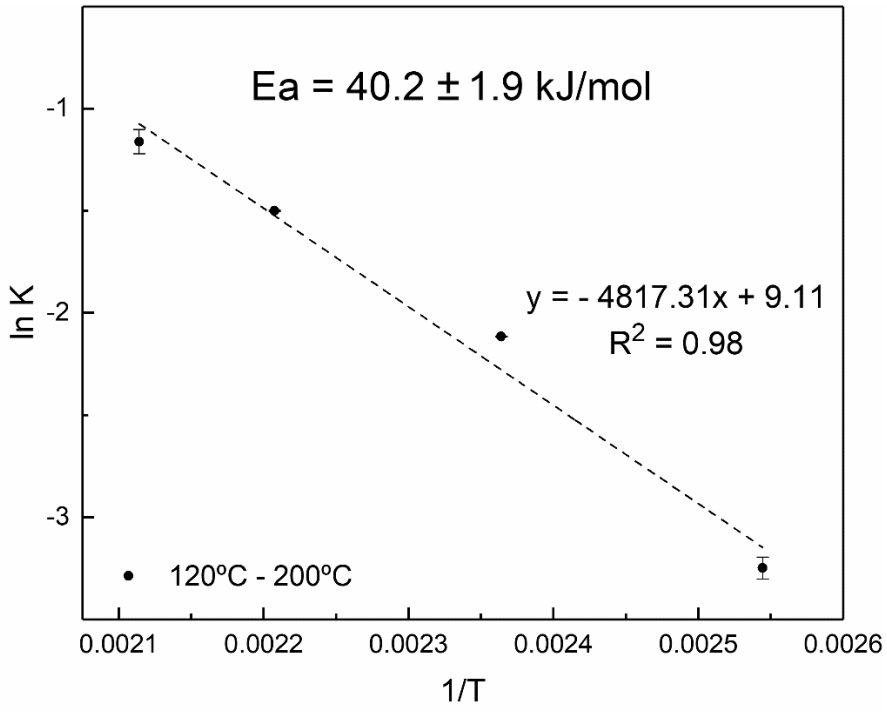

Figure 5.8. Linear fitting of the rate constant K versus the reciprocal of temperature (expressed in Kelvin).

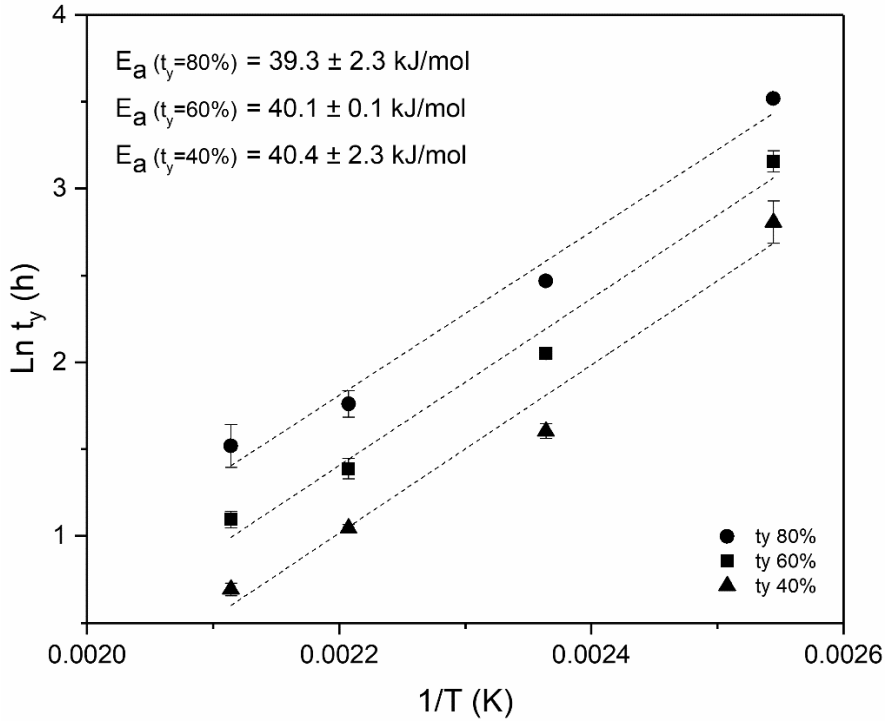

Figure 5.9. Experimental data of the time (lnt_y) for several fractions (Y= 40, 60 and 80%) of transformed anhydrite versus 1/T. The slope of the fitting straight lines corresponds to E_a/R.

5.4. Discussion

5.4.1. Replacement reaction mechanism

Upon interaction with a P-bearing aqueous solution at temperatures between 120°C and 200°C, anhydrite single crystals are replaced by mixtures of β-TCP and Hap. Textural features of the reacted samples are consistent with the replacement taking place through an interface coupled dissolution-reprecipitation reaction (Putnis 2002, 2009b; Putnis and Putnis 2007; Ruiz-Agudo et al. 2014). Firstly, the reaction starts at the surface of anhydrite and progresses from rim to core through the advancement of a reaction front that appears sharp, well defined, and approximately parallel to the original anhydrite surface. Secondly, the external shape as well as most surface features of anhydrite crystals are preserved throughout the reaction, which has a pseudomorphic character. Thirdly, replaced samples consist of aggregates of crystals of the product phases and contain large amounts of porosity. All these features are characteristic of mineral replacement processes that occur mediated by the presence of a fluid phase. The reaction takes place in the interfacial layer of fluid. When the process starts, the fluid is undersaturated with respect to the primary phase. This drives its dissolution and determines that the interfacial layer of fluid soon becomes supersaturated with respect to the product(s). Anhydrite dissolution releases Ca^{2+} and SO_4^{2-} ions to the interfacial layer of fluid. To evaluate the physicochemical conditions in the interfacial fluid at early stages of replacement process we simulate the dissolution of a small amount of anhydrite in a small volume of fluid using the geochemical code PHREEQC and the lnll.dat database (Parkhurst and Appelo 1999). We consider the successive dissolution of layers of anhydrite whose thickness corresponds to one unit cell (a_0 = 6.993 Å, b_0 = 6.995 Å and c_0 = 6.245 Å; Hawthorne and Ferguson 1975). For a 3 x 3 x 3 mm sized crystal the dissolved anhydrite volume is 3.64 x 10^{-8} cm^3 of $CaSO_4$, which

corresponds to 7.94 x 10^{-10} moles of anhydrite. We consider two realistic thickness for the fluid boundary layer, 100 nm and 1000 nm, which corresponds to a volume of interfacial solution of 5.40 x 10^{-6} cm^3 and 5.4 x 10^{-5} cm^3, respectively (Ruiz-Agudo et al. 2015). The state of supersaturation is defined by the value of the saturation index (SI), which is expressed as:

$$SI = \log (IAP/Ksp) \quad (7),$$

where IAP is the ion activity product and Ksp is the solubility product of the phase considered. SI = 0 indicates that the system is in equilibrium with a given phase, this is saturated, while SI < 0 and SI > = 0 indicate that the system is undersaturated and supersaturated, respectively. At 150°C, the dissolution of one anhydrite monolayer in both 100 nm and 1000 nm boundary layers results in the interfacial fluid layer becoming supersaturated with respect to HAP and β -TCP. Thus, the 100 nm thick boundary layer becomes supersaturated with respect to both, Hap and β -TCP (SI_{Hap} = 23.86, $SI_{\beta\text{-}TCP}$ = 3.42) after the dissolution of one anhydrite monolayer, while still remaining undersaturated with respect to this latter phase (SI_{Anh} = -7.36). Similarly, the 1000 nm thick boundary layer reaches supersaturation with respect to Hap and β -TCP (SI_{Hap} = 19.11, $SI_{\beta\text{-}TCP}$ = 0.56) after the dissolution of one anhydrite monolayer. The simulation of the dissolution of one anhydrite monolayer at other experimental temperatures also yields SI > 0 for both, Hap and β - TCP. The SI value for all the phases involved increases as successive anhydrite monolayers dissolve. Once the interfacial fluid reaches the supersaturation threshold for Hap and β – TCP nucleation, both calcium phosphate phases will precipitate at the reaction front. As a replaced rim forms, the presence of pores within it guarantees a continuous communication between the bulk solution and the reaction front, facilitating mass transport to and from the interface (Putnis et al. 2005; Putnis and Putnis 2007; Pollok et al. 2011; Forjanes et al. 2020b). The progress of the reaction involves the definition

of a dissolution-crystallisation feedback loop. Thus, anhydrite dissolution promotes calcium phosphate precipitation in the interfacial fluid and *vice versa*. The preservation of the external shape of anhydrite crystals requires that the rates of anhydrite dissolution and calcium phosphate precipitation are coupled (Putnis 2002, 2009b; Putnis and Putnis 2007; Pollok et al. 2011; Ruiz-Agudo et al. 2014). In the temperature range of the experiments, the solubility product of anhydrite varies between $10^{-4.36}$ at 120ºC and $10^{-4.83}$ at 200ºC (Freyer and Voigt 2003). The solubility product of Hap strongly decreases with increasing temperature within this temperature range, being $10^{-58.33}$ at 120ºC and $10^{-70.64}$ at 200ºC (Kaufman and Kleinberg 1979). In contrast, the solubility product of β – TCP slightly increases with temperature in the temperature range of the experiments from $10^{-26.63}$ at 120ºC to $10^{-25.42}$ at 200ºC (Wang and Nancollas 2008). Considering the very large differences in solubility between anhydrite and both calcium phosphates, it is likely that the latter phases form under very high supersaturations and can be expected that this process occurs rapidly at any experimental temperature. Therefore, anhydrite dissolution is most likely the rate-limiting process. However, the progress of the reaction requires continuous chemical exchange with the bulk solution and the rate of mass transport through the porous replaced rim may play a significant role modulating the overall kinetics of the anhydrite by calcium phosphate replacement reaction.

5.4.2. Reaction pathway

The mole ratio of β-TCP/Hap vary with temperature and reaction time. At 120°C, β-TCP/Hap mole ratio first increases with reaction time and later slowly decreases. At all other temperatures β-TCP/Hap mole ratio progressively decreases with increasing reaction time. This decrease takes place much more rapidly with increasing temperature. In the temperature range of the experiments, β-TCP is more soluble than Hap (llnl.dat) and, consequently, less

stable. Therefore, β-TCP forms as a thermodynamically metastable phase. Crystallisation of metastable phases often occurs under high supersaturations. The large solubility difference between anhydrite, β-TCP and Hap determines that the layer of fluid at the interface will be very highly supersaturated with respect to both, β-TCP and Hap. Under these conditions, both calcium phosphate phases can nucleate. Indeed, the presence of Hap at very early stages of the replacement process suggests a competition between the nucleation and growth of β-TCP and Hap. Metastable β-TCP latter transforms into Hap according to an Ostwald ripening process. This transformation most likely occurs through a dissolution-reprecipitation reaction since dissolution pits are apparent in the surface of β-TCP and needle-like Hap crystals grow spatially associated to those pits (Fig. 5.4b). The competition between the nucleation and growth of β-TCP and Hap operates longer and plays a more important role at lower temperatures as is evidenced by the initial increase in the β-TCP/Hap mole ratio as well as the large amount of β-TCP in almost fully replaced samples at 120°C.

The replacement reaction can be described through the following equations:

$$3CaSO_4 + 2(NH_4)_2HPO_4(aq) \rightarrow Ca_3(PO_4)_2 + (NH_4)_2SO_4(aq) + 2(NH_4)HSO_4(aq) \quad (5)$$

$$5CaSO_4 + 3(NH_4)_2HPO_4(aq) + H_2O \rightarrow Ca_5(PO_4)_3OH + (NH_4)_2SO_4(aq) + 4(NH_4)HSO_4(aq) \quad (6)$$

$$5Ca_3(PO_4)_2 + 3H_2O \rightarrow 3Ca_5(PO_4)_3OH + H_3PO_4(aq) \quad (7)$$

The precipitation of Hap, as a basic salt, results in a pH decrease in the fluid phase (equations 6 and 7). This is in good agreement with the change from an initial pH_i = 8.1 (1) to a pH of 6.8 (1) measured at the end of the experiments.

5.4.3. Porosity generation

Several factors explain the generation of porosity during pseudomorphic replacement reactions. Porosity balances the loss of volume in reactions that involve a negative molar volume change and guarantees the preservation of the original external shape of the primary phase. In the case of the replacement of anhydrite (V_{Anh}= 45.84 cm^3/mol) by mixtures of β-TCP ($V_{\beta-TCP}$= 33.14) and Hap (V_{Hap}= 31.79 cm^3/mol), all relevant molar volume changes are negative: -12.70 cm^3/mol (27,7%) and -14.05 (30.65%), the changes associated to the transformation of anhydrite into β-TCP and Hap, respectively, and -1.35 (4.07%) the change associated to the transformation of β-TCP into Hap. These molar volume changes only very slightly vary (< 1%) depending on the experimental temperature (Evans 1979; Nakamura et al. 1990). The porosity required to balance the molar volume change associated to the replacement reaction will be around 30%, although the exact value will vary depending on the β-TCP/Hap mole ratio in the calcium phosphate mixture. Since this ratio changes with reaction time and temperature, small differences in porosity can be expected depending on the experimental conditions.

A second source of porosity is the difference in solubility between the primary and product phases (Putnis 2002, 2009b; Pollok et al. 2011). β-TCP and Hap are less soluble than anhydrite. This means that part of the dissolved anhydrite is lost to the solution when this phase is replaced by β-TCP and Hap. The negative solubility change associated to the replacement will also be balanced by generation of porosity that will add up to that that balances the negative molar volume change. The volume of solubility change-related porosity

is also influenced by reaction time and temperature as both parameters determine the β-TCP/Hap in the reacted sample. Differences in the porosity formed during the replacement may influence the mass transport rate and be reflected by the overall kinetics of the replacement reaction (Jonas et al. 2013; Pedrosa et al. 2017).

5.4.4. Textural features and evolution

Mass transport from and to the interface is not only affected by the increase of porosity during the replacement but also by the specific characteristics of this porosity regarding pore shape, size and connectivity (Putnis et al. 2005; Jonas et al. 2013; Putnis 2015; Yuan et al. 2018; Forjanes et al. 2020a). Yuan et al. (2018) studied the porosity generated during the replacement of calcite by cerussite and identified three types of pores: Open pores that directly connect the reaction front and the bulk solution, trapped pores, which are connected through grain boundary diffusion between the crystals of the product phase and open pores to the bulk solution, and isolated pores, located between differently oriented crystals of the product. All types of pores are filled by fluid, but the chemistry of this fluid will vary due to differences in the mass transport rate. Chemical exchange between the interfacial fluid and the bulk will be more efficient if the porosity mainly consists of open pores, while the predominance of isolated pores will strongly hinder mass transport and the progress of the reaction. Both habit and textural relationships of the product crystals are key features that define the relative amount of open, trapped and isolated pores in replaced samples. The existence/absence of epitactic relationships between the product and the primary phase is another key factor. We observe no evidence of epitatic growth of either β-TCP or Hap on anhydrite surfaces. β-TCP crystals grow randomly oriented, while Hap grow as fan-like bunches of needle-like crystals arranged approximately perpendicular to the

anhydrite surface (Figure 5.4). β-TCP crystals accumulated in the central region of this bunches. Needle-like crystals within bunches that seem to originate at the region occupied by β-TCP crystals are arranged with their long axis approximately parallel between them. This arrangement is characteristic of competitive growth between crystals that nucleate randomly oriented on a surface and have a preferential growth direction. Those crystals oriented with the preferential growth direction perpendicular to the surface can grow freely, while the growth of all differently oriented crystals rapidly becomes prevented by the lack of space. It is noteworthy that the porosity generated during replacement reactions has a transient nature, and its features evolve along time. In the case of the replacement of anhydrite by calcium phosphate, the very different habit of β-TCP and Hap crystals will determine differences in the relative abundance of different types of pores depending on the mole β-TCP/Hap ratio in the replaced sample. As pores between elongated, parallel crystals tend to be open, it can be expected that the number of open pores in replaced samples will increase as more β-TCP transforms into Hap.

5.4.5. Rate-limiting process

Coupled dissolution-precipitation reactions are heterogeneous processes. Their kinetics is either limited by the dissolution of the primary phase or by the precipitation of the product phase(s). Several observations give support to the interpretation that the dissolution of anhydrite is the limiting step of the anhydrite by calcium phosphate replacement reaction Moreover, textural features of the reacted samples indicate that the reaction progresses from rim to core. This has been interpreted by different authors as evidence of the precipitation of the product(s) taking place at a faster rate than the dissolution of the primary phase. Altree-Williams et al. (2015, 2017) pointed out that mineral replacement reactions which are rate-limited by the precipitation of the product

also result in the formation of pseudomorphs. However, external features of these pseudomorphs are less accurately preserved as the formation of overgrowths blurs them. Moreover, these pseudomorphs show hollow cores. Neither the development of overgrowths nor the formation of a hollow core is observed during the formation of calcium phosphate pseudomorphs after anhydrite.

Altree-Williams et al. (2019) calculated an average empirical activation energy (E_a) of 46.2 ± 7.6 kJ/mol for the carbonation of anhydrite. These authors interpreted the slightly lower value of this activation energy compared to previously reported values of the activation energy for anhydrite dissolution [50 kJ/mol, Bildstein et al. (2001); 61.0 ± 1.0 kJ/mol, Kontrec et al. (2002)] as indicative of anhydrite dissolution being the rate-limiting event of anhydrite carbonation kinetics. Moreover, they concluded that, since the reported values of the activation energy for the diffusion of dissolved calcium are much smaller (E_a = 12.6 kJ/mol), mass transport of species from the bulk solution to the reaction interface and backwards must occur a faster rate compared to anhydrite dissolution. The average empirical activation energy of the anhydrite by calcium phosphate replacement reaction determined in this work using the isoconversional method is 39.9 ± 1.6 kJ/mol. The similarity of this value to the previously reported activation energy for anhydrite carbonation supports that anhydrite dissolution also controls the kinetics of anhydrite phosphation.

The experimental data fitted the Avrami model yields an E_a = 40.2 ± 1.9 kJ/mol, which is identical to that obtained using the isoconversional method regardless of the transformed fraction considered. The calculated A is 9045.3 $(hours)^{-1}$ and the resulting integral law is $Y_{CaP} = 9045.3e^{(-40/RT)}t$. Applying the law equation and assuming that the reaction mechanism is the same as that controlling the process in the 120-200°C range, it can be estimated that at 20°C

the time required to for the complete replacement of anhydrite single crystals by calcium phosphate will be around 4 months. However, similar experiments performed under lower temperature conditions need to be performed to confirm the soundness of this approach.

The shape of the rate curves in Figure 5.6 is approximately the same for those corresponding to 150°C, 180°C and 200°C and the curves can be described as isokinetic. Consistently, the Avrami reaction exponents (n) corresponding to these three temperatures show almost identical values (~ 1.35). The shape of the rate curve corresponding to 120°C is slightly different, which correlates with a larger Avrami exponent (~ 1.66 at 120°C) (Figure 5.6). The value of Avrami exponents is characteristic of the rate-limiting kinetic mechanism that operates at each temperature (Redfern 1987). All calculated Avrami exponents in this work stand between those defined by Hancock and Sharp (1972) for first-order and higher-order processes. However, it is important to keep into mind that Hancock and Sharp (1972) studied solid-state transformations, while the replacement of anhydrite by calcium phosphate phase takes place mediated by the presence of a fluid phase. Several authors have interpreted changes in the value of the Avrami exponent with temperature as reflecting a balance between changes in the solubilities of the primary and secondary phases combined with changes that affect mass transport processes (Zhao et al. 2009; Altree-Williams et al. 2019). The solubility of anhydrite and apatite decrease with increasing temperature. However, this decrease follows a different trend depending on the phase (Gregory et al. 1974; McDowell et al. 1977; Otálora and García-Ruiz 2014; llnl database from PHREEQC code). Moreover, in the temperature range of the experiments the solubility of β–TCP shows a positive dependence with temperature. These differences in solubility evolution may be reflected by the Avrami exponent. Anhydrite phosphation does not only involve the dissolution of anhydrite to form Hap. β–TCP precipitation is metastable and, as the reaction

progresses, β–TCP dissolves to form Hap. The formation of β–TCP and its transformation into Hap may also weigh differently on the overall kinetics of the replacement depending on the reaction temperature. Reported values of the empirical activation energy of β–TCP dissolution are around 16.3 kJ/mol, which is much smaller a value than that of the activation energy for the dissolution of anhydrite and very close to the activation energy for the diffusion of dissolved calcium (Bohner et al. 1997). Although its activation energy is small, the influence of β–TCP dissolution may sufficiently influence the kinetics of Hap formation as to explain changes in the Avrami exponent. Moreover, the β–TCP into Hap transformation differently affect textural features of the reacted samples depending on the temperature. After complete replacement of anhydrite by calcium phosphate, β–TCP content is highest in samples reacted at 120°C (~20%), followed by those reacted at 150°C (~13%). Given the very different morphology of β–TCP crystals compared to those of hydroxyapatite as well as the slightly larger molar volume of the former, differences in porosity and pores arrangement may further explain small kinetics changes at different reaction temperatures (Putnis et al. 2005; Jonas et al. 2013; Putnis 2015; Pedrosa et al. 2017).

CHAPTER 6

GENERAL DISCUSSION

6. General discussion

Minerals can undergo phase transformations due to variations in the physico-chemical conditions in the system, resulting in changes of chemical composition and/or crystalline structure. These processes, which include transformations between minerals with the same composition (polymorphs) or involve both, structural and chemical changes (newly formed phases, pseudormophic replacements), occur on different time scales and play a key role in the cycling of elements in all geological environments. At water free environments, solid state diffusion may become a feasible mechanism for mineral transformation, especially at increasing temperatures deeper within the Earth. However when surface and sub-surface conditions prevail, the presence of fluid phases promotes the development of solvent-mediated reactions. Under these low temperature conditions, reactions occurs at a rate too fast to be explained by solid-state mechanisms, and take place far from thermodynamic equilibrium, whereby kinetic factors playing an important role in mineral transformation processes (Putnis 2002, 2009a). The reaction between fluids and mineral surfaces usually involves different sorption mechanisms, such as adsorption, sorption and surface precipitation being relevant in several mineral transformations. The prevalence of one of the sorption processes over the other ones will depend on the minerals involved as well as the physical and chemical properties of the system. For instance, adsorption contribution to sorption is significant in those minerals as zeolites, whose structures contain large and interconnected channels that allow ion exchange to occur at relevant rates (Tahervand and Jalali 2017). However, the kinetics of ion diffusion through carbonate and sulphate mineral structures is relatively slow and absorption can be considered negligible at room temperature. On the contrary, dissolution-crystallisation reactions are common processes in surface and subsurface

geological environments, involving mineral phases of highly different solubility, from highly soluble, like halite, moderately soluble, like gypsum and anhydrite, or sparingly soluble like calcite, aragonite and silicate minerals (Putnis and Putnis 2007; Putnis 2009a; Pollok et al. 2011; Ruiz-Agudo et al. 2014). When these dissolution-crystallisation reactions occur with the coupling of dissolution and precipitation rates, the original shape and volume of the primary mineral can be preserved, leading to pseudomorphic replacements, where porosity generation is required to ensure continuous communication between the interface and the bulk fluid, promoting the progress of the replacement reaction. These reactions are known as interface couple dissolution-precipitation (ICDP) reactions (Putnis 2002, 2009a, 2015; Zhao et al. 2009; Jonas et al. 2013; Ruiz-Agudo et al. 2014).

Previous works point out that dissolution-precipitation reactions involving sulphates, carbonates and phosphates can be considered an effective long-term way of removing different inorganic pollutants from natural water and wastewaters (Pina et al. 2000; Rodríguez-Blanco et al. 2007; Pinto et al. 2009; Prieto et al. 2013; Wang et al. 2013; Morales et al. 2014). Furthermore, the use of biogenic $CaCO_3$ materials (biominerals) as heavy metal scavengers has also been explored (Köhler et al. 2007; Alidoust et al. 2015; Zhou et al. 2017). Although numerous studies have shown that, the sorption of heavy metals by mineral surfaces or into crystalline structures control the reduction of dissolved contaminants in water, however, physicochemical factors that govern both evolution and kinetics of reactions under epigenetic conditions remains poorly understood. This PhD thesis aims to understand the factors that control the progress of ICDP reactions and the evolution of textures of the secondary phases formed during these mineral transformations by studying the interaction of dissolved Pb with calcium carbonates and gypsum and P with anhydrite under Earth's surface conditions and hydrothermal conditions, respectively.

As previously mentioned, lead is one of the most dangerous heavy metal causing long-lasting damage in underwater environments and has increased over the last decades as a result of its use in numerous industries. In this context, the amount of dissolved Pb in wastewater must be effectively reduced to avoid, or at least minimize, contamination of aquifers and surface waters. In addition to heavy metals, other elements such as phosphorous have become an environmental problem due to their excessive use as fertiliser in extensive agriculture to intensify production. The overuse of phosphorus as a fertiliser causes eutrophication of water bodies and consequent pollution of aquifers and flowing waters (Smith 2003; Wei and Bailey 2021). The differences between the volumes of phosphates used in different industries versus the amounts of P recovered (40-50%) (Egle et al. 2016), as well as their limited resources, significantly affect phosphate resources for its use in the near future. Due to the main role of P in the life cycle, the scarcity of this element in the Earth's crust and its ability to pollute soils, sediments and ground and running waters, developing methods for the recovery of P through the precipitation of phosphate phases on the surface of pre-existing minerals would have an outstanding importance.

Based on all previous studies, the starting materials used in the experiments carried out in this research consist of some of the most common rock-forming mineral in sedimentary basins (calcium carbonates and calcium sulphates) and biogenic calcium carbonates to study their reactivity under near-surface conditions. The mineral - pollutant - water systems investigated in this PhD thesis show that dissolution-precipitation is the main mechanism for the removal of Pb or P from the fluid. However, several factors such as the solubility of the solid phases, the reactive surface of the primary phase, the formation of solid solutions, the epitaxial relationships between the primary and secondary phases or the arrangement of porosity in the newly formed phases determine the effectiveness of dissolution-precipitation reactions for the removal of these

heavy metals. In the case of systems of environmental interest, interactions of Pb-rich aqueous solutions with both common rock-forming minerals (gypsum and calcite) and biogenic calcium carbonates (biocalcite and bioaragonite) have been carried out to understand the physicochemical factors that control the removal of Pb from polluted aqueous solutions. In addition, the study of the pseudomorphic replacement of anhydrite by polycrystalline calcium phosphates under diagenetic conditions sheds light on the formation of calcium phosphates. This chapter is a general discussion of the results presented in previous chapters of this thesis that may contribute to a better understanding of the fate of dissolved P and Pb species in diverse Earth systems.

6.1. Dissolution-precipitation reactions: Pb removal

The interaction of Pb-bearing solutions with inorganic minerals (calcite and /or gypsum) or biogenic calcium carbonates (bio-calcite or bio-aragonite) results in a reduction of the Pb concentration in the fluid due to the precipitation of newly formed Pb-bearing solid phases. In this experimental work, very high initial concentrations of Pb (from 2230 mg/L to 230 mg/L) have been used, of which large amounts (between 90 and 99%) have been removed. However, the final Pb concentration in the liquid phase was always well above the maximum permitted in drinking water (0.01 mg/L). Figure 6.1 summarizes the results of the Pb-mineral-water systems, for which variations of an order of magnitude in both grain size and the amount of original minerals have been considered. The amounts of Pb remaining in the solution after interaction with phases of geological or biogenic origin have been compared with the results obtained by Di Lorenzo et al. (2020).

In the case of the interaction of aqueous solutions bearing Pb with gypsum and /or calcite, it is worthwhile to mention that all previous

experimental studies by interacting polluted-bearing aqueous solutions were conducted by considering these phases separately (Godelitsas et al. 2003; Astilleros et al. 2010). Thus, no previous study had taken into consideration that the dissolution of any of these Ca-bearing minerals significantly alters the physicochemical characteristics of the aqueous solution and this change affects the progress of the mineral-fluid phase interaction. In the present study, the effectiveness of mixtures of gypsum and calcite crystals as Pb scavengers has been compared with the effectiveness of these minerals when they are considered separately. The interaction resulted in a Pb removal that could be fast and extensive when gypsum was present in the system, but progressed at a comparably extremely slow rate in the absence of this phase. Regardless of its kinetics, in all the systems studied coprecipitation of Pb-bearing mineral phases was the main mechanism of Pb removal. These Pb-bearing phases formed as a result of the reaction between dissolved Pb and SO_4^{2-} and/or CO_3^{2-} ions released during the dissolution of the primary phases, gypsum, and/or calcite. Interaction of Pb-bearing solutions with gypsum results in the early formation of anglesite ($PbSO_4$) both in the bulk and on the surface of crystals of the primary phase(s) leading to a rapid drop in Pb concentration to ~3 mg/L. No further Pb removal was achieved through interaction of Pb-bearing solutions only with gypsum, no matter the duration of the interaction. Thus, this system seems to be controlled by the formation of relatively insoluble anglesite ($Ksp=10^{-7.79}$) (Parkhurst and Appelo 1999). These results are in agreement with those published by other authors reporting similar decrease in Pb concentration after interaction with calcium sulphates (Astilleros et al. 2010; Morales et al. 2014). However, when Pb-bearing solutions interacted with calcite, the sluggish kinetics of calcite dissolution made Pb removal through precipitation of lead carbonates (cerussite and hydrocerussite) a very slow process, which resulted a very inefficient one compared to the precipitation of anglesite, at least within the time set of the

experiments in the present research. This contrasts with the findings of Godelitsas et al. (2003), who reported a higher decrease in Pb concentration. The large difference in the size of the calcite crystals used in both studies, which were much smaller in Godelitsas et al. (2003) research, may be a plausible explanation for these differences. The smaller crystal size results in a larger crystal surface area exposed to the interaction with the Pb-bearing aqueous solutions, resulting in a much faster release of calcium and carbonate ions into the liquid phase, leading to supersaturation of the Pb-bearing solution with respect to the lead carbonate phases. In contrast, the simultaneous interaction of Pb-bearing aqueous solutions with crystals of both phases, gypsum-calcite, resulted in Pb removals that, depending on the initial Pb concentration (between 1 and 10mM), were from as much as up to 5 times and up to 500 times larger than those attained through interaction only with gypsum or calcite, respectively.

From an environmental point of view, the most striking result is the highest effectiveness of both biogenic calcium carbonates polymorphs (BIO-calcite and BIO-aragonite) to remove Pb from fluids. Previous studies had demonstrated that the interaction between Pb polluted waters and calcium carbonate polymorphs, namely calcite and aragonite samples of abiogenic origin, conducted to the removal of Pb from the liquid phase (Godelitsas et al. 2003; Chada et al. 2005; Pérez-Garrido et al. 2007, 2009; Di Lorenzo et al. 2019). However, few studies have investigated the potential of biogenic $CaCO_3$ materials as heavy metal scavengers (Köhler et al. 2007; Alidoust et al. 2015; Zhou et al. 2017). In the present research, it has been applied the same experimental procedure that had been used by Di Lorenzo et al. (2019) to study the sorption of Pb by purely inorganic $CaCO_3$ (calcite and aragonite). Therefore, the kinetic data obtained in the present study allow a fully consistent comparison with those derived from the study with inorganic minerals. The experimental observations suggest that the large difference in solubility between the two

polymorphs of calcium carbonate ($Ksp_{aragonite}=10^{-8.34}$ and $Ksp_{calcite}=10^{-8.48}$) and cerussite ($Ksp_{cerussite}=10^{-13.13}$) explains that, as soon as the first phases begin to dissolve, the fluid becomes supersaturated with respect to cerussite. Thus, the cerussite formation appears to be the predominant Pb uptake mechanism, which is controlled by a dissolution-precipitation reaction that takes place at the surfaces of biocarbonates. This conclusion is in good agreement with previously reported studies on Pb sequestration by inorganic calcium carbonate minerals (Godelitsas et al. 2003; Yuan et al. 2016, 2018; Di Lorenzo et al. 2019, 2020; Roza Llera et al. 2021).

Dissolution-crystallisation reactions have been considered by different authors as the main mechanism responsible for the removal of various dissolved components from aqueous solutions interacting with calcium carbonates and sulphates (Godelitsas et al. 2003; Rodríguez et al. 2008; Astilleros et al. 2010; Morales et al. 2014; Di Lorenzo et al. 2019). Similarly, dissolution-precipitation is the mechanism responsible for the removal of dissolved lead solutions by the biominerals studied in this thesis. However, there is a major difference between biominerals and inorganic minerals, the organic matter content. Most biogenic calcium carbonates are materials composed of two closely interrelated components: mineral component and biopolymers (Addadi and Weiner 1992; Checa et al. 2016). The presence of these biopolymers and the nano-crystalline nature of biogenic calcium carbonates may contribute to increase both their solubility and surface area compared to their geologic counterparts. A comparison of the results obtained by interaction of Pb-bearing aqueous solutions with biominerals and geologic calcium carbonates shows that the former are five times more efficient removing lead from the solution (Figure 4.9). However, the interaction of Pb-bearing solutions (10 mM) with gypsum and calcite mixtures removes higher concentrations of Pb than the interaction with BIO-ARG (Figure 6.1), which could be due to the higher solubility of gypsum

with respect to calcium carbonates. It should be noted that solid/liquid ratio may algo play and influence. While in experiments carried out with mixtures of gypsum + calcite this ratio was 20 g/L, in experiments with biominerals (BIO-ARG and BIO-CAL) it was 2 g/L (as used by Di Lorenzo et al. (2019)). This clearly shows that the effectiveness in lead removal is higher when biominerals are used, even when a small amount of these materials are used in the interactions compared to the volume of Pb-bearing aqueous solution. Furthermore, biominerals (BIO-ARG and BIO-CAL) are significantly more efficient as Pb scavengers than their inorganic counterparts (Figure 6.1). As explained above, the presence of biopolymers can increase the solubility, although in the case of BIO-CAL and BIO-ARG it will be necessary to carry out specific experiments in future to quantify their specific solubility as each material have a different biopolymer content and the nature of the biopolymers can also be very different.

Regarding the adsorption of Pb^{2+} on biopolymers exposed to the interaction with the aqueous solution in the surface of biocarbonate fragments, it cannot fully be disregarded that this process may play a role in enhancing the apparent removal of Pb^{2+} by biogenic samples compared to geological ones. The results in this work show that calcite biomineral is a more efficient Pb-sequester (99.9 % Pb removal) than the aragonite one (99.0 % Pb removal). The enhance Pb scavenging capacity of biocarbonates can be attributed to their specific microstructure that grants them significantly larger specific areas and reactivity compared to their inorganic counterparts (Köhler et al. 2007). More efficient Pb-sequestration by biocalcite as compared to bioaragonite is explained by differences in the degree of structural matching between the substrate and precipitate. While isostructural relationships between cerussite and aragonite facilitate the initial nucleation of cerussite on the bioaragonite, the surface quickly becomes passivated. Contrarily, the structural differences between calcite and cerussite prevent extensive passivation of biocalcite and enable the

persistent supply of carbonate ions necessary to maintain the solution at the primary phase-secondary phase interface supersaturated with respect to cerussite, even at very low Pb concentrations.

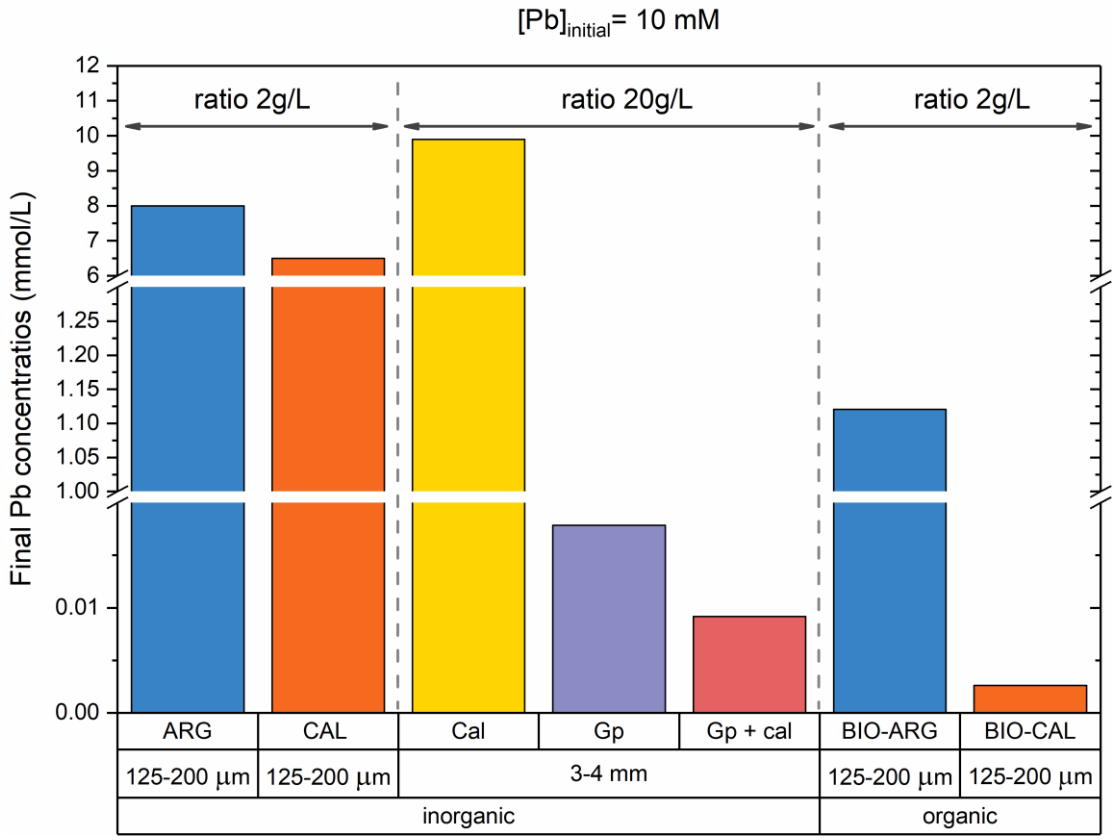

Figure 6.1. Evolution of Pb uptake by Calcite (Cal), Gypsum (Gp), mixtures of Gypum and calcite (Gp + Cal) and biominerals (BIO-ARG and BIO-CAL). Data obtained for inorganic minerals calcite (CAL) and aragonite (ARG) by Di Lorenzo et al. (2019) are plotted for comparison.

The findings reported in this study support the concept that coupled dissolution-crystallisation reactions are most effective metal sequestering mechanism. The precipitation of heavy metal-containing, sparingly soluble carbonates appears as an efficient immobilization mechanism. The higher specific surface areas and reactivity of biocarbonates make these excellent candidates for being incorporated into strategies for sequestering Pb2+ from contaminated waters. Since the canning industry yearly produces millions of tons of waste biocarbonates, this incorporation can contribute to the circular

economy, providing and added value to these materials. Experiments performed in this study define simplified systems. Further research will be needed to gain knowledge on the factors that may modulate the reactivity of biocarbonates and their ability to efficiently sequester dissolved Pb as well as other heavy metals.

6.2. Interface coupled dissolution-precipitation (ICDP) reactions: P recovery

The study Ca-phosphate-sulphate system shed light on processes occurring in the context of diagenesis. The present experimental study provides clear evidences that the transformation of anhydrite single crystals into aggregates of calcium phosphates phases (β-TCP and Hap) takes place through a coupled dissolution-precipitation reaction whose rate-limiting process is the dissolution of anhydrite. This reaction results in the formation of pseudomorphs, which together to the external shape, some textural features of the pristine mineral are preserved. These results agree well with those of previous studies of other replacement reactions that involved a variety of mineral phases, from silica, carbonate, halides, sulphurs and oxides to silicates (Putnis 2002, 2009a; Putnis and Putnis 2007; Ruiz-Agudo et al. 2014). Under hydrothermal conditions (120°C – 200°C), the interaction of P-bearing solutions with anhydrite single crystals results in the dissolution of the latter leading to the supersaturation of the fluid, at least in the interfacial layer, with respect to calcium phosphates (β-TCP and Hap). Thus, when the fluid reaches the supersaturation threshold for the nucleation of β-TCP and Hap, both calcium phosphates precipitate at the reaction front. The replacement reaction progresses through the formation of a porosity network that ensures a continuous communication between the reaction front and the bulk solution (Putnis et al. 2005; Putnis and Putnis 2007; Pollok et al. 2011; Forjanes et al. 2020b). Thus, the reaction starts at the surface of anhydrite and progresses from rim to core through the advancement of a sharp

reaction front. The pseudomorphic nature of the replacement of anhydrite single crystals by aggregates of calcium phosphate crystals explains the generation of large amounts of porosity. This porosity balances the volume loss associated to the reaction which involves a negative molar volume change (V_{Anh} = 45.84 cm^3/mol, $V_{\beta\text{-}TCP}$ = 33.14 cm^3/mol and V_{Hap} = 31.79 cm^3/mol) thereby guaranteeing the preservation of the external shape of the pristine anhydrite sample. This preservation requires that the coupling between the rates of anhydrite dissolution and calcium phosphate precipitation is very tight. Dissolution-precipitation reactions that involve calcium sulphate mineral phases, particularly anhydrite, and P-bearing aqueous solutions appear as feasible processes occurring during diagenesis which could explain the origin of some calcium phosphate deposits associated to sedimentary basins. The kinetics of the the anhydrite by calcium phosphate mineral replacement is characterized by an activation energie, Ea, around 40 kJ/mol, as determined by both, the Avrami equation and the isoconversional method. This value is similar to that determined by Altree-Williams et al. (2019) for the carbonation of anhydrite, which is a process rate-limited by anhydrite dissolution. However, the Avrami exponents of the anhydrite by calcium carbonate mineral replacement stand between those defined by Hancock and Sharp (1972) for first-order and higher-order processes. This is in apparent contradiction with anhydrite dissolution being the rate-limiting process in this case, which reflects the complexity of coupled dissolution-precipitation reactions. The kinetics of these reactions is modulated by a number of factors, including the existence/absence of crystallographic relationships between the primary and secondary phases, the nature and textural features of the primary phase, which determine its dissolution rate, the volume, connectivity and permeability of the porosity formed during the replacement, the precipitation rate of the secondary phase(s) and the textural evolution of the latter. In the case of the anhydrite by calcium

phosphate mineral replacement, a competition between the nucleation and growth of β-TCP and Hap exist at early stages of the replacement, and this competition last longer when the reaction takes at lower temperatures. Because the morphology of β-TCP and Hap crystals is very different, the textural characteristics of the replacement regarding pore arrangement within the replaced layer is strongly influenced by this competition. In turn, the characteristics of the newly formed porosity strongly influences, mass transfer from and to the interfacial fluid and, consequently, the kinetics of the reaction. Thus, findings in the study of the anhydrite by calcium phosphate mineral replacement highlight that the formation of transient metastable precursor phases and the Ostwald ripening processes that they undergo play an important role in defining the overall kinetics of coupled dissolution-precipitation reactions. Furthermore, the knowledge gained from studying the replacement of anhydrite by calcium phosphates under hydrothermal conditions constitutes and excellent grounds for in future addressing the research of dissolution-precipitation reactions that can lead to the effective removal and immobilization of an important pollutant, P, in Earth's surface environmental settings.

CHAPTER 7

CONCLUSIONS

7. Conclusions

This thesis comprise the experimental study of three systems, Ca-Pb-carbonates-sulphates, Ca-Pb-Biogenic carbonates and Ca-phosphate-sulphate, which are addressed aiming to improve our current understanding of the factors that control the progress of dissolution-precipitation reactions under epigenetic conditions. In agreement with the results discussed in previous chapters, and to conclude the manuscript of this doctoral thesis, the main conclusions have been divided into two sections according to the environmental and diagenetic interest of the mineral-water systems.

The mineral transformations in both Ca-Pb-carbonates-sulphates and Ca-Pb-biogenic carbonate systems have an environmental interest. The main conclusions are detailed bellow:

- The interaction of minerals of geological origin (gypsum, calcite, or mixtures of gypsum and calcite crystals) with Pb-bearing aqueous solutions results in a Pb removal from aqueous solution that is both fast and extensive when gypsum is present in the system.

- In all the Ca-Pb-carbonates-sulphates systems studied here, the main mechanism of Pb removal takes place through the coprecipitación of Pb-bearing minerals. The newly Pb-rich phases are formed as a result of the reaction between dissolved Pb and SO_4^{2-} and/or CO_3^{2-} ions released during the dissolution of the primary phases, gypsum and/or calcite.

- Interaction of Pb-bearing solutions with calcite lead to the precipitation of cerussite ($PbCO_3$) and hydrocerussite ($Pb_3(CO_3)_2(OH)_2$), while the interaction of those solutions with gypsum results in the formation of anglesite ($PbSO_4$). Indeed, cerussite, hydrocerussite and anglesite

precipitates on the surface of primary minerals after interaction with mixtures of gypsum and calcite.

- The sluggish kinetics of calcite dissolution makes Pb removal through precipitation of lead carbonates a very slow process, which results less efficient compared to the precipitation of anglesite, at least within the time set of experiments in this study.

- The simultaneous interaction of Pb-bearing aqueous solutions with crystals of both phases, gypsum-calcite crystals results in Pb removals that, depending on $[Pb]_i$, are from as much as up to 5 times larger than those attain through interaction only with gypsum, and up to 500 times larger than those attain when solutions only interact with calcite.

- The interaction of biominerals, BIO-CAL and BIO-ARG, with Pb-bearing solutions leads to cerussite precipitation being the predominant mechanism of Pb uptake, which is controlled by dissolution-precipitation reaction at the surface of biocarbonates.

- Calcite biomineral (*Chlamys opercularis*) is an overall more efficient Pb-sequester (99.9 % Pb removal) than the aragonite (*Sepia Officinalis*) one (99.0 % Pb removal). This is explained by differences in the degree of structural matching between the substrate and precipitate.

- Isostructural relationships between cerussite and aragonite facilitate the initial nucleation of cerussite on the bioaragonite, which quickly passivates the surface.

- Structural differences between calcite and cerussite prevent extensive passivation of biocalcite and enable persistent supply of carbonate ions necessary to maintain supersaturation of the solution with respect to

cerussite event at very low Pb concentrations necessary for cerussite precipitation.

- Pb removal yields are around five times larger for biocarbonates than previously found for inorganic carbonates of geological origin.

- The higher specific surface areas and reactivity of biocarbonates makes these excellent candidates for being incorporated into strategies for sequestering Pb^{2+} from contaminated waters.

- Coupled dissolution-crystallisation reactions are an effective metal sequestering mechanism and the precipitation of heavy metal-containing carbonates appears as efficient immobilization in form of insoluble minerals.

The mineral transformations taking place in the Ca-phosphate-sulphate system under hydrothermal conditions presents a diagenetic interest. The main conclusions are detailed bellow:

- The interaction of anhydrite single crystals with P-bearing aqueous solutions leads to the replacement of anhydrite by aggregates of calcium phosphates, hydroxyapatite and β-TCP under hydrothermal conditions (from 120 to 200 °C). The external shape and volume of anhydrite crystals is preserved, and thus the replacement is pseudomorphic.

- The replacement of anhydrite by calcium phosphates involves the dissolution of anhydrite to precipitate β-TCP, which is metastable and dissolves to form Hap as the reaction progresses over the entire temperature range used in this study.

- At early stages of the replacement of anhydrite by calcium phosphates, there is a competition between nucleation and the growth of β-TCP and Hap. This competition lasts longer the lower the reaction temperature is.

- In the temperature range of 120 – 200°C, the solubility of β-TCP shows a positive dependence with temperature, which facilitates the fast dissolution of β-TCP to form Hap at higher temperatures.

- The kinetic of the replacement of anhydrite by aggregates of calcium phosphates has been assessed by fitting the experimental results to both, the Avrami equation and the isoconversional method. Under the conditions used in this research, the activation energies, Ea, reaches values around 40 kJ/mol.

- The different morphological features of β-TCP and Hap crystals strongly influence the texture and the pores arrangement during the progress of the replacement, which in turn modulate mass transfer from and to the fluid. Overall, it emphasises that the presence of metastable precursor phases (β-TCP) and Ostwald ripening processes play a key role on the kinetics of coupled dissolution-precipitation reactions.

- The replacement of evaporitic minerals is a feasible mechanism for the formation of some calcium phosphate accumulations in sedimentary basins during diagenesis.

CHAPTER 8

RESUMEN

8. Resumen

Introducción y objetivos

En la corteza terrestre tienen lugar diferentes procesos como la diagénesis, el metamorfismo o el metasomatismo, dónde la circulación de fluidos facilita el desarrollo y progreso de diferentes reacciones minerales. En las últimas décadas, el estudio de los procesos que involucran la interacción de fluidos acuosos con las superficies minerales se ha convertido en un importante tema de investigación debido a sus implicaciones diagenéticas y medioambientales. Cuando la superficie de un mineral entra en contacto con una disolución acuosa, se producen una serie de reacciones que operan de manera simultánea como son, la disolución del mineral primario, el transporte de las especies en disolución (iones o moléculas), la adsorción de iones en posiciones reactivas de la superficie mineral, o la precipitación de fases secundarias cuando las concentraciones de iones disueltos son lo suficientemente elevadas.

Trabajos de investigación previos a esta tesis, han demostrado que las interacciones entre minerales y fluidos pueden controlar la movilidad y concentración de contaminantes ambientales peligrosos, como los metales pesados (Hochella 2002; Godelitsas and Astilleros 2010), a través de diferentes mecanismos de sorción (adsorción, absorción y coprecipitación). Además de estos procesos de sorción, son muy comunes las reacciones acopladas de disolución-precipitacion (denominadas ICDP de aquí en adelante) en contextos naturales. En este caso, las propiedades termodinámicas y cinéticas de los minerales, junto con las condiciones fisicoquímicas de los fluidos, pueden promover un acoplamiento entre la velocidad de disolución de la fase primaria y la velocidad de precipitación de la secundaria. El progreso de las reacciones ICDP requiere una comunicación continua entre la fase fluida y la interfase fase

primaria-fase secundaria, que está asegurada por la formación de porosidad y/o fracturas durante la reacción de reemplazamiento mineral (Putnis 2002, 2009b; Fernández-Díaz et al. 2009; Ruiz-Agudo et al. 2014). Además, la existencia de relaciones epitaxiales entre fases primarias y secundarias puede desempeñar un papel importante, tanto en las reacciones de sustitución minerales como en los procesos de sorción (Van Der Merwe 1978; Astilleros et al. 2003, 2010; Prieto et al. 2003; Pérez-Garrido et al. 2007; Chernov 2012; Cuesta Mayorga et al. 2018; Forjanes et al. 2020a). A lo largo del último siglo, diversas industrias químicas, farmacéuticas, mineras, entre otras han contribuido significativamente a la contaminación suelos y aguas subterráneas por compuestos tóxicos de origen orgánico e inorgánico (Hassaan et al. 2016). Entre estos últimos, los metales pesados suponen un importante riesgo para la salud de los seres humanos, ya los organismos vivos pueden absorber y acumular cantidades importantes de elementos tóxicos. Durante las últimas décadas, se han desarrollado metodologías encaminadas a la descontaminación de suelos y acuíferos. Aunque se han obtenido buenos resultados, un inconveniente común de estas técnicas es su elevado coste, que hace imposible su aplicación en los países desarrollados. Por lo tanto, es esencial la investigación y el desarrollo de estrategias de descontaminación más eficientes y menos costosas (Crini and Lichtfouse 2019; Guo et al. 2021). En este contexto, resulta de máximo interés el estudio de las reacciones de disolución-precipitación que se desarrollan en condiciones de la superficie terrestre y con implicaciones medioambientales o diagenéticas. Para ello, es preciso seleccionar minerales abundantes en la corteza terrestre como carbonatos cálcicos (calcita y aragonito) y sulfatos cálcicos (yeso y anhidrita).

El objetivo principal de esta tesis es comprender los factores que intervienen en procesos de disolución-cristalización que tienen lugar en ambientes de la superficie terrestre y diagenéticos. Para ello, se han seleccionado los siguientes sistemas: Ca-Pb-carbonatos-sulfatos, Pb-carbonatos de calcio

biogénicos y Ca-fosfatos-sulfatos. En concreto, se propone estudiar el mecanismo y la cinética de reemplazamiento de anhidrita por fosfatos de calcio, así como determinar la naturaleza y el comportamiento de cristalización de fases secundarias de Pb (sulfatos y carbonatos) que se originan por la interacción de Pb en disolución con sulfatos (yeso) y carbonatos de calcio (calcita, aragonito y biominerales). Para abordar este objetivo principal, se plantean los siguientes objetivos específicos:

- Analizar la evolución de la composición química del fluido durante la interacción de disoluciones acuosas ricas en Pb con dos sistemas: a) calcita - yeso y b) biocalcita o bioaragonito.

- Determinar el mecanismo de eliminación del Pb durante su interacción con monocristales de calcita y yeso y sus mezclas, o con carbonatos de calcio biogénicos.

- Evaluar y comparar la eficacia en la eliminación del plomo disuelto por diferentes carbonatos cálcicos biogénicos y abiogénicos.

- Estudiar el reemplazamiento de monocristales de anhidrita por fosfatos de calcio al interaccionar con disoluciones acuosas ricas en P, analizando la influencia de factores fisicoquímicos y texturales.

- Determinar el mecanismo y la cinética de la reacción de reemplazamiento en el sistema Ca-fosfatos-sulfatos.

Para alcanzar estos objetivos, se han diseñado experimentos específicos para cada sistema con el fin de reproducir el escenario más preciso en función del interés ambiental o diagenético de los metales seleccionados. En el capítulo 2 se describe de forma global los experimentos y técnicas empleadas en esta tesis doctoral y se ha dividido en 4 categorías: (2.1) experimentos a temperatura

ambiente, (2.2) experimentos hidrotermales, (2.3) caracterización de fases líquidas y (2.4) caracterización de fases sólidas. Los procedimientos experimentales llevados a cabo para cada sistema estudiado se detallan en los capítulos correspondientes a cada sistema.

Para el estudio del sistema Ca-Pb-carbonatos-sulfatos (capítulo 3) se han seleccionado fragmentos de calcita y yeso. A pesar de que estos minerales aparecen a menudo asociados en cuencas sedimentarias, todos los estudios experimentales previos de la interacción entre disoluciones de Pb con calcita o yeso se habían realizado considerando estas fases por separado, sin tener en cuenta que la disolución de cualquiera de estos minerales, puede alterar significativamente las características fisicoquímicas de la solución acuosa pudiendo influir en las características de la interacción de la fase fluida con el mineral. Por ello, se han llevado a cabo experimentos de interacción entre disoluciones de plomo con yeso, calcita y con mezclas de yeso y calcita.

La mayoría de estudios experimentales sobre la eliminación de metales pesados, a través de la interacción con superficies minerales de carbonatos de calcio, utilizan como material inicial calcita y aragonito de origen geológico. Sin embargo, hay muchos menos trabajos que hayan investigado la sorción de metales pesados con carbonatos de calcio de origen biogénico. En esta tesis doctoral se estudia el sistema Ca-Pb-Carbonatos biogénicos (capítulo 4) donde se han realizado experimentos de interacción entre disoluciones de plomo y biominerales de composición calcítica (*Chlamys opercularis*) y aragonítica (*Sepia officinalis*).

Por último, con el objetivo de avanzar en el estudio de los mecanismos de eliminación de P a través de reacciones acopladas de disolución – cristalización (ICDP) y en el origen de las acumulaciones de apatito asociadas a rocas sedimentarias evaporíticas, se ha llevado a cabo el estudio del tercer

sistema Ca-fosfatos-sulfatos (capítulo 5). En este sistema se han efectuado experimentos de interacción entre cristales de anhidrita y disoluciones acuosas de P en condiciones hidrotermales.

Resultados y discusión

Sistema Ca-Pb-carbonatos-sulfatos

Cuando las disoluciones ricas en plomo interactúan con yeso, independientemente de la concentración inicial de Pb, se llega a eliminar entre un 98-99.8% de plomo. Sin embargo en el caso de la interacción de calcita con disoluciones de Pb, la eliminación de este elemento pesado depende en gran medida de la concentración inicial de Pb siendo un 13% para $[Pb]_i$ = 10 mM y 99% para $[Pb]_i$ = 1 mM. Sin embargo, cuando se realizan estos experimentos de interacción con mezclas de yeso y calcita se obtienen concentraciones finales de plomo cinco veces más bajas que las alcanzadas mediante la interacción de yeso y hasta 500 veces menores a las obtenidas cuando solo interaccionan con calcita. En todos los casos, se observa la precipitación de sulfatos de plomo (anglesita) o de carbonatos de plomo (cerusita e hidrocerusita) que son los responsables de la eliminación del plomo disuelto. Independientemente de su cinética, en todos los sistemas estudiados la coprecipitación fue el principal mecanismo de sorción mediante el cual se eliminó el Pb de la disolución.

Sistema Ca-Pb-Carbonatos biogénicos

Los resultados obtenidos permiten confirmar que los biominerales son más eficaces en la eliminación del Pb de disoluciones acuosas que lo minerales inorgánicos, calcita y aragonito. Esta eliminación de plomo es el resultado de la disolución de los biominerales y la precipitación de carbonatos de plomo mediante mecanismo de sorción denominado coprecipitación. El biomineral de

composición aragonítica Sepia Officinalis es muy eficaz en periodos cortos de tiempo, sin embargo, el biomineral de composición calcítica, Chlamys opercularis, presenta mejores valores de eliminación de plomo para tiempos más largos de interacción siendo finalmente más efectivo. En el caso de los biominerales de composición aragonítica, el hecho de que el carbonato de plomo que precipita (cerusita) cristalice en el mismo sistema cristalino que el aragonito (ortorrómbico) facilita el crecimiento epitaxial de cerusita sobre sobre las superficies de los biominerales aragoníticos, de tal modo que tapiza las superficies evitando que siga disolviéndose el biomineral y por tanto pueda seguir precipitando más cerusita. Este fenómeno no es posible en el caso del biomineral con composición calcítica debido a las diferencias estructurales entre cerusita y calcita (sistema trigonal). Además, los resultados de esta tesis permiten confirmar que los biominerales estudiados son más efectivos que calcita y aragonito de origen inorgánico.

Los resultados de los sistemas Ca-Pb-carbonatos-sulfatos y Ca-Pb-Carbonatos biogénicos confirman que las reacciones acopladas de disolución-cristalización son el mecanismo de eliminación de metales pesados más eficaz. La precipitación de carbonatos poco solubles que contienen estos metales parece ser un mecanismo de inmovilización eficaz. Las mayores áreas de superficie específica y reactividad de los biocarbonatos los convierten en excelentes candidatos para ser incorporados a estrategias de remediación ambiental de aguas contaminadas por Pb^{2+}. Dado que la industria conservera produce anualmente millones de toneladas de residuos de biocarbonatos, esta incorporación puede contribuir a la economía circular, aportando un valor añadido a estos materiales.

Sistema Ca-fosfatos-sulfatos

Los resultados obtenidos en el estudio del sistema Ca-fosfatos-sulfatos indican que el reemplazamiento completo de anhidrita por hidroxiapatito (Hap) a 120°C no se alcanza hasta los 3 días, mientras que en pocas horas (10 horas) a 200°C los cristales de anhidrita se ha transformado por completo. Existe una competición entre la nucleación y el crecimiento de dos fases de fosfatos de calcio Hap y β-Tricalcium fosfato (β –TCP) en etapas tempranas de la sustitución, que duran más cuanto menor es la temperatura de reacción. Debido a las diferentes características morfológicas de los cristales de β-TCP y Hap, esta competición influye fuertemente en la textura originada por el reemplazamiento y en la disposición de sus poros. El cálculo de la energía de activación (Ea) se llevó a cabo mediante la ecuación de Avrami y el método isoconversional obteniéndose para ambos energías de activación experimentales, Ea, en torno a 40 kJ/mol. Este valor es similar al determinado por Altree-Williams et al. (2019) para la carbonatación de la anhidrita. Sin embargo, los exponentes de Avrami del reemplazamiento de anhidrita por carbonato cálcico se sitúan entre los definidos por Hancock y Sharp (1972) para procesos de primer orden y de orden superior. Esto está en aparente contradicción con que la disolución de anhidrita sea el proceso limitante de la velocidad de la reacción, lo que refleja la complejidad de las reacciones acopladas de disolución-precipitación. La cinética de estas reacciones está controlada por una serie de factores, como la existencia/ausencia de relaciones cristalográficas entre las fases minerales primaria y secundaria, la naturaleza y las características texturales de la fase primaria, que determinan su velocidad de disolución, el volumen, la conectividad y la permeabilidad de la porosidad formada durante el reemplazamiento, la velocidad de precipitación de la fase o fases secundarias y la evolución textural de estas últimas. Además, los resultados obtenidos a partir del estudio del reemplazamiento de anhidrita por fosfatos de calcio en condiciones hidrotermales constituyen una base

excelente para abordar en el futuro la investigación de reacciones de disolución-precipitación que puedan conducir a la eliminación e inmovilización efectiva del fósforo, que es un importante contaminante cuando se encuentra en altas concentraciones en entornos de la superficie terrestre.

CHAPTER 9

CONCLUSIONES

9. Conclusiones

Esta tesis comprende el estudio experimental de tres sistemas, Ca-Pb-carbonatos-sulfatos, Ca-Pb-carbonatos biogénicos y Ca-fosfato-sulfato, que se abordan con el objetivo de mejorar nuestra comprensión actual de los factores que controlan el progreso de las reacciones de disolución-precipitación en condiciones epigenéticas. De acuerdo con los resultados discutidos en los capítulos anteriores, y para concluir el manuscrito de esta tesis doctoral, las principales conclusiones se han dividido en dos secciones según el interés ambiental y diagenético de los sistemas mineral-fluido.

Las transformaciones minerales que se producen en los sistemas Ca-Pb-carbonatos-sulfatos y Ca-Pb-carbonatos biogénicos tienen interés medioambiental. A continuación, se detallan las principales conclusiones:

- La interacción de minerales de origen geológico (yeso, calcita o mezclas de cristales de yeso y calcita) con disoluciones acuosas ricas en Pb da lugar a una rápida y considerable eliminación de Pb de la solución acuosa cuando el yeso está presente en el sistema.

- En todos los sistemas Ca-Pb-carbonatos-sulfatos estudiados en esta tesis, el principal mecanismo de eliminación de Pb tiene lugar a través de la coprecipitación de fases minerales de Pb. Las nuevas fases ricas en Pb se forman como resultado de la reacción entre el Pb disuelto y los iones SO_4^{2-} y/o CO_3^{2-} liberados durante la disolución de las fases minerales primarias, yeso y/o calcita.

- La interacción de disoluciones acuosas ricas en Pb con calcita conduce a la precipitación de cerusita ($PbCO_3$) e hidrocerusita ($Pb_3(CO_3)_2(OH)_2$), mientras que la interacción de esas disoluciones con yeso da lugar a la

formación de anglesita ($PbSO_4$). Además, la cerusita, la hidrocerusita y la anglesita precipitan en la superficie de fases minerales primarias tras la interacción con mezclas de yeso y calcita.

- La cinética de disolución de la calcita hace que la eliminación de Pb a través de la precipitación de carbonatos de plomo sea un proceso muy lento, que resulta menos eficiente en comparación con la precipitación de anglesita, al menos dentro del tiempo establecido en los experimentos de este estudio.

- La interacción simultánea de disoluciones acuosas ricas en Pb con cristales de ambas fases, yeso-calcita, da lugar a eliminaciones de Pb que, dependiendo de $[Pb]_i$, son hasta 5 veces mayores que las obtenidas mediante la interacción sólo con yeso, y hasta 500 veces mayores que las obtenidas cuando las disoluciones sólo interaccionan con calcita.

- En la interacción de biominerales, BIO-CAL y BIO-ARG, con disoluciones ricas de Pb el principal mecanismo de eliminación de Pb es la precipitación de cerusita y está controlado por la reacción de disolución-precipitación en la superficie de los biocarbonatos.

- El biomineral de calcita (*Chlamys opercularis*) es más eficaz eliminando Pb de la disolución (99,9 % de eliminación de Pb) que el biomineral de aragonito (*Sepia Officinalis*) (99,0 % de eliminación de Pb). Esto se explica por las diferencias en el grado de coincidencia de elementos cristalográficos entre el sustrato y la fase precipitada.

- Las relaciones isoestructurales entre cerusita y aragonito facilitan la nucleación inicial de cerusita sobre el biomineral de aragonito, pasivando rápidamente la superficie.

- Las diferencias estructurales entre calcita y cerusita impiden la pasivación de la superficie del biomineral de calcita y permiten que pueda seguir disolviéndose, aportando iones carbonato, de modo que puede mantenerse la sobresaturación de la disolución con respecto a cerusita incluso con concentraciones muy bajas de Pb.

- Los biocarbonatos son cinco veces más efectivos en la eliminación de Pb de las disoluciones acuosas que los carbonatos de calcio inorgánicos.

- La mayor superficie específica y reactividad de los biocarbonatos los convierte en excelentes candidatos para su incorporación a estrategias de remediación ambiental de aguas contaminadas por Pb^{2+}.

- Las reacciones acopladas de disolución-cristalización son un mecanismo eficaz en la eliminación de metales pesados como el plomo, además los biocarbonatos y sulfatos de calcio se presentan como eficaces inmovilizadores de estos contaminantes.

Las transformaciones minerales que tienen lugar en el sistema Ca-fosfato-sulfato en condiciones hidrotermales presentan un interés diagenético. Las principales conclusiones se detallan a continuación:

- La interacción de monocristales de anhidrita con disoluciones acuosas ricas en P en condiciones hidrotermales (de 120 a 200°C), conduce al reemplazamiento de la anhidrita por agregados de fosfatos de calcio, hidroxiapatito y β-TCP. La forma externa y el volumen de los cristales de anhidrita se conservan, por lo que la sustitución es pseudomórfica.

- El reemplazamiento de anhidrita por fosfatos de calcio implica la disolución de la anhidrita para precipitar β-TCP, fase metaestable que se

disuelve, precipitando finalmente hidroxiapatito a medida que progresa la reacción en todo el rango de temperaturas utilizado en este estudio.

- En las primeras fases del reemplazamiento de la anhidrita por fosfatos de calcio, existe una competencia entre la nucleación y el crecimiento de β-TCP e hidroxiapatito. Esta competencia dura más cuanto menor es la temperatura de reacción.

- En el rango de temperaturas de 120 - 200°C, la solubilidad del β-TCP aumenta de la misma con la temperatura, lo que facilita la rápida disolución del β-TCP para formar hidroxiapatito a temperaturas más altas.

- La cinética del reemplazamiento de anhidrita por agregados de fosfatos de calcio se ha determinado ajustando los resultados experimentales tanto a la ecuación de Avrami como al método isoconversional. En las condiciones experimentales utilizadas en esta investigación, las energías de activación, Ea, alcanzan valores en torno a 40 kJ/mol.

- Las diferencias morfológicas entre los cristales de β-TCP y de hidroxiapatito influyen fuertemente en la textura y la disposición de los poros durante el progreso del reemplazamiento, que a su vez modulan la transferencia de masa desde y hacia el fluido. En general, la presencia de fases precursoras metaestables (β-TCP) y los procesos de maduración de Ostwald desempeñan un papel clave en la cinética de las reacciones acopladas de disolución-precipitación.

- El reemplazamiento de minerales evaporíticos es un mecanismo factible para la formación de algunas acumulaciones de fosfato de calcio en cuencas sedimentarias durante la diagénesis.

CHAPTER 8

REFERENCES

10.References

Addadi, L., and Weiner, S. (1992) Control and Design Principles in Biological Mineralization. Angewandte Chemie International Edition in English, 31, 153–169.

Aizenberg, J., Hanson, J., Koetzle, T.F., Weiner, S., and Addadi, L. (1997) Control of Macromolecule Distribution within Synthetic and Biogenic Single Calcite Crystals. Journal of the American Chemical Society, 119, 881–886.

Al Aji, B., Yavuz, Y., and Koparal, A.S. (2012) Electrocoagulation of heavy metals containing model wastewater using monopolar iron electrodes. Separation and Purification Technology, 86, 248–254.

Alidoust, D., Kawahigashi, M., Yoshizawa, S., Sumida, H., and Watanabe, M. (2015) Mechanism of cadmium biosorption from aqueous solutions using calcined oyster shells. Journal of Environmental Management, 150, 103–110.

Altree-Williams, A., Pring, A., Ngothai, Y., and Brugger, J. (2015) Textural and compositional complexities resulting from coupled dissolution–reprecipitation reactions in geomaterials. Earth-Science Reviews, 150, 628–651.

Altree-Williams, A., Pring, A., Ngothai, Y., and Brugger, J. (2017) The Carbonatation of Anhydrite: Kinetics and Reaction Pathways. ACS Earth and Space Chemistry, 1, 89–100.

Altree-Williams, A., Brugger, J., Pring, A., and Bedrikovetsky, P. (2019) Coupled reactive flow and dissolution with changing reactive surface and porosity. Chemical Engineering Science, 206, 289–304.

Arvanitoyannis, I.S., and Kassaveti, A. (2008) Fish industry waste: treatments, environmental impacts, current and potential uses. International Journal of Food Science & Technology, 43, 726–745.

Astilleros, J.M., Pina, C.M., Fernández-Díaz, L., and Putnis, A. (2003) Nanoscale growth of solids crystallising from multicomponent aqueous solutions. Surface Science, 545, L767–L773.

Astilleros, J.M., Godelitsas, A., Rodríguez-Blanco, J.D., Fernández-Díaz, L., Prieto, M., Lagoyannis, A., and Harissopulos, S. (2010) Interaction of gypsum with lead in aqueous solutions. Applied Geochemistry, 25, 1008–1016.

Audry, S., Schäfer, J., Blanc, G., and Jouanneau, J.-M. (2004) Fifty-year sedimentary record of heavy metal pollution (Cd, Zn, Cu, Pb) in the Lot River reservoirs (France). Environmental Pollution, 132, 413–426.

Baronnet, A. (1982) Crystal-Growth of mienrals-recent contrinbution and tem. Journal De Microscopie Et De Spectroscopie Electroniques, 7, 417–423.

Baturin, G. (1989) The origin of marine phosphorites. International Geology Review, 31, 327–342.

Belcari, P., Sartor, P., Sanchez, P., Demestre, M., Tsangridis, A., Leondarakis, P., Lefkaditou, E., and Papaconstantinou, C. (2002) Exploitation patterns of the cuttlefish, Sepia officinalis (Cephalopoda, Sepiidae), in the Mediterranean Sea. Bulletin of marine science, 71, 187–196.

Bentor, Y. (1980) Phosphorites—the unsolved problems. In Marine Phosphorites-Geochemistry, Occurrence, Genesis Vol. 29, pp. 3–18. SEPM Society for Sedimentary Geology, Tulsa.

Berman, A., Hanson, J., Leiserowitz, L., Koetzle, T.F., Weiner, S., and Addadi, L. (1993) Biological control of crystal texture: a widespread strategy for adapting crystal properties to function. Science, 259, 776–779.

Berner, R.A. (1980) Early diagenesis: a theoretical approach. Princeton University Press.

Bildstein, O., Worden, R., and Brosse, E. (2001) Assessment of anhydrite dissolution as the rate-limiting step during thermochemical sulfate reduction. Chemical geology, 176, 173–189.

Bohner, M., Lemaître, J., and Ring, T.A. (1997) Kinetics of dissolution of β-tricalcium phosphate. Journal of colloid and interface science, 190, 37–48.

Bradl, H. (2005) Heavy metals in the environment: origin, interaction and remediation Vol. 6. Elsevier.

Brown, G., Parks, G., and O'Day, P. (1995a) Mineral Surfaces, Vaughan, DJ, Pattrick, RAD, Eds.

Brown, G., Parks, G., and O'day, P. (1995b) Sorption at mineral-water interfaces: macroscopic and microscopic perspectives. Mineral Surfaces, 5, 129–183.

Callagon, E.B.R., Lee, S.S., Eng, P.J., Laanait, N., Sturchio, N.C., Nagy, K.L., and Fenter, P. (2017) Heteroepitaxial growth of cadmium carbonate at dolomite and calcite surfaces: Mechanisms and rates. Geochimica et Cosmochimica Acta, 205, 360–380.

Chada, V.G.R., Hausner, D.B., Strongin, D.R., Rouff, A.A., and Reeder, R.J. (2005) Divalent Cd and Pb uptake on calcite {101¯4} cleavage faces: An XPS and AFM study. Journal of Colloid and Interface Science, 288, 350–360.

Charlesworth, S., De Miguel, E., and Ordóñez, A. (2011) A review of the distribution of particulate trace elements in urban terrestrial environments and its application to considerations of risk. Environmental geochemistry and health, 33, 103–123.

Chattopadhyay, G., Lin, K.C.-P., and Feitz, A.J. (2003) Household dust metal levels in the Sydney metropolitan area. Environmental Research, 93, 301–307.

Checa, A.G., Esteban-Delgado, F.J., and Rodríguez-Navarro, A.B. (2007) Crystallographic structure of the foliated calcite of bivalves. Journal of structural biology, 157, 393–402.

Checa, A.G., Cartwright, J.H.E., Sánchez-Almazo, I., Andrade, J.P., and Ruiz-Raya, F. (2015) The cuttlefish Sepia officinalis (Sepiidae, Cephalopoda) constructs cuttlebone from a liquid-crystal precursor. Scientific Reports, 5, 11513.

Checa, A.G., Macías-Sánchez, E., Harper, E.M., and Cartwright, J.H. (2016) Organic membranes determine the pattern of the columnar prismatic layer of mollusc shells. Proceedings of the Royal Society B: Biological Sciences, 283, 20160032.

Checa, A.G., Harper, E.M., and González-Segura, A. (2018) Structure and crystallography of foliated and chalk shell microstructures of the oyster Magallana: the same materials grown under different conditions. Scientific Reports, 8, 7507.

Checa, A.G., Yáñez-Ávila, M.E., González-Segura, A., Varela-Feria, F., Griesshaber, E., and Schmahl, W.W. (2019) Bending and branching of calcite laths in the foliated microstructure of pectinoidean bivalves occurs at coherent crystal lattice orientation. Journal of Structural Biology, 205, 7–17.

Chernov, A.A. (2012) Modern crystallography III: crystal growth Vol. 36. Springer Science & Business Media.

Cole, W., and Lancucki, C. (1974) A refinement of the crystal structure of gypsum CaSO4. 2H2O. Acta Crystallographica Section B: Structural Crystallography and Crystal Chemistry, 30, 921–929.

Comodi, P., Nazzareni, S., Zanazzi, P.F., and Speziale, S. (2008) High-pressure behavior of gypsum: A single-crystal X-ray study. American Mineralogist, 93, 1530–1537.

Crini, G., and Lichtfouse, E. (2019) Advantages and disadvantages of techniques used for wastewater treatment. Environmental Chemistry Letters, 17, 145–155.

Cubillas, P., Köhler, S., Prieto, M., Chaïrat, C., and Oelkers, E.H. (2005) Experimental determination of the dissolution rates of calcite, aragonite, and bivalves. Chemical Geology, 216, 59–77.

Cuesta Mayorga, I., Astilleros, J.M., Fernández-Díaz, L., Morales, J., Prieto, M., Roncal-Herrero, T., and Benning, L.G. (2018) Epitactic overgrowths of calcite (CaCO3) on anhydrite (CaSO4) cleavage surfaces. Crystal Growth & Design, 18, 1666–1675.

Di Lorenzo, F., Ruiz-Agudo, C., and Churakov, S.V. (2019) The key effects of polymorphism during Pb II uptake by calcite and aragonite. CrystEngComm, 21, 6145–6155.

Di Lorenzo, F., Cametti, G., Vanhecke, D., and Churakov, S.V. (2020) The Role of Interfaces in Controlling Pb2+ Removal by Calcium Carbonate Minerals. Crystal Growth & Design, 20, 6157–6169.

Di Lorenzo, F., Arnold, T., and Churakov, S.V. (2021) Pb2+ Uptake by Magnesite: The Competition between Thermodynamic Driving Force and Reaction Kinetics. Minerals, 11.

Du, Y., Lian, F., and Zhu, L. (2011) Biosorption of divalent Pb, Cd and Zn on aragonite and calcite mollusk shells. Environmental Pollution, 159, 1763–1768.

Duncan, P.F., Brand, A.R., Strand, Ø., and Foucher, E. (2016) Chapter 19 - The European Scallop Fisheries for Pecten maximus, Aequipecten opercularis, Chlamys islandica, and Mimachlamys varia. In S.E. Shumway and G.J. Parsons, Eds., Developments in Aquaculture and Fisheries Science Vol. 40, pp. 781–858. Elsevier.

Dyer, A. (1995) Mineral Surfaces. Ed. DJ. Vaughan and RAD Pattrick, Chapman and Hall, London, 333–354.

Dzombak, R.M., and Sheldon, N.D. (2020) Weathering Intensity and Presence of Vegetation Are Key Controls on Soil Phosphorus Concentrations: Implications for Past and Future Terrestrial Ecosystems. Soil Systems, 4.

Egle, L., Rechberger, H., Krampe, J., and Zessner, M. (2016) Phosphorus recovery from municipal wastewater: An integrated comparative technological, environmental and economic assessment of P recovery technologies. Science of The Total Environment, 571, 522–542.

Elzinga, E.J., Rouff, A.A., and Reeder, R.J. (2006) The long-term fate of Cu2+, Zn2+, and Pb2+ adsorption complexes at the calcite surface: An X-ray absorption spectroscopy study. Geochimica et Cosmochimica Acta, 70, 2715–2725.

Evans, H.T. (1979) The thermal expansion of anhydrite to 1000° C. Physics and Chemistry of Minerals, 4, 77–82.

Ewing, R.C., and Wang, L. (2002) Phosphates as nuclear waste forms. Reviews in mineralogy and geochemistry, 48, 673–699.

Fernández-Díaz, L., Pina, C.M., Astilleros, J.M., and Sánchez-Pastor, N. (2009) The carbonatation of gypsum: Pathways and pseudomorph formation. American Mineralogist, 94, 1223–1234.

Filippelli, G.M. (2002) The Global Phosphorus Cycle. Reviews in Mineralogy and Geochemistry, 48, 391–425.

Fiorito, E., Porcedda, G.E., Brundu, L., Passiu, C., Atzei, D., Ennas, G., Elsener, B., Fantauzzi, M., and Rossi, A. (2022) Calcium carbonate as sorbent for lead removal from wastewaters. Chemosphere, 296, 133897.

Florek, M., Fornal, E., Gómez-Romero, P., Zieba, E., Paszkowicz, W., Lekki, J., Nowak, J., and Kuczumow, A. (2009) Complementary microstructural and chemical analyses of Sepia officinalis endoskeleton. Materials Science and Engineering: C, 29, 1220–1226.

Forjanes, P., Gómez-Barreiro, J., Morales, J., Astilleros, J.M., and Fernández-Díaz, L. (2020a) Epitactic growth of celestite on anhydrite: substrate induced twinning and morphological evolution of aggregates. CrystEngComm, 22, 5743–5759.

Forjanes, P., Astilleros, J.M., and Fernández-Díaz, L. (2020b) The Formation of Barite and Celestite through the Replacement of Gypsum. Minerals, 10, 189.

Forjanes, P., Simonet Roda, M., Greiner, M., Griesshaber, E., Lagos, N.A., Veintemillas-Verdaguer, S., Astilleros, J.M., Fernández-Díaz, L., and Schmahl, W.W. (2022) Experimental burial diagenesis of aragonitic biocarbonates: from organic matter loss to abiogenic calcite formation. Biogeosciences, 19, 3791–3823.

Freyer, D., and Voigt, W. (2003) Crystallization and Phase Stability of CaSO4 and CaSO4 – Based Salts. Monatshefte für Chemie / Chemical Monthly, 134, 693–719.

Fulghum, J.E., Bryan, S.R., Linton, R.W., Bauer, C.F., and Griffis, D.P. (1988) Discrimination between adsorption and coprecipitation in aquatic particle standards by surface analysis techniques: lead distributions in calcium carbonates. Environmental science & technology, 22, 463–467.

Gaffey, S.J. (1988) Water in skeletal carbonates. Journal of Sedimentary Research, 58, 397–414.

Gaffey, S.J., Kolak, J.J., and E. Bronnimann, C. (1991) Effects of drying, heating, annealing, and roasting on carbonate skeletal material, with geochemical and diagenetic implications. Geochimica et Cosmochimica Acta, 55, 1627–1640.

Godelitsas, A., and Astilleros, J.M. (2010) Dissolution, sorption/(re) precipitation, formation of solid solutions and crystal growth phenomena on mineral surfaces: implications for the removal of toxic metals from the environment. EMU Notes in Mineralogy, 10, 289–324.

Godelitsas, A., Astilleros, J.M., Hallam, K., Harissopoulos, S., and Putnis, A. (2003) Interaction of Calcium Carbonates with Lead in Aqueous Solutions. Environmental Science & Technology, 37, 3351–3360.

Goffredo, S., Vergni, P., Reggi, M., Caroselli, E., Sparla, F., Levy, O., Dubinsky, Z., and Falini, G. (2011) The Skeletal Organic Matrix from Mediterranean Coral Balanophyllia europaea Influences Calcium Carbonate Precipitation. PLOS ONE, 6, e22338.

Gopal, R., and Calvo, C. (1972) Structural relationship of whitlockite and βCa3 (PO4) 2. Nature Physical Science, 237, 30–32.

Gray, N.F. (2008) Drinking water quality: problems and solutions. Cambridge University Press.

Gregory, T., Moreno, E., Patel, J., and Brown, W. (1974) Solubility of β-Ca3(PO4)2 in the system Ca(OH)2-H3PO4-H2O at 5, 15, 25, and 37°C. J Res Natl Bur Stand 78:667-674. Journal of Research of the National Bureau of Standards. Section A, Physics and Chemistry, 78, 667.

Griesshaber, E., Checa, A.G., Salas, C., Hoffmann, R., Yin, X., Neuser, R., Rupp, U., and Schmahl, W.W. (2023) Biological light-weight materials: The endoskeletons of cephalopod mollusks. Journal of Structural Biology, 215, 107988.

Guo, Z., Boeing, W.J., Borgomeo, E., Xu, Y., and Weng, Y. (2021) Linking reservoir ecosystems research to the sustainable development goals. Science of The Total Environment, 146769.

Guren, M.G., Putnis, C.V., Montes-Hernandez, G., King, H.E., and Renard, F. (2020) Direct imaging of coupled dissolution-precipitation and growth processes on calcite exposed to chromium-rich fluids. Chemical Geology, 552, 119770.

Hancock, J.D., and Sharp, J.H. (1972) Method of Comparing Solid-State Kinetic Data and Its Application to the Decomposition of Kaolinite, Brucite, and BaCO3. Journal of the American Ceramic Society, 55, 74–77.

Hans von Storch, C.H. (2004) Controlling Lead Concentrations in Human Blood by Regulating the Use of Lead in Gasoline. AMBIO: A Journal of the Human Environment, 33, 126-132–7.

Harper, E.M., Checa, A.G., and Rodríguez-Navarro, A.B. (2009) Organization and mode of secretion of the granular prismatic microstructure of Entodesma navicula (Bivalvia: Mollusca). Acta Zoologica, 90, 132–141.

Hartman, and Perdok, W. (1955a) On the relations between structure and morphology of crystals. I. Acta Crystallographica, 8, 49–52.

——— (1955b) On the relations between structure and morphology of crystals. II. Acta Crystallographica, 8, 521–524.

Hassaan, M.A., El Nemr, A., and Madkour, F.F. (2016) Environmental assessment of heavy metal pollution and human health risk. American Journal of Water Science and Engineering, 2, 14–19.

Hawthorne, F., and Ferguson, R. (1975) Anhydrous sulphates; II, Refinement of the crystal structure of anhydrite. The Canadian Mineralogist, 13, 289–292.

Heijnen, W., and Hartman, P. (1991) Structural morphology of gypsum (CaSO4· 2H2O), brushite (CaHPO4· 2H2O) and pharmacolite (CaHAsO4· 2H2O). Journal of Crystal Growth, 108, 290–300.

Hejami, A.A., Davis, M., Prete, D., Lu, J., and Wang, S. (2020) Heavy metals in indoor settled dusts in Toronto, Canada. Science of The Total Environment, 703, 134895.

Herman, A., Addadi, L., and Weiner, S. (1988) Interactions of sea-urchin skeleton macromolecules with growing calcite crystals— a study of intracrystalline proteins. Nature, 331, 546–548.

Hochella, M. (2002) Sustaining Earth: Thoughts on the present and future roles of mineralogy in environmental science. Mineralogical Magazine, 66, 627–652.

Hövelmann, J., and Putnis, C.V. (2016) In situ nanoscale imaging of struvite formation during the dissolution of natural brucite: implications for phosphorus recovery from wastewaters. Environmental Science & Technology, 50, 13032–13041.

Howells, M., Hermann, S., Welsch, M., Bazilian, M., Segerström, R., Alfstad, T., Gielen, D., Rogner, H., Fischer, G., and Van Velthuizen, H. (2013) Integrated analysis of climate change, land-use, energy and water strategies. Nature Climate Change, 3, 621–626.

Hughes, J.M., Cameron, M., and Crowley, K.D. (1989) Structural variations in natural F, OH, and Cl apatites. American Mineralogist, 74, 870–876.

Jang, Y.-C., and Townsend, T.G. (2003) Leaching of Lead from Computer Printed Wire Boards and Cathode Ray Tubes by Municipal Solid Waste Landfill Leachates. Environmental Science & Technology, 37, 4778–4784.

Johnson, P.D., Girinathannair, P., Ohlinger, K.N., Ritchie, S., Teuber, L., and Kirby, J. (2008) Enhanced removal of heavy metals in primary treatment using coagulation and flocculation. Water environment research, 80, 472–479.

Jonas, L., John, T., and Putnis, A. (2013) Influence of temperature and Cl on the hydrothermal replacement of calcite by apatite and the development of porous microstructures. American Mineralogist, 98, 1516–1525.

Jonas, L., John, T., King, H.E., Geisler, T., and Putnis, A. (2014) The role of grain boundaries and transient porosity in rocks as fluid pathways for reaction front propagation. Earth and Planetary Science Letters, 386, 64–74.

Jung, M.C., and Thornton, I. (1997) Environmental contamination and seasonal variation of metals in soils, plants and waters in the paddy fields around a Pb◎Zn mine in Korea. Science of The Total Environment, 198, 105–121.

Kasioptas, A., Geisler, T., Putnis, C.V., Perdikouri, C., and Putnis, A. (2010) Crystal growth of apatite by replacement of an aragonite precursor. Journal of Crystal Growth, 312, 2431–2440.

Kasioptas, A., Geisler, T., Perdikouri, C., Trepmann, C., Gussone, N., and Putnis, A. (2011) Polycrystalline apatite synthesized by hydrothermal replacement of calcium carbonates. Geochimica et Cosmochimica Acta, 75, 3486–3500.

Kaufman, H.W., and Kleinberg, I. (1979) Studies on the incongruent solubility of hydroxyapatite. Calcified Tissue International, 27, 143.

Keir, R.S. (1980) The dissolution kinetics of biogenic calcium carbonates in seawater. Geochimica et Cosmochimica Acta, 44, 241–252.

Khan, A.E., Ireson, A., Kovats, S., Mojumder, S.K., Khusru, A., Rahman, A., and Vineis, P. (2011) Drinking Water Salinity and Maternal Health in Coastal Bangladesh: Implications of Climate Change. Environmental Health Perspectives, 119, 1328–1332.

Khanam, R., Kumar, A., Nayak, A.K., Shahid, Md., Tripathi, R., Vijayakumar, S., Bhaduri, D., Kumar, U., Mohanty, S., Panneerselvam, P., and others (2020) Metal(loid)s (As, Hg, Se, Pb and Cd) in paddy soil: Bioavailability and potential risk to human health. Science of The Total Environment, 699, 134330.

Kile, D.E., Eberl, D.D., Hoch, A.R., and Reddy, M.M. (2000) An assessment of calcite crystal growth mechanisms based on crystal size distributions. Geochimica et Cosmochimica Acta, 64, 2937–2950.

Kim, Y., Tekawade, A., Lee, S.S., and Fenter, P. (2023) Morphological and crystallographic controls in the replacement of calcite and aragonite by cerussite and otavite. Geochimica et Cosmochimica Acta, 341, 16–27.

Kim, Y.-Y., Carloni, J.D., Demarchi, B., Sparks, D., Reid, D.G., Kunitake, M.E., Tang, C.C., Duer, M.J., Freeman, C.L., and Pokroy, B. (2016) Tuning hardness in calcite by incorporation of amino acids. Nature materials, 15, 903–910.

Knudsen, A.C., and Gunter, M.E. (2002) Sedimentary Phosphorites—An Example: Phosphoria Formation, Southeastern Idaho, U.S.A. Reviews in Mineralogy and Geochemistry, 48, 363–389.

Köhler, S.J., Cubillas, P., Rodríguez-Blanco, J.D., Bauer, C., and Prieto, M. (2007) Removal of Cadmium from Wastewaters by Aragonite Shells and the Influence of Other Divalent Cations. Environmental Science & Technology, 41, 112–118.

Kontrec, J., Kralj, D., and Brečević, L. (2002) Transformation of anhydrous calcium sulphate into calcium sulphate dihydrate in aqueous solutions. Journal of Crystal Growth, 240, 203–211.

Kuhn, T., Herzig, P.M., Hannington, M.D., Garbe-Schönberg, D., and Stoffers, P. (2003) Origin of fluids and anhydrite precipitation in the sediment-hosted Grimsey hydrothermal field north of Iceland. Chemical Geology, 202, 5–21.

Lagos, N.A., Benítez, S., Grenier, C., Rodriguez-Navarro, A.B., García-Herrera, C., Abarca-Ortega, A., Vivanco, J.F., Benjumeda, I., Vargas, C.A., Duarte, C., and others (2021) Plasticity in organic composition maintains biomechanical performance in shells of juvenile scallops exposed to altered temperature and pH conditions. Scientific Reports, 11, 24201.

Laidlaw, M.A.S., Filippelli, G.M., Sadler, R.C., Gonzales, C.R., Ball, A.S., and Mielke, H.W. (2016) Children's Blood Lead Seasonality in Flint, Michigan (USA), and Soil-Sourced Lead Hazard Risks. International Journal of Environmental Research and Public Health, 13.

Lang, A., Mijowska, S., Polishchuk, I., Fermani, S., Falini, G., Katsman, A., Marin, F., and Pokroy, B. (2020) Acidic Monosaccharides become Incorporated into Calcite Single Crystals**. Chemistry – A European Journal, 26, 16860–16868.

Laptikhovsky, V., Cooke, G., Drerup, C., Jackson, A., MacLeod, E., and Robin, J.-P. (2023) Spatial and temporal variability of common cuttlefish, Sepia officinalis, L. spawning grounds off North Europe. Fisheries Research, 263, 106688.

Lasaga, A.C. (1998) Kinetic theory in the earth sciences Vol. 811. Princeton, NJ: Princeton university press.

Lee, H.H., Kim, S.Y., Owens, V.N., Park, S., Kim, J., and Hong, C.O. (2018) How Does Oyster Shell Immobilize Cadmium? Archives of Environmental Contamination and Toxicology, 74, 114–120.

Lee, S.W., Kim, Y.M., Kim, R.H., and Choi, C.S. (2008) Nano-structured biogenic calcite: a thermal and chemical approach to folia in oyster shell. Micron, 39, 380–386.

Li, M., Wang, L., Zhang, W., Putnis, C.V., and Putnis, A. (2016) Direct Observation of Spiral Growth, Particle Attachment, and Morphology Evolution of Hydroxyapatite. Crystal Growth & Design, 16, 4509–4518.

Li, Z., Ma, Z., van der Kuijp, T.J., Yuan, Z., and Huang, L. (2014) A review of soil heavy metal pollution from mines in China: Pollution and health risk assessment. Science of The Total Environment, 468–469, 843–853.

Lippmann, F. (1977) The solubility products of complex minerals, mixed crystals, and three-layer clay minerals.

——— (1980) Phase diagrams depicting the aqueous solubility of mineral systems. Neues Jahrbuch Mineralogische Abhandlungen, 139, 1–25.

Lippmann, F. (1991) Aqueous solubility of magnesian calcites with different endmembers. Acta Mineral Petrogr, 32, 5–19.

Lowenstam, H.A., and Weiner, S. (1989) On biomineralization. Oxford University Press on Demand.

Lu, H., Wang, Y., and Wang, J. (2015) Recovery of Ni2+ and pure water from electroplating rinse wastewater by an integrated two-stage electrodeionization process. Journal of Cleaner Production, 92, 257–266.

Luo, X.-S., Ding, J., Xu, B., Wang, Y.-J., Li, H.-B., and Yu, S. (2012) Incorporating bioaccessibility into human health risk assessments of heavy metals in urban park soils. Science of The Total Environment, 424, 88–96.

Ma, Q.Y., Traina, S.J., Logan, T.J., and Ryan, J.A. (1993) In situ lead immobilization by apatite. Environmental Science & Technology, 27, 1803–1810.

Malferrari, D., Fermani, S., Galletti, P., Goisis, M., Tagliavini, E., and Falini, G. (2013) Shaping Calcite Crystals by Means of Comb Polyelectrolytes Having Neutral Hydrophilic Teeth. Langmuir, 29, 1938–1947.

Mallin, M.A., and Cahoon, L.B. (2020) The Hidden Impacts of Phosphorus Pollution to Streams and Rivers. BioScience, 70, 315–329.

Mapanda, F., Mangwayana, E., Nyamangara, J., and Giller, K. (2005) The effect of long-term irrigation using wastewater on heavy metal contents of soils under vegetables in Harare, Zimbabwe. Agriculture, Ecosystems & Environment, 107, 151–165.

Mavropoulos, E., Rossi, A.M., Costa, A.M., Perez, C.A.C., Moreira, J.C., and Saldanha, M. (2002) Studies on the Mechanisms of Lead Immobilization by Hydroxyapatite. Environmental Science & Technology, 36, 1625–1629.

McDowell, H., Gregory, T.M., and Brown, W.E. (1977) Solubility of Ca(5)(PO(4))(3)OH in the System Ca(OH)(2)-H(3)PO(4)-H(2)O at 5, 15, 25, and 37 °C. Journal of Research of the National Bureau of Standards. Section A, Physics and Chemistry, 81A, 273–281.

Metzler, R.A., Tribello, G.A., Parrinello, M., and Gilbert, P.U.P.A. (2010) Asprich Peptides Are Occluded in Calcite and Permanently Disorder Biomineral Crystals. Journal of the American Chemical Society, 132, 11585–11591.

Morales, J., Astilleros, J.M., Fernández-Díaz, L., Álvarez-Lloret, P., and Jiménez, A. (2013) Anglesite (PbSO4) epitactic overgrowths and substrate-induced twinning on anhydrite (CaSO4) cleavage surfaces. Journal of Crystal Growth, 380, 130–137.

Morales, J., Astilleros, J.M., Jiménez, A., Göttlicher, J., Steininger, R., and Fernández-Díaz, L. (2014) Uptake of dissolved lead by anhydrite surfaces. Applied Geochemistry, 40, 89–96.

Murray, R.C. (1964) Origin and diagenesis of gypsum and anhydrite. Journal of Sedimentary Research, 34, 512–523.

Nakamura, S., Otsuka, R., Aoki, H., Akao, M., Miura, N., and Yamamoto, T. (1990) Thermal expansion of hydroxyapatite-β-tricalcium phosphate ceramics. Thermochimica Acta, 165, 57–72.

Nečas, D., and Klapetek, P. (2012) Gwyddion: an open-source software for SPM data analysis, 10, 181–188.

Njati, S.Y., and Maguta, M.M. (2019) Lead-based paints and children's PVC toys are potential sources of domestic lead poisoning–A review. Environmental pollution.

Nkutha, C.S., Naidoo, E.B., and Shooto, N.D. (2021) Adsorptive studies of toxic metal ions of Cr(VI) and Pb(II) from synthetic wastewater by pristine and calcined coral limestones. South African Journal of Chemical Engineering, 36, 43–57.

Noguera, C., Fritz, B., Clément, A., and Baronnet, A. (2006) Nucleation, growth and ageing scenarios in closed systems I: A unified mathematical framework for precipitation, condensation and crystallization. Journal of Crystal Growth, 297, 180–186.

Nriagu, J.O., and Pacyna, J.M. (1988) Quantitative assessment of worldwide contamination of air, water and soils by trace metals. Nature, 333, 134–139.

Obeng-Gyasi, E. (2019) Sources of lead exposure in various countries. Reviews on environmental health, 34, 25–34.

Oelkers, E.H., Golubev, S.V., Pokrovsky, O.S., and Bénézeth, P. (2011) Do organic ligands affect calcite dissolution rates? Geochimica et Cosmochimica Acta, 75, 1799–1813.

Olivarius, M., Weibel, R., Hjuler, M.L., Kristensen, L., Mathiesen, A., Nielsen, L.H., and Kjøller, C. (2015) Diagenetic effects on porosity–permeability relationships in red beds of the Lower Triassic Bunter Sandstone Formation in the North German Basin. Sedimentary Geology, 321, 139–153.

Oliver, M. (1997) Soil and human health: a review. European Journal of Soil Science, 48, 573–592.

Oller, I., Malato, S., and Sánchez-Pérez, Ja. (2011) Combination of advanced oxidation processes and biological treatments for wastewater decontamination—a review. Science of the total environment, 409, 4141–4166.

Otálora, F., and García-Ruiz, J. (2014) Nucleation and growth of the Naica giant gypsum crystals. Chemical Society Reviews, 43, 2013–2026.

Parkhurst, D.L., and Appelo, C. (1999) User's guide to PHREEQC (Version 2): A computer program for speciation, batch-reaction, one-dimensional transport, and inverse geochemical calculations. Water-resources investigations report, 99, 312.

——— (2013) Description of input and examples for PHREEQC version 3: a computer program for speciation, batch-reaction, one-dimensional transport, and inverse geochemical calculations. US Geological Survey.

Pedersen, B.F., and Semmingsen, D. (1982) Neutron diffraction refinement of the structure of gypsum, CaSO4. 2H2O. Acta Crystallographica Section B: Structural Crystallography and Crystal Chemistry, 38, 1074–1077.

Pedrosa, E.T., Putnis, C.V., and Putnis, A. (2016) The pseudomorphic replacement of marble by apatite: The role of fluid composition. Chemical Geology, 425, 1–11.

Pedrosa, E.T., Boeck, L., Putnis, C.V., and Putnis, A. (2017) The replacement of a carbonate rock by fluorite: Kinetics and microstructure. American Mineralogist, 102, 126–134.

Penel, G., Leroy, G., Rey, C., and Bres, E. (1998) MicroRaman Spectral Study of the PO4 and CO3 Vibrational Modes in Synthetic and Biological Apatites. Calcified Tissue International, 63, 475–481.

Peng, C., Jin, R., Li, G., Li, F., and Gu, Q. (2014) Recovery of nickel and water from wastewater with electrochemical combination process. Separation and Purification Technology, 136, 42–49.

Pérez-Garrido, C., Fernández-Díaz, L., Pina, C.M., and Prieto, M. (2007) In situ AFM observations of the interaction between calcite (10$\bar{1}$4) surfaces and Cd-bearing aqueous solutions. Surface Science, 601, 5499–5509.

Pérez-Garrido, C., Astilleros, J.M., Fernández-Díaz, L., and Prieto, M. (2009) In situ AFM study of the interaction between calcite {1 0 1$\bar{4}$} surfaces and supersaturated Mn2+–CO32− aqueous solutions. Journal of Crystal Growth, 311, 4730–4739.

Piekut, A., Gut, K., Ćwieląg-Drabek, M., Domagalska, J., and Marchwińska-Wyrwał, E. (2019) The relationship between children's non-nutrient exposure to cadmium, lead and zinc and the location of recreational areas-Based on the Upper Silesia region case (Poland). Chemosphere, 223, 544–550.

Pina, C.M., Fernández-Díaz, L., Prieto, M., and Putnis, A. (2000) In situ atomic force microscope observations of a dissolution–crystallisation reaction: the phosgenite–cerussite transformation. Geochimica et Cosmochimica Acta, 64, 215–221.

Pinto, A.J., Jimenez, A., and Prieto, M. (2009) Interaction of phosphate-bearing solutions with gypsum: Epitaxy and induced twinning of brushite (CaHPO4· 2H2O) on the gypsum cleavage surface. American Mineralogist, 94, 313–322.

Pinto, A.J., Ruiz-Agudo, E., Putnis, C.V., Putnis, A., Jiménez, A., and Prieto, M. (2010) AFM study of the epitaxial growth of brushite (CaHPO4· 2H2O) on gypsum cleavage surfaces. American Mineralogist, 95, 1747–1757.

Pinto, A.J., Carneiro, J., Katsikopoulos, D., Jiménez, A., and Prieto, M. (2012) The Link between Brushite and Gypsum: Miscibility, Dehydration, and Crystallochemical Behavior in the CaHPO4·2H2O–CaSO4·2H2O System. Crystal Growth & Design, 12, 445–455.

Pirkle, J.L., Kaufmann, R.B., Brody, D.J., Hickman, T., Gunter, E.W., and Paschal, D.C. (1998) Exposure of the U.S. population to lead, 1991-1994. Environmental Health Perspectives, 106, 745–750.

Plummer, L.N., and Busenberg, E. (1987) Thermodynamics of aragonite-strontianite solid solutions: Results from stoichiometric solubility at 25 and 76°C. Geochimica et Cosmochimica Acta, 51, 1393–1411.

Poikane, S., Kelly, M.G., Herrero, F.S., Pitt, J.-A., Jarvie, H.P., Claussen, U., Leujak, W., Solheim, A.L., Teixeira, H., and Phillips, G. (2019) Nutrient criteria for surface waters under the European Water Framework Directive: Current state-of-the-art, challenges and future outlook. Science of the Total Environment, 695, 133888.

Pokroy, Fitch, A.N., Marin, F., Kapon, M., Adir, N., and Zolotoyabko, E. (2006a) Anisotropic lattice distortions in biogenic calcite induced by intra-crystalline organic molecules. Journal of Structural Biology, 155, 96–103.

Pokroy, Fitch, A.N., Lee, P.L., Quintana, J.P., Caspi, E.N., and Zolotoyabko, E. (2006b) Anisotropic lattice distortions in the mollusk-made aragonite: A widespread phenomenon. Journal of Structural Biology, 153, 145–150.

Pokroy, Fitch, A., and Zolotoyabko, E. (2006c) The Microstructure of Biogenic Calcite: A View by High-Resolution Synchrotron Powder Diffraction. Advanced Materials, 18, 2363–2368.

Pokroy, B., Quintana, J.P., Caspi, E.N., Berner, A., and Zolotoyabko, E. (2004) Anisotropic lattice distortions in biogenic aragonite. Nature Materials, 3, 900–902.

Pollok, K., Putnis, C.V., and Putnis, A. (2011) Mineral replacement reactions in solid solution-aqueous solution systems: Volume changes, reactions paths and end-points using the example of model salt systems. American Journal of Science, 311, 211–236.

Popov, S.V. (1986) Composite prismatic structure in bivalve shell. Acta Palaeontologica Polonica, 31.

Prieto, M. (2009) Thermodynamics of Solid Solution-Aqueous Solution Systems. Reviews in Mineralogy and Geochemistry, 70, 47–85.

Prieto, M., Putnis, A., and Fernandez-Diaz, L. (1993) Crystallization of solid solutions from aqueous solutions in a porous medium: zoning in (Ba, Sr)SO4. Geological Magazine, 130, 289–299.

Prieto, M., Putnis, A., Fernández-Díaz, L., and López-Andrés, S. (1994) Metastability in diffusing-reacting systems. Journal of Crystal Growth, 142, 225–235.

Prieto, M., Cubillas, P., and Fernández-Gonzalez, Á. (2003) Uptake of dissolved Cd by biogenic and abiogenic aragonite: a comparison with sorption onto calcite. Geochimica et Cosmochimica Acta, 67, 3859–3869.

Prieto, M., Astilleros, J.M., and Fernández-Díaz, L. (2013) Environmental remediation by crystallization of solid solutions. Elements, 9, 195–201.

Putnis, A. (1992) An introduction to mineral sciences, 457 p. Cambridge University Press.

Putnis, A. (2002) Mineral replacement reactions: from macroscopic observations to microscopic mechanisms. Mineralogical Magazine, 66, 689–708.

Putnis, A. (2009a) Mineral Replacement Reactions. Reviews in Mineralogy and Geochemistry, 70, 87–124.

——— (2009b) Mineral replacement reactions. Reviews in mineralogy and geochemistry, 70, 87–124.

——— (2015) Transient Porosity Resulting from Fluid–Mineral Interaction and its Consequences. Reviews in Mineralogy and Geochemistry, 80, 1–23.

Putnis, A., and Putnis, C.V. (2007) The mechanism of reequilibration of solids in the presence of a fluid phase. Journal of Solid State Chemistry, 180, 1783–1786.

Putnis, C.V., and Fernández-Díaz, L. (2010) Ion partitioning and element mobilization during mineral replacement reactions in natural and experimental systems.

Putnis, C.V., Tsukamoto, K., and Nishimura, Y. (2005) Direct observations of pseudomorphism: compositional and textural evolution at a fluid-solid interface. American Mineralogist, 90, 1909–1912.

Putnis, C.V., Geisler, T., Schmid-Beurmann, P., Stephan, T., and Giampaolo, C. (2007) An experimental study of the replacement of leucite by analcime. American Mineralogist, 92, 19–26.

Rahimpour-Bonab, H., Esrafili-Dizaji, B., and Tavakoli, V. (2010) Dolomitization and anhydrite precipitation in Permo-Triassic carbonates at the South Pars gas Field, Offshore Iran: controls on reservoir quality. Journal of Petroleum Geology, 33, 43–66.

Rakovan, J., and Reeder, R.J. (1996) Intracrystalline rare earth element distributions in apatite: Surface structural influences on incorporation during growth. Geochimica et Cosmochimica Acta, 60, 4435–4445.

Rangel-Porras, G., García-Magno, J.B., and González-Muñoz, M.P. (2010) Lead and cadmium immobilization on calcitic limestone materials. Desalination, 262, 1–10.

Redfern, S.A.T. (1987) The kinetics of dehydroxylation of kaolinite. Clay Minerals, 22, 447–456.

Reeder, R.J. (1983) Crystal chemistry of the rhombohedral carbonates. Reviews in Mineralogy and Geochemistry, 11, 1–47.

Reinares-Fisac, D., Veintemillas-Verdaguer, S., and Fernández-Díaz, L. (2017) Conversion of biogenic aragonite into hydroxyapatite scaffolds in boiling solutions. CrystEngComm, 19, 110–116.

Rodríguez, J.D., Jiménez, A., Prieto, M., Torre, L., and García-Granda, S. (2008) Interaction of gypsum with As (V)-bearing aqueous solutions: Surface precipitation of guerinite, sainfeldite, and Ca2NaH (AsO4) 2· 6H2O, a synthetic arsenate. American Mineralogist, 93, 928–939.

Rodríguez, L., Ruiz, E., Alonso-Azcárate, J., and Rincón, J. (2009) Heavy metal distribution and chemical speciation in tailings and soils around a Pb–Zn mine in Spain. Journal of Environmental Management, 90, 1106–1116.

Rodríguez-Blanco, J.D., Jiménez, A., and Prieto, M. (2007) Oriented Overgrowth of Pharmacolite (CaHAsO4·2H2O) on Gypsum (CaSO4·2H2O). Crystal Growth & Design, 7, 2756–2763.

Roncal-Herrero, T., Astilleros, J.M., Bots, P., Rodríguez-Blanco, J.D., Prieto, M., Benning, L.G., and Fernández-Díaz, L. (2017) Reaction pathways and textural aspects of the replacement of anhydrite by calcite at 25° C. American Mineralogist, 102, 1270–1278.

Rouff, A.A., Elzinga, E.J., Reeder, R.J., and Fisher, N.S. (2004) X-ray Absorption Spectroscopic Evidence for the Formation of Pb(II) Inner-Sphere Adsorption Complexes and Precipitates at the Calcite–Water Interface. Environmental Science & Technology, 38, 1700–1707.

——— (2005) The influence of pH on the kinetics, reversibility and mechanisms of Pb(II) sorption at the calcite-water interface. Geochimica et Cosmochimica Acta, 69, 5173–5186.

——— (2006) The Effect of Aging and pH on Pb(II) Sorption Processes at the Calcite−Water Interface. Environmental Science & Technology, 40, 1792–1798.

Roy, D.M., and Linnehan, S.K. (1974) Hydroxyapatite formed from coral skeletal carbonate by hydrothermal exchange. Nature, 247, 220–222.

Royer, J., Pierce, G.J., Foucher, E., and Robin, J.P. (2006) The English Channel stock of Sepia officinalis: Modelling variability in abundance and impact of the fishery. Trends and Assessment of Cephalopod Fisheries., 78, 96–106.

Roza Llera, A., Jimenez, A., and Fernández-Díaz, L. (2021) Removal of Pb from Water: The Effectiveness of Gypsum and Calcite Mixtures. Minerals, 11, 66.

Różycka, M., Coronado, I., Brach, K., Olesiak-Bańska, J., Samoć, M., Zarębski, M., Dobrucki, J., Ptak, M., Weber, E., Polishchuk, I., and others (2019) Lattice Shrinkage by Incorporation of Recombinant Starmaker-Like Protein within Bioinspired Calcium Carbonate Crystals. Chemistry – A European Journal, 25, 12740–12750.

Ruiz-Agudo, E., Putnis, C.V., Rodriguez-Navarro, C., and Putnis, A. (2012) Mechanism of leached layer formation during chemical weathering of silicate minerals. Geology, 40, 947–950.

Ruiz-Agudo, E., Putnis, C.V., and Putnis, A. (2014) Coupled dissolution and precipitation at mineral–fluid interfaces. Chemical Geology, 383, 132–146.

Ruiz-Agudo, E., Putnis, C.V., Hövelmann, J., Álvarez-Lloret, P., Ibañez-Velasco, A., and Putnis, A. (2015) Experimental study of the replacement of calcite by calcium sulphates. Geochimica et Cosmochimica Acta, 156, 75–93.

Ruiz-Agudo, E., King, H.E., Patiño-López, L.D., Putnis, C.V., Geisler, T., Rodriguez-Navarro, C., and Putnis, A. (2016) Control of silicate weathering by interface-coupled dissolution-precipitation processes at the mineral-solution interface. Geology, 44, 567–570.

Ryan, Huet N, and MacIntosh D L (2000) Longitudinal investigation of exposure to arsenic, cadmium, and lead in drinking water. Environmental Health Perspectives, 108, 731–735.

Saidian, M., Godinez, L.J., and Prasad, M. (2016) Effect of clay and organic matter on nitrogen adsorption specific surface area and cation exchange capacity in shales (mudrocks). Journal of Natural Gas Science and Engineering, 33, 1095–1106.

Sánchez-Pastor, N., Pina, C.M., Astilleros, J.M., Fernández-Díaz, L., and Putnis, A. (2005) Epitaxial growth of celestite on barite (001) face at a molecular scale. Surface Science, 581, 225–235.

Sánchez-Pastor, N., Pina, C.M., and Fernández-Díaz, L. (2007) A combined in situ AFM and SEM study of the interaction between celestite (0 0 1) surfaces and carbonate-bearing aqueous solutions. Surface science, 601, 2973–2982.

Sancho-Tomás, M., Fermani, S., Durán-Olivencia, M.A., Otálora, F., Gómez-Morales, J., Falini, G., and García-Ruiz, J.M. (2013) Influence of Charged Polypeptides on Nucleation and Growth of CaCO3 Evaluated by Counterdiffusion Experiments. Crystal Growth & Design, 13, 3884–3891.

Seknazi, E., and Pokroy, B. (2018) Residual Strain and Stress in Biocrystals. Advanced Materials, 30, 1707263.

Sheldon, R.P. (1981) Ancient Marine Phosphorites. Annual Review of Earth and Planetary Sciences, 9, 251–284.

Shtukenberg, A.G., Astilleros, J.M., and Putnis, A. (2005) Nanoscale observations of the epitaxial growth of hashemite on barite (0 0 1). Surface Science, 590, 212–223.

Simón, M., Ortiz, I., García, I., Fernández, E., Fernández, J., Dorronsoro, C., and Aguilar, J. (1999) Pollution of soils by the toxic spill of a pyrite mine (Aznalcollar, Spain). Science of The Total Environment, 242, 105–115.

Smith, V.H. (2003) Eutrophication of freshwater and coastal marine ecosystems a global problem. Environmental Science and Pollution Research, 10, 126–139.

Soto, D. (2009) Integrated mariculture: a global review. Food and Agriculture Organization of the United Nations (FAO).

Sposito, G. (1986) Distinguishing adsorption from surface precipitation. ACS Publications.

Stipp, S.L., Hochella, M.F., Parks, G.A., and Leckie, J.O. (1992) Cd2+ uptake by calcite, solid-state diffusion, and the formation of solid-solution: Interface processes observed with near-surface sensitive techniques (XPS, LEED, and AES). Geochimica et Cosmochimica Acta, 56, 1941–1954.

Stipp, S.L.S., Kulik, A.J., Franzreb, K., Benoit, W., and Mathieu, H.J. (1997) A combination of SFM and TOF-SIMS imaging for observing local inhomogenieties in morphology and composition: aged calcite surfaces. Surface and Interface Analysis, 25, 959–965.

Sturchio, N.C., Chiarello, R.P., Cheng, L., Lyman, P.F., Bedzyk, M.J., Qian, Y., You, H., Yee, D., Geissbuhler, P., Sorensen, L.B., and others (1997) Lead adsorption at the calcite-water interface: Synchrotron X-ray standing wave and X-ray reflectivity studies. Geochimica et Cosmochimica Acta, 61, 251–263.

Subhas, A.V., Rollins, N.E., Berelson, W.M., Erez, J., Ziveri, P., Langer, G., and Adkins, J.F. (2018) The dissolution behavior of biogenic calcites in seawater and a possible role for magnesium and organic carbon. Marine Chemistry, 205, 100–112.

Tahervand, S., and Jalali, M. (2017) Sorption and desorption of potentially toxic metals (Cd, Cu, Ni and Zn) by soil amended with bentonite, calcite and zeolite as a function of pH. Journal of Geochemical Exploration, 181, 148–159.

Thevenon, F., Graham, N.D., Chiaradia, M., Arpagaus, P., Wildi, W., and Poté, J. (2011) Local to regional scale industrial heavy metal pollution recorded in sediments of large freshwater lakes in central Europe (lakes Geneva and Lucerne) over the last centuries. Science of The Total Environment, 412–413, 239–247.

Tong, S., Schirnding, Y.E. von, and Prapamontol, T. (2000) Environmental lead exposure: a public health problem of global dimensions. Bulletin of the world health organization, 78, 1068–1077.

Traina, S.J., and Laperche, V. (1999) Contaminant bioavailability in soils, sediments, and aquatic environments. Proceedings of the National Academy of Sciences, 96, 3365–3371.

Tukker, A., Buist, H., Oers, L. van, and Voet, E. van der (2006) Risks to health and environment of the use of lead in products in the EU. Resources, Conservation and Recycling, 49, 89–109.

Van Der Merwe, J.H. (1978) The role of lattice misfit in epitaxy. Critical Reviews in Solid State and Material Sciences, 7, 209–231.

Vetter, T., Iggland, M., Ochsenbein, D.R., Hänseler, F.S., and Mazzotti, M. (2013) Modeling Nucleation, Growth, and Ostwald Ripening in Crystallization Processes: A Comparison between Population Balance and Kinetic Rate Equation. Crystal Growth & Design, 13, 4890–4905.

Walter, L.M., and Morse, J.W. (1984) Reactive surface area of skeletal carbonates during dissolution; effect of grain size. Journal of Sedimentary Research, 54, 1081–1090.

Wang, L., and Nancollas, G.H. (2008) Calcium Orthophosphates: Crystallization and Dissolution. Chemical Reviews, 108, 4628–4669.

Wang, L., Ruiz-Agudo, E., Putnis, C.V., Menneken, M., and Putnis, A. (2012a) Kinetics of Calcium Phosphate Nucleation and Growth on Calcite: Implications for Predicting the Fate of Dissolved Phosphate Species in Alkaline Soils. Environmental Science & Technology, 46, 834–842.

Wang, L., Li, S., Ruiz-Agudo, E., Putnis, C.V., and Putnis, A. (2012b) Posner's cluster revisited: direct imaging of nucleation and growth of nanoscale calcium phosphate clusters at the calcite-water interface. CrystEngComm, 14, 6252–6256.

Wang, L., Putnis, C.V., Ruiz-Agudo, E., King, H.E., and Putnis, A. (2013) Coupled dissolution and precipitation at the cerussite-phosphate solution interface: Implications for immobilization of lead in soils. Environmental science & technology, 47, 13502–13510.

Wang, L., Putnis, C.V., Ruiz-Agudo, E., Hövelmann, J., and Putnis, A. (2015) In situ Imaging of Interfacial Precipitation of Phosphate on Goethite. Environmental Science & Technology, 49, 4184–4192.

Warren, J.K. (2006) Evaporites: sediments, resources and hydrocarbons. Springer Science & Business Media.

Wei, X., and Bailey, R.T. (2021) Evaluating nitrate and phosphorus remediation in intensively irrigated stream-aquifer systems using a coupled flow and reactive transport model. Journal of Hydrology, 598, 126304.

Weiner, S., and Dove, P.M. (2003) An overview of biomineralization processes and the problem of the vital effect. Reviews in mineralogy and geochemistry, 54, 1–29.

Weiner, S., and Traub, W. (1984) Macromolecules in mollusc shells and their functions in biomineralization. Philosophical Transactions of the Royal Society of London. B, Biological Sciences, 304, 425–434.

Xia, F., Brugger, J., Chen, G., Ngothai, Y., O'Neill, B., Putnis, A., and Pring, A. (2009) Mechanism and kinetics of pseudomorphic mineral replacement reactions: A case study of the replacement of pentlandite by violarite. Geochimica et Cosmochimica Acta, 73, 1945–1969.

Yang, Y., Wu, Q., Wang, M., Long, J., Mao, Z., and Chen, X. (2014) Hydrothermal Synthesis of Hydroxyapatite with Different Morphologies: Influence of Supersaturation of the Reaction System. Crystal Growth & Design, 14, 4864–4871.

Yu, L., Daniels, L.M., Mulders, J.J., Saldi, G.D., Harrison, A.L., Liu, L., and Oelkers, E.H. (2019) An experimental study of gypsum dissolution coupled to CaCO3 precipitation and its application to carbon storage. Chemical Geology, 525, 447–461.

Yuan, K., Lee, S.S., De Andrade, V., Sturchio, N.C., and Fenter, P. (2016) Replacement of Calcite (CaCO3) by Cerussite (PbCO3). Environmental Science & Technology, 50, 12984–12991.

Yuan, K., De Andrade, V., Feng, Z., Sturchio, N.C., Lee, S.S., and Fenter, P. (2018) Pb2+–Calcite Interactions under Far-from-Equilibrium Conditions: Formation of Micropyramids and Pseudomorphic Growth of Cerussite. The Journal of Physical Chemistry C, 122, 2238–2247.

Zachara, J.M., Cowan, C.E., and Resch, C.T. (1991) Sorption of divalent metals on calcite. Geochimica et Cosmochimica Acta, 55, 1549–1562.

Zhao, J., Brugger, J., Grundler, P.V., Xia, F., Chen, G., and Pring, A. (2009) Mechanism and kinetics of a mineral transformation under hydrothermal conditions: Calaverite to metallic gold. American Mineralogist, 94, 1541–1555.

Zheng, N., Wang, Q., and Zheng, D. (2007) Health risk of Hg, Pb, Cd, Zn, and Cu to the inhabitants around Huludao Zinc Plant in China via consumption of vegetables. Science of The Total Environment, 383, 81–89.

Zheng, N., Liu, J., Wang, Q., and Liang, Z. (2010) Health risk assessment of heavy metal exposure to street dust in the zinc smelting district, Northeast of China. Science of The Total Environment, 408, 726–733.

Zhou, X., Liu, W., Zhang, J., Wu, C., Ou, X., Tian, C., Lin, Z., and Dang, Z. (2017) Biogenic Calcium Carbonate with Hierarchical Organic–Inorganic Composite Structure Enhancing the Removal of Pb(II) from Wastewater. ACS Applied Materials & Interfaces, 9, 35785–35793.

Zhu, R., Yu, R., Yao, J., Wang, D., and Ke, J. (2008) Morphology control of hydroxyapatite through hydrothermal process. Journal of Alloys and Compounds, 457, 555–559.

Zhuang, P., McBride, M.B., Xia, H., Li, N., and Li, Z. (2009) Health risk from heavy metals via consumption of food crops in the vicinity of Dabaoshan mine, South China. Science of The Total Environment, 407, 1551–1561.

Appendix A. Conference Contributions

XXXVII Reunión SEM (Sociedad Española de Mineralogía):

Presentación tipo póster. Celebrado en Madrid.

"Formación de jarositas en condiciones ambientales".

Pedro Granda, Ana Roza y Amalia Jiménez

ECM31 2018 31st European Crystallographic Meeting:

Presentación tipo póster. Celebrado en Oviedo.

"Crystal growth of lead bearing phases at acidic conditions".

Ana Roza, Ester Benito and Amalia Jiménez

EGU General Assembly 2019:

Presentación tipo póster. Celebrado en Viena.

"Effect of pH on crystallization of lead bearing phases on gypsum at ambient conditions".

Ana Roza, Amalia Jiménez and Lurdes Fernández-Díaz.

"Interaction of dissolved lead with calcite in the pH range between 2.5 and 7.9"

Amalia Jiménez, Ana Roza and Lurdes Fernández-Díaz.

Goldschmidt Conference 2019:

Presentación tipo póster. Celebrado en Barcelona.

"Interaction of dissolved lead with calcite and gypsum at acidic conditions".

Ana Roza, Lurdes Fernández-Díaz and Amalia Jiménez.

EGU: Sharing Geoscience Online 2020. Congreso online debido a la pandemia originada por el Covid-19:

"Replacement of anhydrite by hydroxyapatite: kinetic and textural characteristics".

Ana Roza, Amalia Jiménez and Lurdes Fernández-Díaz.

Goldschmidt Conference 2021 Virtual:

Presentación PowerPoint. Online.

"Kinetic of the replacement reaction of anhydrite by calcium phosphates".

Ana Roza, Amalia Jiménez and Lurdes Fernández-Díaz.

EMC 2020 3rd European Mineralogical Conference Cracow Poland:

Presentación PowerPoint. Online.

"Pseudomorphic replacement of anhydrite by calcium phosphate: kinetics, reaction pathway, and textural features".

Ana Roza, Amalia Jiménez and Lurdes Fernández-Díaz.

"Stability of natrojarosite and precipitation of anglesite under acidic conditions".

Ana Roza, Gregorio Marban and Amalia Jiménez.

Formación de natrojarosita en condiciones ambientales

Pedro Granda Ibáñez (1), Ana Roza Llera (1), Amalia Jiménez (1*)

(1) Departamento de Geología. Universidad de Oviedo, 33005, Oviedo (España)
* corresponding author: amjimenez@uniovi.es

Palabras Clave: natrojarosita, precipitación, morfología. | **Key Words:** natrojarosite, precipitation, morphology.

INTRODUCCIÓN

La formación de minerales del grupo de la jarosita $(AFe_3(SO_4)_2(OH)_6$ donde A = Na^+, K^+, Ag^+, Rb^+, H_3O^+, NH_4^+, Pb^{+2}) está asociada a procesos geológicos y geoquímicos que tienen lugar en la superficie terrestre. Estos minerales que se encuentran en depósitos supergénicos y aguas ácidas de minas también son componentes principales de grandes volúmenes de residuos en la industria metalúrgica o se usan para atrapar cantidades significativas de metales pesados tóxicos o metaloides. En la hidrometalurgia de zinc, se utiliza la precipitación de jarosita para eliminar eficazmente el exceedente de hierro que está presente en las concentraciones de sulfuro de Zn (Dutrizac y Jambor, 2000). La identificación de jarosita en Marte (Papike et al., 2006), aporta un interés adicional a los minerales de este grupo como indicadores de la presencia de agua y por tanto de las condiciones geoquímicas de la superficie de este planeta.

A pesar del interés que genera este grupo mineral, aún no se conocen en profundidad algunos datos específicos y concluyentes sobre sus condiciones de formación. Por ello, el propósito de este trabajo es un estudio experimental sobre la síntesis de natrojarositas (en un sistema abierto y condiciones ambientales controladas de laboratorio) a partir de una mezcla de disoluciones acuosas a temperaturas inferiores a 50°C.

METODOLOGÍA EXPERIMENTAL

Los experimentos de precipitación se llevaron a cabo mediante la mezcla de dos disoluciones de NaOH (1M) y $Fe_2(SO_4)_3$ (0.3 M) con una proporción de 40:60 a distintas temperaturas (20°C, 35°C y 50°C). Para cada temperatura se realizaron experimentos de envejecimiento durante periodos de tiempo creciente desde 1h hasta 120 horas. Una vez transcurrido el tiempo de reacción se midió el pH de las fases acuosas finales que coexisten con el precipitado y se separaron ambas fases mediante centrifugación. Los sólidos se analizaron por difracción de rayos X y SEM. Los difractogramas obtenidos mediante DRX fueron tratados con programas informáticos (X'Pert HighScore Plus) obteniendo datos de composición y estructura cristalina de las fases precipitadas. A partir de los diagramas de rayos X se han refinado los parámetros de celda unidad de cada precipitado por el método de mínimos cuadrados y se ha estimado el grado de cristalinidad a partir de la anchura a media altura (FWHM) de las reflexiones. La composición de las disoluciones acuosas se analizó mediante espectrometría de masas (ICP/MS).

RESULTADOS

La figura 1 muestra los difractogramas de las muestras precipitadas a 50° C para tiempos de reacción creciente. Como se puede observar, todos los diagramas presentan reflexiones bien diferenciadas que corresponden a una sustancia cristalina que ha sido identificada como natrojarosita (PDF 36-425). En los diagramas de 1h y 6h aparece una reflexión adicional (d= 10.20 Å) que se ha identificado como un hidróxido de aluminio metoxido (PDF 22-1538) y que se atribuye a precipitados metaestables que desaparecen para tiempos de reacción más prolongados. En los difractogramas de los sólidos obtenidos a 35° C sólo se identificó natrojarosita.

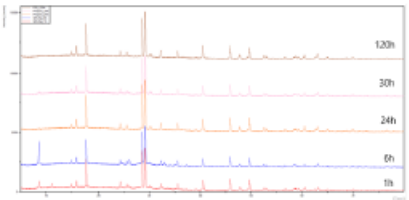

Fig 1. Difractogramas a 50°C para distintos tiempos de reacción

En la figura 2 se presentan los diagramas de rayos X correspondientes a los experimentos de 20°C. El difractograma del precipitado obtenido a 3h muestra evidencias claras de su baja cristalinidad, como es el elevado ruido de fondo y algunas reflexiones incipientes muy anchas. Para tiempos de envejecimiento más largos, se aprecian reflexiones mejor definidas que se han identificado como 021 y 113 en el patrón de natrojarosita (PDF 36-425). En general, la intensidad de estas reflexiones aumenta para tiempos de envejecimiento más prolongados. A partir de la figura 2 se han obtenido

31st European Crystallographic Meeting • Oviedo, Spain 22-27 August

MS15-P08

Crystal growth of lead bearing phases at acidic conditions

Ana Roza Llera[1], Amalia Jiménez[1], Ester Benito[1]

1. Department of Geology. University of Oviedo., Oviedo, Spain

email: ana.roza@gmail.com

Dissolution - crystallization reactions can control the uptake of heavy metal such as lead, which is harmful to human health if inhaled or ingested. When Pb-bearing aqueous solution interacts with carbonates and sulfates, the formation of secondary phases at the interface mineral-water plays an important role on both the migration and accumulation of this pollutant in earth surface systems. The interaction of lead dissolved with calcium bearing minerals has been previously studied at pH between 4.75 and 6.8 [1-2]. However, less attention has been paid to the crystallization of Pb-bearing minerals in high acidic environments, in which the availability and mobility of dissolved Pb increase. Here, we have studied the interaction of Pb dissolved with both calcite and gypsum at highly acidic and atmospheric conditions. The main goals of this work were (a) to analyse the physicochemical evolution of the system and (b) to study the nature and morphology of the neo-formed phases. With these aims, a set of macroscopic experiments has been carried out by placing 1 g of crystals of a mix of calcite and gypsum (3.0 – 4.0 mm) in batch reactors containing 100 mL of Pb-bearing aqueous solution at pH= 2.5. Then, the vessels were closed with parafilm to minimize evaporation during reaction times (from 1 hour to 48 hours). The parent solution was prepared using reagent-grade $Pb(NO_3)_2$ and high-purity deionized water to yield $[Pb_{aq}]_{initial}$ of 500 mg/L. After given period of time, the solid phases were analysed by glancing incident X-ray diffraction (GIXRD), Raman spectroscopy (RS) and Scanning Electron Microscopy (SEM). The initial and final pH were monitored and Ca^{2+} and Pb^{2+} in the aqueous solutions were analysed by ICP-OES.

Results show that dissolution of calcite and gypsum is simultaneous to elimination of the almost Pb^{2+}. Anglesite ($PbSO_4$) were identified using RS and GIRDX in all interaction experiments with gypsum. SEM reveals the heterogeneous nucleation of anglesite crystals, which are distributed randomly without covering all the gypsum surface. Different morphologies of anglesite are identified, including small rhombus-shaped single crystals, aggregates of identical crystals growing in parallel and contact twins. On the contrary, calcite is dissolving during the entire period of reaction and lead-bearing carbonates are not detected on the calcite surfaces. These data show that anglesite is a stable phase responsible of the Pb elimination under acidic conditions. The evolution of the anglesite morphologies after given reaction periods are discussed.

References:

[1] Astilleros, J.M., Godelitsas, A., Rodriguez–Blanco, J.D. Fernández–Díaz, L., Prieto, M, Lagoyannis, A. and Harissopulos, S. (2010). Applied Geochemistry, 25, 1008-1016.
[2] Godelitsas, A., Astilleros, J.M., Hallam K, Harissopulos, S. and Putnis A. (2003). Envion. Sci. Technol., 37, 3351-3360.

Keywords: Lead, Calcite, Gypsum

Geophysical Research Abstracts
Vol. 21, EGU2019-10107, 2019
EGU General Assembly 2019

Effect of pH on crystallization of lead bearing phases on gypsum at ambient conditions.

Ana Roza (1), Lurdes Fernández-Díaz (2,3), and Amalia Jiménez Bautista (1)

(1) Department of Geology. University of Oviedo. Spain, (2) Department of Mineralogy and Petrology. Complutense University of Madrid. Spain, (3) Institute of Geosciences (UCM, CSIC). Spain

Pollution of surface waters and groundwaters by Pb2+ and other heavy metals is a common feature in a variety of geological settings due to both, natural processes and human activities. The bioavailability of metal contaminants is strongly dependent on the type of minerals that are most abundant in those settings because the interaction of their surfaces with polluted waters give raise to sorption processes that sequester metals and reduce their concentration in the aqueous phase. Calcium sulphate minerals, namely gypsum and anhydrite, are highly abundant in sedimentary basins. Dissolution-crystallization processes occurring as a result of the interaction between these sulphates and Pb-bearing waters are involved in the sequestration of this pollutant and their development has been previously studied in the pH range between 4.75 and 6.8 [1]. Much less attention has been paid so far to the development of these processes in highly acidic environments, where the weathering of Pb-bearing minerals is accelerated and the availability and mobility of dissolved Pb is likely to be increased. Here, we present the results of interaction experiments between dissolved Pb and gypsum surfaces at acidic to slightly basic pHs (2.5, 5.5 and 7.9) during increasing reaction times (from 5 minutes to 24 hours) at atmospheric conditions. The main goals of this work are (a) to analyse the physicochemical evolution of the system and (b) to identify and characterize the neo-formed phases that can effectively reduce Pb bioavailability.

SEM imagining of gypsum surfaces after short interaction with dissolved Pb2+ evidence the simultaneous development of etch pits and the formation of newly formed secondary phases. The chemical evolution of the aqueous phase, which is characterised by a rapid decrease of Pb2+ concentration and a parallel increase of Ca2+ concentration, is consistent with the concomitance of gypsum dissolution and Pb-bearing phases precipitation. The nature of the Pb-bearing phases is strongly influenced by the initial pH of the aqueous solution. Thus, anglesite ($PbSO_4$) is the only phase that precipitates under acidic conditions (pH = 2.5 and 5.5) as deduced from both XRD and Raman spectroscopy analyses. Anglesite crystals initially nucleate randomly oriented on gypsum surface, quickly carpeting large areas. Anglesite crystals initially appear as tabular rhombus-shaped single crystals that evolve towards elongated along [100] crystals with a "double arrow" habit as growth proceeds. In contrast, under alkaline conditions Pb-bearing precipitates consist of nanometric to micrometric sized flake-like particles. The nature of these particles is unclear. We discuss the influence of pH in the mineralogy of neo-formed Pb-bearing phases as well as the morphological evolution of anglesite on the basis of physicochemical and crystal chemical considerations.

[1] Astilleros, J.M., Godelitsas, A., Rodríguez–Blanco, J.D. Fernández–Díaz, L., Prieto, M, Lagoyannis, A. and Harissopulos, S. (2010). Applied Geochemistry, 25, 1008-1016.

Geophysical Research Abstracts
Vol. 21, EGU2019-10049-1, 2019
EGU General Assembly 2019

Interaction of dissolved lead with calcite in the pH range between 2.5 and 7.9.

Amalia Jimenez (1), Ana Roza (1), Lurdes Fernández-Díaz (2,3)

(1) Department of Geology. University of Oviedo. Spain. amjimenez@uniovi.es, (2) Department of Mineralogy and Petrology. Complutense University of Madrid. Spain., (3) Institute of Geosciences (UCM, CSIC). Spain

Fresh water pollution by heavy metals is an important threat to human health in many regions in the world. The concentration of heavy metals in fresh water, as well as their mobility, can be reduced as a result of the development of dissolution - crystallization reactions that take place as fresh waters interact with mineral surfaces. Pb is one of the heavy metals that is most widespread in aqueous environments worldwide and whose effects on human health is most negative. Calcium carbonate minerals, namely calcite and aragonite, are main constituents of chemical sedimentary rocks. The interaction of calcite and aragonite crystal surfaces with Pb-bearing aqueous solutions plays a major role in controlling both, Pb migration and accumulation and, as result, contribute to define Pb bioavailability in natural setting where sedimentary carbonates are abundant.

Godelitsas et al [1] studied the dissolution-crystallization reactions that result from the interaction of calcite and aragonite with aqueous phases that had Pbaq contents lower than 1000 ppm and whose pH varied between 4.75 and 6.8. In comparison, Pb sorption processes by calcium carbonate minerals that take place when pH conditions are more acidic, and/or the concentration of this pollutant is significantly higher have hardly been explored. Aiming to contribute to fill this gap, in this work we focus on calcite and investigate its interaction with Pb-highly concentrated aqueous solutions in the pH range between 2.5 and 7.9 by conducting macroscopic batch-type experiments at ambient conditions. Analysis of the chemical evolution of the aqueous phase indicates that its interaction with calcite results in a rapid removal of Pb when the aqueous solution initial pH was higher than 2.5. SEM observations on calcite crystal surfaces evidence that under these pH conditions Pb removal is the consequence of the coupling between calcite dissolution and the precipitation of secondary phases precipitation. Crystals of these newly formed phases show two types of morphologies, prismatic and platy. Raman spectroscopy analysis confirms the former as cerussite ($PbCO_3$) and the latter as hydrocerussite ($Pb3(CO_3)2(OH)2$). Interestingly, during calcite interaction with Pb- bearing aqueous solutions at pH 2.5 the formation of secondary phases is only detected at the latter stages of the experiment. This is consistent with the chemical evolution of the aqueous solution, characterized by a progressive increase of Ca concentration that runs parallels to a pH increases during the entire period of interaction, while Pb remains constant over most of the experiment to only decrease at the end of reaction time. This evolution points to a continuous dissolution of calcite over the whole duration of the experiment at pH = 2.5, eventually accompanied by the precipitation of secondary phases after prolonged interaction. The different chemical evolution trends as well as the changes in the morphological characteristics of secondary phases observed as a function of the initial pH of the aqueous solution are interpreted taking into consideration thermodynamic and kinetic arguments.

[1] Godelitsas, A., Astilleros, J.M., Hallam K, Harissopulos, S. and Putnis A. (2003). Envion. Sci. Technol., 37, 3351-3360.

Goldschmidt2019 Abstract

Interaction of dissolved lead with calcite and gypsum at acidic conditions

A. ROZA[1], L. FERNÁNDEZ-DÍAZ[2] AND A. JIMÉNEZ[1]

[1]Dpt. Geology, Univ. Oviedo, Oviedo, Spain. rozaana@uniovi.es, amjimenez@uniovi.es

[2]Dpt. Mineralogy and Petrology, Univ. Complutense, Madrid, Spain. lfdiaz@geo.ucm.es

Clean water reservoirs have been continuously decreasing in the Earth due to anthropogenic effects. Contamination by Pb^{2+} is a real threat for the quality of drinking water not only in developing countries but also in specific settings in developed economies. Water lead pollution has an especially negative impact on the health of children, affecting their neurological development with long-lasting effects. Different researches have highlighted the remarkable ability of the surfaces of sedimentary rock-forming minerals like gypsum ($CaSO_4{\cdot}2H_2O$) [1] and calcite ($CaCO_3$) [2] to uptake Pb^{2+} and reduce its concentration in natural waters to values close to the maximum admissible. In previous studies the Pb^{2+} uptake behavior of gypsum and calcite surfaces has been investigated independently. Here we study the removal of dissolved Pb^{2+} as a result of the interaction of the lead-bearing solution (2072 ppm) with mixtures of gypsum and calcite (1:1). Lead uptake has been explored for two initial pHs (2.5 and 5.5) of the aqueous solution during increasing reaction times (from 5 minutes to 24 hours) at atmospheric conditions.

Our results show a rapid decrease of Pb^{2+} concentration in the aqueous solution, which is accompanied by a concomitant increase of both, Ca^{2+} concentration and pH. This evolution of the aqueous solution chemistry is consistent with Pb^{2+} removal taking place through the coupling of gypsum and calcite dissolution and the precipitation of Pb-bearing solid phases. Regardless the initial pH the formation of secondary anglesite ($PbSO_4$) and cerussite ($PbCO_3$) is confirmed by SEM and XRD analyses. The formation of hydrocerussite ($Pb_3(CO_3)_2(OH)_2$ crystals is also observed when the solution initial pH is 5. In all the cases anglesite is the first phase to precipitate, forming on the surfaces of both, gypsum and calcite as well as in the bulk solution. Cerussite and hydrocesrussite are only observed to form on the surface of calcite crystals. We interpret the precipitation sequence taking into consideration the dissolution kinetics of gypsum and calcite and the solubilities of the primary and secondary mineral phases.

[1] Godelitsas et al. (2003). *Envion. Sci. Technol.*, **37**, 3351.
[2] Astilleros et al. *Appl. Geochem.*, **25**, 1008.

EGU2020-17842
EGU General Assembly 2020

Replacement of anhydrite by hydroxyapatite: kinetic and textural characteristics

Ana Roza[1], Amalia Jiménez[1], and Lurdes Fernández-Díaz[2]
[1]Department of Geology. University of Oviedo. Spain (rozaana@uniovi.es)
[2]Department of Mineralogy and Petrology. Complutense University of Madrid. Institute of Geosciences (UCM, CSIC). Spain

Interface-coupled dissolution-precipitation (ICDP) reactions lead to the pseudomorphic replacement of minerals in a wide range of geological settings, exerting a significant impact in geochemical cycles (Putnis 2002). ICDP reactions play a major role in the diagenetic evolution of sedimentary rocks, specially of limestones and evaporites. Recent experimental works have studied ICDP reactions that lead to the formation of $CaCO_3$ pseudomorphs after anhydrite ($CaSO_4$), upon interaction of the latter phase with carbonated aqueous solutions. These pseudomorphs are highly porous polycrystalline aggregates that mainly consist of calcite (Roncal-Herrero et al. 2018; Altree-Williams et al. 2017). The formation of a large volume of interconnected microporosity that balances the molar volume loss associated to the anhydrite-calcite transformation as well as the specific arrangement of this microporosity, influenced by the existence of epitactic relationships between anhydrite and calcite, facilitate the progress of the ICDP reaction.

Here, we study the ICDP reaction that leads to the formation of hydroxyapatite ($Ca_5(PO_4)_3(OH)$) pseudomorphs after the interaction of anhydrite with phosphate-bearing aqueous solutions at temperatures 90 to180ºC during times that range from one hour to five weeks. The X-ray diffraction Rietveld analysis of the transformed samples indicates that the kinetics of the pseudomorphic transformation of anhydrite into hydroxyapatite strongly depends on temperature. Thus, while at 180ºC a 100% transformation yield is attained in few hours, it takes five weeks of interaction at 90ºC. Scanning Electron Microscopy imagining of transformed samples shows the very good preservation of both, the original external shape and microtopographic features of anhydrite crystals. On cross-cut sections of partially replaced by hydroxyapatite anhydrite crystals we observe that the transformation advances from the surface inwards, with sharp separating the by replaced layer from the unreacted anhydrite core. Furthermore, this replaced layer is structured into a compact ~ 50 µm thick outer rim, which consists of coalescent small (~ 5 µm) hydroxyapatite crystals, and a progressively thickening inner region formed by hydroxyapatite columnar crystals in a stockade-like arrangement. This latter region is highly porous. We interpret these results taking into consideration the differences in solubility and molar volume between anhydrite and hydroxyapatite as well as the similarities/differences between the crystal structures of these phases. By comparing the characteristics of different ICDP reactions that involve anhydrite in sedimentary basins we derive implications about the diagenetic evolution of calcium sulphate evaporites.

Goldschmidt 2021 Abstract
https://doi.org/10.7185/gold2021.7133

Kinetic of the replacement reaction of anhydrite by calcium phosphates

ANA ROZA LLERA[1], AMALIA JIMENEZ[1] AND LURDES FERNÁNDEZ-DÍAZ[2,3]

[1]University of Oviedo
[2]Universidad Complutense de Madrid
[3]Instituto de Geociencias IGEO (CSIC-UCM)
Presenting Author: rozaana@uniovi.es

Interface-coupled dissolution-precipitation (ICDP) reactions are widely common during the diagenesis of sedimentary rocks, namely, limestones and evaporites. In a broad range of diagenetic sceneries, ICPD reactions result in pseudomorphic replacements that often involve carbonate and sulfate minerals, both as primary and secondary phases [1-2]. Phosphate-rich rocks can be found in sedimentary rocks of all ages since the Early Proterozoic. The origin of some of these phosphate-rich rocks has been related to diagenetic processes [3], which brings up the question of whether ICPD reactions involving the interaction between P-rich aqueous solution and mineral phases common in sediments may have played a role in their formation.

Here, we investigate the hydrothermal interaction between anhydrite, a common component of evaporites, and phosphate-rich aqueous solutions during times set between 1 and 72 hours in the temperature regime between 120 and 200ºC. The characterization of the reacted samples by X-ray diffraction (XRD), Scanning Electron Microscopy, Infrared and Raman spectroscopies shows anhydrite crystals are partially to totally replaced by mixtures of hydroxyapatite and β-tricalcium phosphate in proportions that vary with time and temperature. The replacement reaction initiates at the surface of the anhydrite crystals and advances inwards, defining a sharp reaction front. The formation of a significant volume of porosity, which balances the molar volume loss associated to the anhydrite into calcium phosphate transformation, guarantees the continuous communication between the phosphate-rich solution and the reaction front, facilitating the progress of the anhydrite dissolution-calcium phosphate precipitation reaction. The good coupling between the rate of both processes explains the pseudomorphic nature of the replacement, which takes place with an almost perfect preservation of the original external shape of the anhydrite crystal all along the ICDP reaction. Finally, we determine anhydrite replaced fractions as a function of reaction time and temperature using XRD Rietveld analysis and apply the rate constant and the time to a given fraction methods to estimate the empirical activation energy Ea (kJ/mol) for the replacement reaction.

[1] Putnis A. (2002): *Mineralogical Magazine* 66.5, 689-208.

[2] Pedrosa E. et al (2017): *American Mineralogist*, *102*(1), 126-134.

[3] Bentor, Y. K. (1980) "Phosphorites—the unsolved problems".

Book of Abstracts
3rd European Mineralogical Conference
EMC 2020, Cracow, Poland

emc2020
3rd European Mineralogical Conference Cracow Poland
29 August - 2 September 2021

PSEUDOMORPHIC REPLACEMENT OF ANHYDRITE BY CALCIUM PHOSPHATE: KINETICS, REACTION PATHWAY, AND TEXTURAL FEATURES.

Roza-Llera Ana[1], Jiménez Amalia[1], Fernández-Díaz Lurdes[2]

[1]Department of Geology, University of Oviedo, Spain, [2]Department of Mineralogy and Petrology, Complutense University of Madrid, Spain

Mineral replacement phenomena occur in a wide range of geological settings as a result of fluid-solid re-equilibration processes. Most mineral replacements that affect minerals in sedimentary rocks involve the development of interface-coupled dissolution-precipitation (ICDP) reactions and result in the formation of mineral pseudomorphs. The progress of ICPD reactions is commonly associated to the formation of a transient network of porosity that facilitates a continuous communication between the fluid phase and the reaction front located at the primary mineral-secondary mineral interface. Anhydrite ($CaSO_4$) is a most common mineral sulfate that is involved in a variety of mineral replacement processes both during diagenesis and in hydrothermal environments. Previous works have reported on the pseudomorphic replacement of anhydrite by calcite and celestite after interaction with aqueous solutions bearing carbonate and strontium, respectively. Here we study the pseudomorphic replacement of anhydrite by calcium phosphate phases upon interaction with hydrothermal phosphate-bearing aqueous solutions in the temperature regime between 120 and 200°C. Phosphorus (P) is a pollutant that causes water eutrophication and endangers aquatic wildlife. The formation of phosphate minerals through the interaction with the surface of moderately soluble minerals like anhydrite can help to remove phosphate from natural waters and reduce bioavailability of this contaminant.
X-ray diffraction (XRD), Scanning Electron Microscopy (SEM), Micro-CT scanning, Infrared spectroscopy and Raman spectroscopy analyses of anhydrite samples reacted during 1 to 96 hours evidence that: (i) Calcium phosphate pseudomorphs after anhydrite consist of varying weight percentages (wt%) of both, rhombohedron-shaped β-tricalcium phosphate (βTC) and elongated hydroxyapatite (HA) crystals, with the latter phase wt% rapidly increasing with interaction time. (ii) Calcium phosphate pseudomorphs after anhydrite contain a volume of porosity above 26%. (iii) In partially replaced samples, a transformed rim encapsulates an unreacted anhydrite core, defining a sharp reaction front. (iv) In this rim, HA crystals are arranged highly co-oriented, with their length perpendicular to the rim-anhydrite core interface. This arrangement favors the connectivity between pores in the porosity network, making the replaced rim permeable to mass transfer from the fluid to the reaction front. (v) The pseudomorphic replacement of anhydrite by a calcium phosphate is a temperature-dependent process limited by the dissolution of anhydrite. (vi) Both, the time to a given fraction and the rate constant methods yield empirical activation energy (Ea) values around 40 kJ/mol for the anhydrite by calcium phosphate replacement reaction. We discuss these results taking into consideration the solubility and molar volume changes involved in the replacement.

Book of Abstracts
3rd European Mineralogical Conference
EMC 2020, Cracow, Poland

emc2020
3rd European Mineralogical Conference Cracow Poland
29 August - 2 September 2021

STABILITY OF NATROJAROSITE AND PRECIPITATION OF ANGLESITE UNDER ACIDIC CONDITIONS.

Roza-Llera Ana[1], Marban Gregorio[2], Jiménez Amalia[1]

[1]Department of Geology, University of Oviedo, Spain, [2]Instituto Nacional del Carbono, CSIC, Spain

The crystallization behavior of jarosite and schwertmannite has been studied by precipitation-aging experiments performed using different parent-solution concentrations as well as in the presence and absence of dissolved lead under extreme conditions similar to those found in acid mine drainages. Schwertmannite ($Fe_8O_8(OH)_{8-2x}(SO_4)_x \cdot nH_2O$) is a poorly crystalline phase that precipitates initially under atmospheric conditions in all experiments. However, a relatively rapid Ostwald ripening process leads to the transformation of schwertmannite into a Na-rich member of the $(Na,H_3O)Fe_3(SO_4)(OH)_6$ solid solution after aging at 20ºC (1 day) or 70ºC (3 hours). SEM images show that the presence of sodium modifies the morphology of the obtained phases and TEM studies reveal that schwertamannite particles consist of disoriented nanodomains (~6nm) spread in an amorphous bulk whereas natrojarosite particles exhibit a single-domain, highly-crytalline core, the crystallinity decreasing from core to rim. TG and DTG analyses show that the dehydration of schwertmannite favors the transformation into natrojarosite. The transformation mechanism is followed by an internal structural reorganization within the individual nanoparticles in which Fe(III) is transported from the solid to the liquid and the other ions (SO_4^{2-} and Na^+) in the opposite direction as confirmed by spectroscopic analyses. Interestingly, the presence of Pb in acidic sulfate-rich aqueous solutions results in the precipitation of anglesite ($PbSO_4$), which is the only responsible for the removal of lead (98.7-99.2%) in short periods of time of 3h and 7 days at 70 and 20ºC, respectively. The present results highlight the role of the ripening processes in epigenetic conditions and could be crucial in interpreting the formation of jarosite in Earth and Martian surface environments. Finally, these results provide useful insights to understand the geochemical behavior of Pb and open new sceneries for the recovery of Pb from acidic mine wastes.

Appendix B. Peer-Reviewer Manuscripts

Manuscript 1: ***Removal of Pb from Water: The Effectiveness of Gypsum and Calcite Mixtures.***

Authors: Roza-Llera, Ana; Jiménez, Amalia and Fernández-Díaz, Lurdes

Journal: Minerals

Publication Year: 2021

DOI: https://doi.org/10.3390/min11010066

Manuscript 2: ***Mechanism and kinetics of the pseudomorphic replacement of anhydrite by calcium phosphate phases at hydrothermal conditions.***

Authors: Roza-Llera, Ana; Jiménez, Amalia and Fernández-Díaz, Lurdes

Journal: American Mineralogist

Publication Year: 2023

DOI: https://doi.org/10.2138/am-2022-8592

Manuscript 3: ***Pb Removal Efficiency by Calcium Carbonates Calcium: Biogenic versus Abiogenic Materials***

Authors: Roza-Llera, Ana; Di Lorenzo, Fulvio; Churakov, Sergey V.; Jiménez, Amalia and Fernández-Díaz, Lurdes

Journal: Crystal Growth & Design

Publication Year: accepted 2023

DOI: https://doi.org/10.1021/acs.cgd.3c00517